# NOTE TO USERS

UNIVERSITY OF CALGARY

# Improving Ambiguity Convergence in Carrier Phase-Based Precise Point Positioning

by

Xiaobing Shen

A THESIS

SUBMITTED TO THE FACULTY OF GRADUATE STUDIES

IN PARTIAL FULFILMENT OF THE REQUIREMENTS FOR THE

DEGREE OF MASTER OF SCIENCE

DEPARTMENT OF GEOMATICS ENGINEERING

CALGARY, ALBERTA

DECEMBER, 2002

*Your file Votre référence*
*ISBN: 0-612-87425-7*
*Our file Notre référence*
*ISBN: 0-612-87425-7*

UNIVERSITY OF CALGARY

FACULTY OF GRADUATE STUDIES

The undersigned certify that they have read, and recommend to the Faculty of Graduate Studies for acceptance, a thesis entitled " Improving Ambiguity Convergence in Carrier Phase-Based Precise Point Positioning " submitted by Xiaobing Shen in partial fulfilment of the requirements of the degree of Master of Science.

Supervisor, Dr. Yang Gao, Department of Geomatics Engineering

Dr. Naser El-Sheimy, Department of Geomatics Engineering

Dr. Andrew MacIver, Department of Civil Engineering

Dec 20, 2002

Date

# ABSTRACT

This thesis describes the research results in the improvement of a new GPS processing approach: precise point positioning (PPP). Currently, PPP is implemented with the so-called Traditional Model based on the un-differenced dual frequency code and carrier phase observations aided by the precise satellite orbit and clock products. Decimetre to centimetre accuracy is achievable while an average of half an hour of convergence time is required. In order for the PPP system to be used in real-time positioning and navigation applications, accelerating ambiguity convergence therefore is essential for a fast positioning convergence solution. With the newly developed code-phase ionosphere-free combination in this research, an alternative PPP processing method – P1-P2-CP Model – is proposed, which has a lower measurement noise and a smaller residual error. But the biggest gain of the P1-P2-CP Model is the feasibility of the fixed ambiguity resolution which brings fewer unknowns, therefore accelerating solution convergence. In the model's implementation, a variance adjustment procedure was applied to obtain more precise stochastic information of both observations and parameters, and a partial ambiguity searching and fixing approach based on a pseudo-fixing concept was preliminarily developed. Included in this thesis are the numerical results and analyses of float solutions in both static and kinematics processing. Fixed solution results in static processing mode are also presented. Further considerations for the improvements of the convergence performance are also addressed.

# ACKNOWLEDGEMENTS

To begin with, I would like to express my appreciation to my supervisor, Dr. Yang Gao, for his academic and financial support, during the period of my graduate studies.

I would also like to thank Mr. Pierre Héroux of Natural Resources of Canada and his colleagues for their valuable comments and providing the software and all the necessary data that made this research possible. This research work was partially funded by Natural Resources of Canada.

Third, I would like to acknowledge the following graduate students for their all kinds of help: Yan Lu, Lei Dong, Xiaohong Zhang, Changlin Ma, Junjie Liu, Kongzhe Chen, Zhizhao Liu, Mohamed Abdel-salam, Minha Park, Zhe Liu, Mahmoud El-Gizawy, Chaochao Wang, and Jayanti Jessica Sharma. Special thanks go to Suen Lee for spending time reading my thesis and correcting the mistakes.

Many thanks are also sent to my friends Dr. Gordon Smith, Philippe Routier, Evan Tran, and Michael McKiel for their generous help and encouragement, especially to Vincent Mar for helping me prepare my final oral examination and correct my pronunciations.

Finally, I would like to thank my family for their love and support all the years.

# TABEL OF CONTENTS

# LIST OF TABLES

# LIST OF FIGURES AND ILLUSTRATIONS

# NOTATION

## i) Symbols

| | |
|---|---|
| $A$ | design matrix |
| $A_X$ | pseudo-observation design matrix |
| $C_l$ | observation variance-covariance matrix |
| $C_{l_X}$ | covariance matrix of the weighted parameters associated with $l_X$ |
| $C_{\hat{\delta}}$ | correction variance-covariance matrix |
| $C_{\hat{v}}$ | residual variance-covariance matrix |
| $l$ | observation vector |
| $l_X$ | vector of pseudo-observations of the parameters obtained from other sources or previous calculation |
| $m$ | number of observations |
| $r$ | degree of freedom or the system redundancy |
| $u$ | number of unknowns |
| $v$ | residual vector for the observations |
| $V_X$ | vector of residuals or parameter corrections to the pseudo-observables |
| $w$ | misclosure vector |
| $w_X$ | misclosure vector between the approximate values of the weighted station parameters and their observed values. |

| | |
|---|---|
| $X^0$ | approximation of unknown |
| $X$ | unknown parameter vector |
| $\delta$ | correction vector |
| $P(Li)$ | measured pseudorange on Li (m) |
| $\Phi(Li)$ | measured carrier phase on Li (m) |
| $\phi(L_i)$ | measured carrier phase on Li (cycle) |
| $\dot{\Phi}(Li)$ | measured carrier phase rate on Li (m/s) |
| $\rho$ | true geometric range (m) |
| $c$ | speed of light (m/s) |
| $dt$ | satellite clock error (s) |
| $dT$ | receiver clock error (s) |
| $d_{orb}$ | satellite orbit error (m) |
| $d_{trop}$ | tropospheric delay (m) |
| $d_{ion/Li}$ | ionospheric delay on Li (m) |
| $\lambda_i$ | wavelength on Li (m) |
| $N_i$ | integer phase ambiguity on Li (cycle) |
| $\phi_r(t_0, Li)$ | initial phase of the receiver oscillator (cycle) |
| $\phi_s(t_0, Li)$ | initial phase of the satellite oscillator (cycle) |
| $d_{mult/P(Li)}$ | multipath effect in the measured pseudorange on Li (m) |
| $d_{mult/\Phi(Li)}$ | multipath effect in the measured carrier phase on Li (m) |

| | |
|---|---|
| $\varepsilon(.)$ | measurement noise (m) |
| $\dot{d}$ | derivative with respect to time |

**ii) Acronyms**

| | |
|---|---|
| C/A | Coarse Acquisition |
| CACS | Canadian Active Control System |
| DoD | Department of Defense |
| DDGPS | Double Differential GPS |
| DGPS | Differential GPS |
| DOP | Dilution of Precision |
| DRMS | Distance Root Mean Square |
| EFEC | Earth-Fixed Earth-Centered |
| EMR | Electromagnetic Radiation |
| ERP | Earth Rotation Parameters |
| FAA | Federal Aviation Administration |
| GPS | Global Positioning System |
| GPSC | GPS Correction (Service) |
| GSD | Geodetic Survey Division |
| ICD | Interface Control Document |
| IERS | International Earth Rotation Service |
| IGP | Ionospheric Grid Point |

| | |
|---|---|
| IGS | International GPS Service |
| IMSs | Integrity Monitor Station(s) |
| ITRF | International Terrestrial Reference Frame |
| JPL | Jet Propulsion Laboratory |
| MSs | Master Station(s) |
| NRCan | Natural Resources Canada |
| P-Code | Precise Code |
| PPP | Precise Point Positioning with carrier phase observables and precise GPS data |
| PPS | Precise Positioning Service |
| PRN | Pseudo Random Noise |
| RCP | Right Circularly Polarized |
| RINEX | Receiver Independent Exchange Format |
| RMS | Root Mean Square |
| RSs | Reference Stations |
| RTACP | Real-Time Active Control Point |
| RTCM | Radio Technical Commission for Marine |
| SA | Selective Availability |
| SPP | Single Point Positioning |
| SPS | Standard Positioning Service |
| STD | Standard Deviation |
| STEC | Slant Total Electron Content |
| TEC | Total Electron Content |

| | |
|---|---|
| VRS | Virtual Reference Station |
| VTEC | Vertical Total Electron Content |
| WAAS | Wide Area Augmentation System |
| ZPD | Zenith Path Delay |

# CHAPTER 1

# INTRODUCTION

## 1.1 Background

The Global Positioning System (GPS) is a satellite-based, all weather, line-of-sight radio-navigation system providing precise three-dimensional position, navigation, and time information.

The first GPS satellite was launched in 1978. In 1993, the system was fully operational with a constellation of 24 satellites. The initial design goal of the system was to provide two Single Point Positioning (SPP) services: the Standard Positioning Service (SPS) with C/A code for civilian users, and the Precise Positioning Service (PPS) with P code for U.S. military and authorized users. Both services utilize only one receiver and are subject to the effects of all GPS error sources. The claimed real-time positioning accuracy is 50~100 metres for SPS and 10 metres for PPS (2 dRMS) if Selective Availability (SA) is on. SA is the intentional degradation of SPS signals by a two-fold process: the "epsilon" ($\varepsilon$) component consisting of the truncation of the orbital information transmitted within the Navigation Message, and the "delta" ($\delta$) component by dithering the satellite clock output frequency. SA is controlled by the U.S. Department of Defence (DOD) to limit the obtainable positioning

accuracy for non-U.S. military and government users. After SA degradation was permanently turned off on May 1st, 2000, the SPS accuracy has improved to 30 meters or less (2 dRMS). Although the improvement was significant, SPS and PPS still cannot support metre-to-millimetre level positioning and navigation applications, such as geodetic survey, precise farming, and aircraft landing.

Fortunately, the GPS system can do much more than just SPS and PPS. After over 20 years of development with the participation of scientists from all around the world, GPS has matured into a technology that goes far beyond its original design goals. The key breakthrough has been the development of Differential GPS (DGPS).

DGPS is an advanced positioning technique, in which reference station(s) with precisely known coordinates are required in order for rover receivers to achieve high accuracy. It can provide accuracy ranging from couple of meters to several millimetres, dependent on the receiver equipment and the type of GPS measurements used [Abousalem, 1996]. It is built on the fact that major GPS error sources are spatially correlated and can be fully or partially removed by observation differencing techniques. Since it was first applied, DGPS has received widespread acceptance for applications with high accuracy needs, but at the same time it continues to be hindered by the requirement of including data from at least one reference station, which makes the implementation of such a system costly. Another disadvantage of DGPS is that the obtainable accuracy degrades with the growing distance between the reference station and the rover receiver as spatial correlation weakens. As a

result, researchers have started to look for new positioning techniques that could offer globally consistent high precision positioning accuracy without using reference stations.

The recent development of Precise GPS data and the advances in building dual-frequency receivers brings about the concept of Precise Point Positioning (PPP). Precise GPS data includes precise ephemeris and satellite clock corrections, and atmospheric corrections, currently available from various organizations including the International GPS Service (IGS) and Natural Resources of Canada (NRCan). Ever since its introduction, PPP has shown its potential to become a high precision positioning technology. Several developments on PPP model construction have been made. Some milestone research includes metre accurate positioning based on the less accurate GPS code measurements [Lachapelle, 1995], and centimetre accurate positioning based on the phase observations with the PPP Traditional Model [Kouba, 2000; Muellerschoen, 2001]. The latter research has attracted much attention from the GPS community as it shows single-receiver positioning approach can achieve a positioning accuracy of centimetre level similar to conventional DGPS, which was once considered impossible. In the implementation of the PPP Traditional Model, both code and phase observations from a dual-frequency receiver are used as basic observables to generate the ionosphere-free code and phase combinations.

The PPP Traditional Model is easy to implement but has some disadvantages. First, the ambiguity term in the model is a non-linear single combined unknown consisting of both L1 and L2 carrier phase ambiguities. As a result, only a float solution can be obtained since this combined term does not preserve the integer characteristics of the carrier phase ambiguity.

Ambiguity resolution algorithm cannot be implemented based on the traditional model. Second, the measurement noise in the Traditional Model grows three-fold as compared to the corresponding original measurement noise. Third, the traditional ionosphere-free combination cannot remove higher-order ionospheric effects, resulting in greater error residuals. With the Traditional Model, more than 30 minutes are required before a converged position solution can be obtained in a post-processing static mode. The convergence of the ambiguity parameters as well as the position parameters is usually a function of the number of unknowns to be estimated and the combined level of the measurement noise and unmodeled errors. Given a specific amount of information, having fewer unknowns can cause more information to be assigned to each unknown and result in faster convergence. Similarly, a lower measurement noise level can bring about faster convergence to parameter estimation in the early stage of processing and more stable results thereafter. To reduce the required convergence time, fewer unknowns and/or a lower measurement noise level are desired, and observation models that allow for integer ambiguity resolution should be developed.

## 1.2 Objective

The main focus of this research is to investigate the existing model and develop a new observation model for Precise Point Positioning. With the aim of reducing the ambiguity convergence time, the new observation model should have a lower measurement noise level

and allow for the exploitation of the integer property of the carrier phase ambiguities. In order to do this, several research tasks have been set up:

- Analyze the performance of the existing PPP Traditional Model in terms of model stability, achievable accuracy and required convergence time;
- Develop new PPP observation models, compare their pros and cons, analyze their performance, and determine the best one for PPP processing. Research will be concentrated on models that feature smaller noise level and error residuals, and at the same time allow for the implementation of the fixed ambiguity resolution algorithms to reduce the number of unknowns;
- Explore the fixed ambiguity resolution and the related ambiguity fixing criteria. Generate both float and fixed solution results, make comparisons and give conclusions;
- Investigate methods for the precise determination of the stochastic model to facilitate optimal parameter estimations. This stochastic modelling includes two parts: the observations' precision described by standard deviation, and parameters' variance and covariance information.

## 1.3 Thesis Outline

This thesis is organized as follows:

Chapter 2 gives a brief background of the GPS system, including the main system components and the GPS positioning concept. Three basic observables including code, phase and phase rate measurements are described as well as the major GPS error sources and ways to mitigate them.

Chapter 3 introduces the concept of Precise Point Positioning, whose implementation is similar to SPP but its accuracy is significantly improved with the use of precise GPS data. Also discussed in this chapter is the history for the development of precise GPS data generation and its wide variety of products. One PPP processing method, the Traditional Model, is also examined.

A new PPP processing model, called P1-P2-CP Model, is investigated in Chapter 4. The P1-P2-CP Model, based on a new code-phase combination and the traditional ionosphere-free phase observations, has several important features for PPP processing and will be discussed in detail.

In Chapter 5, the positioning results from two PPP processing methods in a static processing mode are presented. Results are analysed in terms of model stability, estimation accuracy, and time of convergence, followed by the fixed solutions results and their analysis.

Chapter 6 presents the numerical results of the PPP kinematics processing using the P1-P2-CP Model. Analyses are made in terms of convergence time and converged positioning accuracy.

Finally, Chapter 7 summarizes the conclusions and recommendations obtained from this research.

# CHAPTER 2

# GPS AND ITS ERROR SOURCES

GPS is affected by different error sources, which limit its performance. Achievable accuracy of different GPS positioning techniques greatly depends on the presence of these errors. This chapter first presents the background information of the GPS system, and then describes the three basic GPS observables. Finally, the error sources and the techniques used to mitigate their effects are introduced.

## 2.1 Global Positioning System

GPS is a satellite-based, all weather, line-of-sight radio navigation and positioning system funded and controlled by the U.S. Department of Defence (DoD). It is nominally formed from a constellation of 24 satellites and their ground stations. There are six orbital planes (nominally with four satellites in each), equally spaced (60 degrees apart), and inclined at about fifty-five degrees with respect to the equatorial plane. This constellation provides the user with between five and eight satellites visible from any point on the Earth. The number of visible satellites may be larger if more satellites are deployed into the orbit.

The GPS Satellites continuously transmit microwave carrier signals on two frequencies: the L1 at 1575.42 MHz, and the L2 at 1227.60 MHz. These signals are modulated with one or two pseudorandom noise (PRN) sequences known as the C/A code and the P code. The chipping frequencies of these signals are 1.023 MHz for C/A code and 10.23 MHz for P code, corresponding to wavelengths of 300 m and 30 m, respectively. The L1 carrier is modulated by both the C/A code and the P code while the L2 carrier is only modulated by the P code. Both C/A code and P code allow determination of the time and position, but with different precisions. The C/A code is unrestricted and used for the Standard Positioning Services (SPS) where a single point positioning accuracy of about 30 m (2 dRMS) can be achieved. P code supports Precise Positioning Services, which is only open to authorized users with a positioning accuracy of about 10 m (2 dRMS). The Navigation message also modulates the L1-C/A code signal. It is a 50 Hz signal consisting of data bits that describe the GPS satellite orbits, clock corrections, and other system parameters.

The concept of positioning with GPS is based on simultaneous ranging to at least four GPS satellites (see Figure 2.1). With the known satellites coordinates acquired from the broadcast ephemerides data in the navigation message, the four dimensional coordinates of the receiver position: 3 spatial parameters X, Y, Z, and the receiver clock error (or offset) $\delta$ T with respect to GPS time, can be determined.

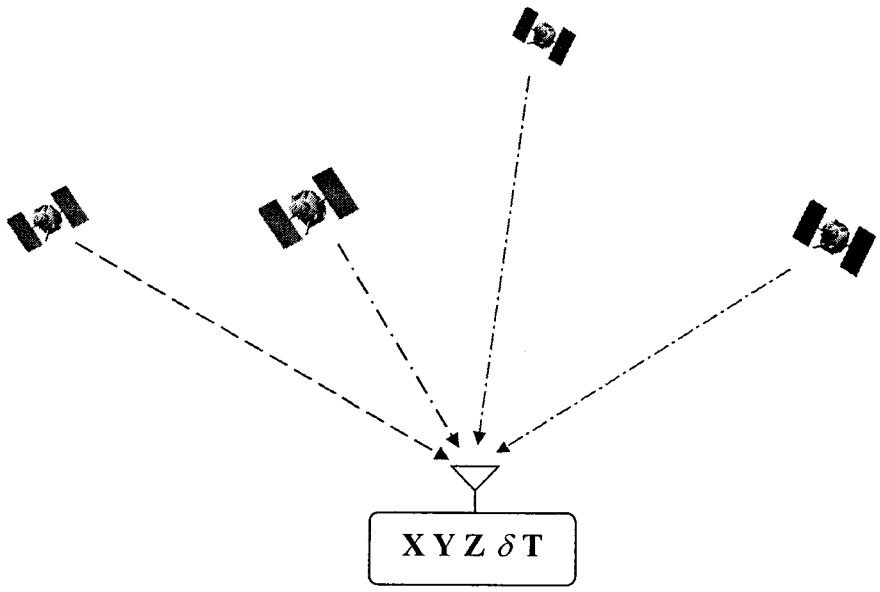


**Figure 2.1 Concept of GPS Positioning**

## 2.2 GPS Observables

There are three basic GPS observables: code, phase, and phase rate. With a dual-frequency GPS receiver, these observables on L1 and L2 between a GPS receiver and a GPS satellite can be described by the following equations [Teunissen, 1998]:

$$P(Li) = \rho + c(dt - dT) + d_{orb} + d_{trop} + d_{ion/Li} + d_{mult/P(Li)} + \varepsilon(P(Li)) \tag{2.1}$$

$$\begin{aligned}\Phi(Li) = {} & \rho + c(dt - dT) + d_{orb} + d_{trop} - d_{ion/Li} + \lambda_i N_i + \lambda_i(\phi_r(t_0, Li) - \phi_s(t_0, Li)) \\ & + d_{mult/\Phi(Li)} + \varepsilon\,(\Phi(Li))\end{aligned} \tag{2.2}$$

$$\dot{\Phi}(Li) = \dot{\rho} + c(\dot{dt} - \dot{dT}) + \dot{d}_{orb} + \dot{d}_{trop} - \dot{d}_{ion/Li} + \dot{d}_{mult/\Phi(Li)} + \dot{\varepsilon}\ (\Phi(Li)) \qquad (2.3)$$

where,

$P(Li)$ is the measured pseudorange on Li (m);

$\Phi(Li)$ is the measured carrier phase on Li (m);

$\dot{\Phi}(Li)$ is the measured carrier phase rate (Doppler) on Li (m/s),

$\rho$ is the true geometric range (m);

$c$ is the speed of light (m/s);

$dt$ is the satellite clock error (s);

$dT$ is the receiver clock error (s);

$d_{orb}$ is the satellite orbit error (m);

$d_{trop}$ is the tropospheric delay (m);

$d_{ion/Li}$ is the ionospheric delay on Li (m);

$\lambda_i$ is the wavelength on Li (m/cycle);

$N_i$ is the integer phase ambiguity on Li (cycle);

$\phi_r(t_0, Li)$ is the initial phase of the receiver oscillator (cycle);

$\phi_s(t_0, Li)$ is the initial phase of the satellite oscillator (cycle);

$d_{mult/P(Li)}$ is the multipath effect in the measured pseudorange on Li (m);

$d_{mult/\Phi(Li)}$ is the multipath effect in the measured carrier phase on Li (m);

$\varepsilon(.)$ is the measurement noise (m), and

$(\dot{d})$ is the derivative with respect to time.

The non-zero initial phase $\lambda_i(\phi_r(t_0, Li) - \phi_s(t_0, Li))$ in Equation (2.2) is a constant value for an observed cycle-slip-free satellite arc but is different among observed satellites during a session. Always less than one full cycle of the wavelength, this term is often merged into the integer ambiguity term $\lambda_i N_i$. In this case, Equation (2.2) can be simplified as:

$$\Phi(Li) = \rho + c(dt - dT) + d_{orb} + d_{trop} - d_{ion/Li} + \lambda_i N_i + d_{mult/\Phi(Li)} + \varepsilon\ (\Phi(Li)) \qquad (2.4)$$

Therefore, the $N_i$ in Equation (2.4) is no longer an integer parameter [Teunissen, 1998]. In the case of double-differencing in satellites and receivers, the initial phase term can be removed, resulting in the integer ambiguity searching approach and the fixed solution.

Several error characteristics need to be pointed out for the observables described in Equations (2.1) through (2.4). First, orbit error, satellite clock error, tropospheric effect, and receiver clock error are frequency independent. The influence of each of these error sources is equal to the code and phase observables from the same satellite. Second, ionospheric effect is proportional to the inverse of the squared frequency. This effect is equal but with opposite sign to the code and phase observables on the same frequency. In other words, code is delayed and phase is advanced in the ionosphere. Third, the code noise, while generally less than 1% of the chipping rate (<3 m for C/A and < 0.3 m for P code), is much bigger than the phase noise which is approximately 2 mm or equivalent to 1% of the wavelength.

Due to the features described above, some useful combinations from dual-frequency GPS observations can be used for error removal or error separation. Two combinations, the traditional ionosphere-free combination and the ionosphere-free code-phase combination, will be presented in the following chapters as they are of interest in PPP processing. Discussions of other useful combinations are given in Appendix B.

## 2.3 GPS Error Sources

Equations (2.1) through (2.3) list several error sources, including the four frequency-independent terms $dt$, $dT$, $d_{orb}$, and $d_{trop}$, and one frequency-dependent term $d_{ion/Li}$. For all GPS applications, these errors are required to be eliminated or mitigated through the use of models or available corrections. The following content discusses the effects of these errors sources and their mitigations, plus noise and multipath, which can only be modeled through a stochastic approach.

### 2.3.1 Satellite Orbit Error

The satellite orbit error is the discrepancy between the true position (and velocity) of a satellite and its known value. This discrepancy can be parameterised in a number of ways. One common way is via the three orbit components: along-track, cross-track and radial. The following comments can be made with regard to the effects of the satellite orbit error on GPS positioning [Rizos, 1999]:

- Height is a relatively weakly determined component, mainly because there are no satellites below the horizon.

- The East-West (longitude) component is slightly weaker than the North-South (latitude) component because of the motion of satellites (particularly in equatorial regions.

- Effect on point positioning can be expressed by the following equation:

  Position error = PDOP * Orbit error (2.5)

There are two basic classes of satellite orbit information:

- Ephemerides that are predicted from past tracking information, and are available to GPS users at the time of observation, and

- Post-processed ephemerides, which are orbit representations valid only for the time interval covered by the tracking data. Obviously this information is not available real-time as there is a delay between collection of the data, transmission of the data to the computer centre, the orbit determination process and the subsequent distribution to GPS users.

The predicted class of information is available via the GPS Navigation Message. Evidence suggests that the accuracy of the broadcast ephemerides is below 10m for a single Navigation Message update per day, and better than 5m when three daily updates are performed [Hofmann-Wellenhof et al, 1998].

Post-processed ephemerides, which come in several forms, are more accurate than predicted ephemerides, with demonstrated accuracies well below the metre level to several centimetres, and will be discussed in detail in the section of Precise GPS Data of the next chapter.

### 2.3.2 Satellite Clock Error

The GPS satellite clock error is described by clock bias, drift, and drift-rate as clock error coefficients broadcast in the navigation message. What is available to users is actually a prediction of the clock behaviour for some time into the future (24 hours or more ahead). As the random deviations of even cesium and rubidium oscillators are not predictable, such deterministic models of satellite clock error are accurate to about 20 nanoseconds, or 6 metres in equivalent range, depending upon the time since the last Navigation Message update.

Two receivers watching the same satellite observe exactly the same satellite clock error, therefore, differential GPS between receivers can completely eliminate this error source. In single point positioning (SPP), the application of precise clock corrections (provided by IGS and other organizations) instead of the broadcast message will minimize the effect of satellite clock errors. Precise clock correction products will be discussed in detail in the section of Precise GPS Data of the next chapter.

### 2.3.3 Ionospheric Effect

The ionosphere is the band of atmosphere extending from about 50 to 1000 kilometres above the Earth's surface. In this layer the sun's ultraviolet radiation ionises gas molecules which then lose an electron. These free electrons in the ionosphere influence the propagation of microwave signals (speed, direction and polarisation) as they pass through the layer. The largest effect is on the speed of the signal, and hence the ionosphere primarily affects the measured range.

The refractive index of microwaves is a function of frequency (and hence the ionosphere has the property of "dispersion") and the density of free electrons, and may be expressed, to a first-order approximation, by [Seeber, 1993; Hofmann-Wellenhof et al, 1998]:

$$n = 1 \pm \frac{A \cdot N_e}{f^2} \tag{2.6}$$

where,

A is a constant,

$N_e$ is the total electron density (TEC) (el/m3), and

$f$ is the frequency.

The sign depends on whether the range (+) or the phase (–) refractive index is required. The propagation speed $v$ is related to the refractive index according to:

$$v = \frac{c}{n} \tag{2.7}$$

where $c$ is the speed of electromagnetic radiation (EMR) in a vacuum.

The above two equations imply that the speed of the carrier wave (the "phase velocity") is actually increased, or "advanced", hence the phase refractive index is less than unity. However, the speed of the ranging codes (the so-called "group velocity", as the ranging codes modulated on the carrier waves are considered a "group" of waves because they have different frequencies) is decreased, and therefore the pseudo-range is considered "delayed", and hence the range (or group) refractive index is greater than unity.

The implication is therefore that the distance as implied by the integrated carrier phase is too short, but the pseudo-range is too long. The correction terms are, of course, quantities with a reversed sign, that is, the carrier phase correction is positive, while the pseudo-range correction is negative.

The expression for the ionospheric group delay $d_{ion/Li}$ (in units of metres) and the ionospheric phase delay $\phi_{ion/Li}$ (in the unit of cycle) for a microwave propagating from a satellite to the ground can then be described as:

$$d_{ion/Li} = -\phi_{ion/Li} \cdot \frac{c}{f_{Li}} \approx 40.28 \cdot \frac{STEC}{f_{Li}^2} \approx \frac{40.28}{\sin E} \cdot \frac{VTEC}{f^2} \tag{2.8}$$

where,

$E$ is the elevation angle,

*STEC* is the Slant Total Electron Content, expressed as the number of free electrons per square metre ($el/m^2$), and

*VTEC* is the Vertical Total Electron Content (zenith direction) ($el/m^2$).

The range of observed TEC is from about $10^{16}$ to $10^{19}$ $el/m^2$. The maximum value of vertical range bias caused by the ionosphere is about 30m on L1 observations, and about 50m on L2 observations. The effect on pseudo-range point positioning can therefore be quite severe. To aid single receiver navigation users, a crude predicted ionospheric correction model is included within the transmitted Navigation Message. However, this model can only reduce the RMS of the measurements (comparing observation residuals after solution, with and without including the ionospheric model correction) by approximately 50% [Rizos, 1999].

In precise point positioning, the ionosphere-free observation combinations are usually applied. In the case where only a single frequency receiver is used, the localized ionospheric corrections from thin-shell grid model parameters available from IGS or other organizations have to be applied in order to enjoy high quality of precise satellite orbit and clock correction data. Grid modelling is carried out by a wide-area network of reference stations. Based on the information collected in these stations, the variation of ionospheric effects or total electron contents (TEC) for the large area can be approximately mapped, and a vertical delay value is given to each grid point with constant latitude and longitude intervals. The ionospheric correction related to the location of the receiver is a result of an interpolation process within the correction grid done by the receiver. The receiver knows the satellite positions (elevation angle, azimuth) from the Navigation Message, it calculates the pierce points of the single

path on the ionospheric shell and interpolates delay values to these points (see Figure 2.2). One example of grid model is made by University of Berne, Switzerland, which uses more than 80 stations dotted globally to calculate the electron density of a 5×2.5 grid in every two hours. NRCan has also been working on the implementation of its own grid model based on the country's CACS network.

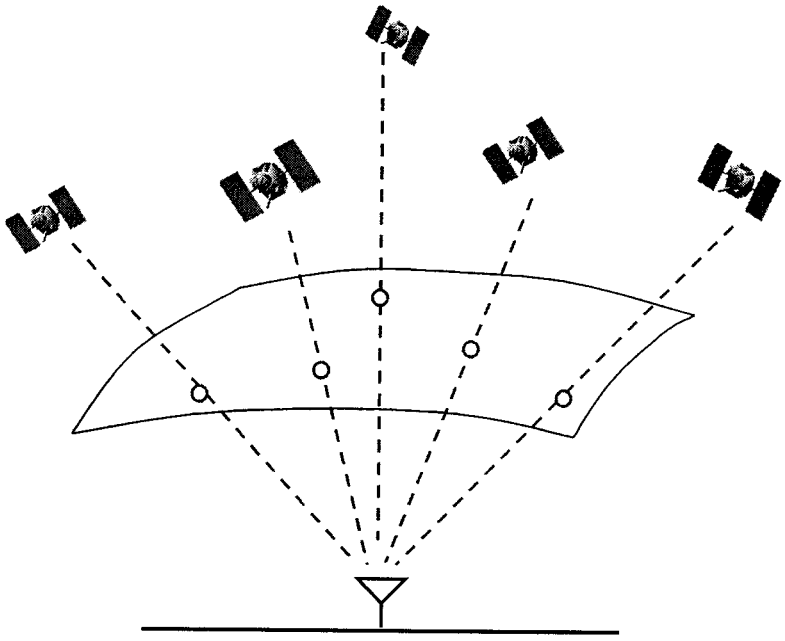

**Figure 2.2 Thin Shell Ionospheric Grid Model**

### 2.3.4 Tropospheric Delay

Tropospheric delay is an error source that is difficult to be totally eliminated because it is not only a function of the satellite elevation angle and the altitude of the receiver, but also dependent on the atmospheric pressure, temperature, and water vapour pressure. The tropospheric delay can be partitioned into two components, one for the dry (hydrostatic) part of the atmosphere and the other for the wet part:

$$d_{trop} = d_{dry} + d_{wet} \tag{2.9}$$

About 90% of the magnitude of the tropospheric delay arises from the dry component, and the remaining 10% from the wet component [Parkinson and Spilker, 1996]. The wet component is much more difficult to model because of the strong variations in the distribution of atmospheric water vapour in space and over time.

The Hopfield Model is the one most commonly used for the estimation of tropospheric effect. This model calculates the zenith path delay according to the receiver location and standard meteorological data or surface meteorological readings. The zenith path delay is then scaled by an appropriate mapping function to any arbitrary elevation angle. The equation can be expressed as follows.

$$d_{trop} = d^{z}_{dry} \cdot m_{dry} + d^{z}_{wet} \cdot m_{wet} \tag{2.10}$$

where,

$d^z_{dry}, d^z_{wet}$ are dry and wet components for zenith path delay respectively, and

$m_{dry}, m_{wet}$ are appropriate mapping functions for dry and wet components.

Most available troposphere modeling methods perform well in the modeling of the zenith dry tropospheric delay, but are unable to model the wet delay in a precise way. For example, the zenith dry tropospheric delay at sea level is of the order of 2.3m. The zenith wet tropospheric delay, however, may vary from a few millimetres to as much as 40cm. The variability of the dry component is relatively low and can be estimated with a precision approaching 1% when pressure is known (to mm accuracy). On the other hand, the wet component of the delay is notoriously difficult to estimate and errors of 10-20% are common [Rizos, 1999].

Since the residual of the wet zenith troposphere delay could be significant after the use of a tropospheric correction model, it can be treated as an unknown parameter to be estimated along with position, and receiver clock offset parameter. This tropospheric unknown has been implemented in some PPP processing [Kouba and Héroux, 2000; Gao and Shen, 2001].

Tropospheric estimation can only give the precise zenith path delay. For each observed satellite, the slant tropospheric delay equals to the value of zenith path delay scaled by the deterministic mapping function, which cannot reflect the real complicated atmospheric variation. When scaled by the total zenith delay, the error on the range could come to approximately 50 mm at 10-degree elevation with most of the existing models, and there is also no way to predict the wet delay correction change with the azimuth [Janes, 1991; Parkinson, B.W., Spilker, J.J., 1996].

### 2.3.5 Receiver Clock Offset

GPS receivers are usually equipped with quartz crystal oscillators, which have the advantages that they are small, consume little power and are relatively inexpensive. In addition, quartz crystal oscillators have good short-term frequency (or time-keeping) stability.

The clock offset, usually in the range of several thousands of nanoseconds with regard to the GPS time, is treated as unknown parameter together with the three coordinate components. Another approach to remove the receiver clock error is via observation differencing between satellites.

### 2.3.6 Measurement Noise

With the measurement of pseudorange and phase comes a noise component associated with the receiver itself. It arises primarily from limitations of receiver electronics. It is a result of thermal noise intercepted by the antenna, noise from the receiver oscillator and other hardware components. Fortunately, the receiver noise tends to be small in magnitude, uncorrelated between measurements, and can be well modelled by a Gaussian distribution. Code tracking errors vary considerably between GPS receiver models, but are generally in the range of 0.03 to 1.0% of the C/A code chip length, or 0.1 m to 3 m. The L1 carrier phase noise is generally less than 0.3 cm. The effect of this error source can be mitigated using state-of-the-art equipment, especially at the reference stations in a GPS network.

### 2.3.7 Multipath

The carrier wave propagates along an almost straight line even though there are small bending effects due to the presence of the atmosphere. Multipath is caused by extraneous reflections from nearby metallic objects, ground or water surfaces reaching the antenna. This has a number of effects: it may cause signal interference between the direct and reflected signal leading to noisier measurement, or it may confuse the tracking electronics of the hardware resulting in a biased measurement that is the sum of the satellite-to-reflector distance and the reflector-to-antenna distance [Rizos, 1999].

The theoretical maximum multipath bias that can occur in pseudo-range data is approximately half the code chip length or 150m for C/A code ranges and 15m for P(Y) code ranges. Typical errors are much lower (generally < 10m). The carrier phase multipath does not exceed about one-quarter of the wavelength – 5~6cm for L1 and L2. Some options for reducing the multipath effect are:

- to make a careful selection of antenna site in order to avoid reflective environments;
- to use a good quality antenna that is multipath-resistant;
- to use an antenna ground plane or choke-ring assembly;
- to use a receiver that can internally digitally filter out the effect of multipath signal disturbance;

- not to observe low elevation satellites whose signals are more susceptible to multipath;
- in the case of pseudo-range positioning (single point or differential), to average the computed results over a period of time in order to reduce the contribution of multipath errors on the averaged pseudo-range solution.

In order to compare the discussed error sources and their different effects to the GPS system, Table 2.1 summarizes their error budgets and ways of mitigations.

**Table 2.1 Summary of GPS Major Error Sources**

| Errors | Error Budget* [Parkinson, 1996] | Ways of Mitigations |
|---|---|---|
| Satellite orbit | 2.1 m | Navigation Message; DGPS; Precise GPS data |
| Satellite clock | 2.1 m | Navigation Message; Differencing between receivers; Precise GPS data |
| Troposphere | 0.7 m | Troposphere model; DGPS; estimated as an unknown |
| Ionosphere | 4.0 m | Ionosphere model; Precise GPS data; DGPS; ionosphere-free combination from dual-frequency receivers |
| Receiver Noise | 0.5 m | Modelled by a Gaussian distribution; use high-end GPS receivers |
| Multipath | 1.4 m | Modelled by a Gaussian distribution as receiver noise; Multipath-friendly site; multipath-resistant antenna; high quality GPS receiver |

* The error budget shows the one-sigma error after applying the standard error model, which is the first option in the column "Ways of Mitigations".

# CHAPTER 3

# PRECISE POINT POSITIONING

Precise Point Positioning (PPP) has the same user's implementation with only a single GPS receiver as Single Point Positioning, but its accuracy can be significantly improved with the use of the globally or regionally distributed precise GPS data, which currently includes precise satellite orbit and clock corrections. The major advantages of PPP lie in two aspects: system simplicity at the user's end, and a globally consistent positioning accuracy.

The purpose of this chapter is to present the PPP concept, the development of precise orbit and clock products, followed by the PPP Traditional Method built on GPS dual-frequency observations.

## 3.1 Concept of PPP

The PPP goal is to obtain an accurate coordinate solution with a single GPS receiver. For over a decade, such accurate positioning has been achieved by operating in differential positioning mode with respect to one or multiple reference stations, or processing double-difference carrier phase observations in a baseline or network estimation approach, a relative mode. Relative and differential processing modes have received widespread acceptance but

continue to be hindered by the requirement of including data from at least one, often distant, reference station.

Fortunately, the advent of precise GPS data from IGS and several other organizations has brought about the concept of PPP to single-receiver users, allowing them to achieve comparable DGPS accuracy in certain cases.

For less than a decade of development, many progresses have been made on the PPP model construction and versatility of PPP products. The early research included the PPP metre accurate positioning based on the less accurate GPS code measurements [Lachapelle, 1995]. But the metre level obviously couldn't reflect the PPP high accuracy potential. Kouba and Héroux (2000) described a post-processing approach using IGS final precise orbit/clock products in 2000. Their model applies the dual-frequency pseudorange and carrier phase observations from a single GPS receiver to estimate station coordinates, the tropospheric zenith path delay, and receiver clock offset. The results have shown centimetre global positioning accuracy is achievable with the most accurate precise GPS data. Muellerschoen et al. (2001) have generated similar results in a similar model construction to Kouba's. Gao and Shen (2001) developed a new PPP processing method and obtained slightly better post-processing results. However, the big gain of this new method is the concept of ambiguity pseudo-fixing, which is able to accelerate positioning convergence to only a few minutes with 3~4 decimetres accuracy.

The PPP research has attracted much attention from the GPS community as it shows a single receiver can achieve comparable DGPS accuracy, a feat once considered impossible. As

precise GPS orbit and clock products continue to improve in precision and timeliness, and real-time phase-based wide-area/global ionospheric corrections become available, PPP for real-time decimetre to centimetre positioning and navigation will become possible in the near future for single-frequency GPS receiver users.

## 3.2 Precise GPS Data

Precise GPS data includes satellite ephemerides (GPS orbits) data, satellite clock data, and atmospheric effects (troposphere and ionosphere). Satellite orbit data are either in a form of coordinate corrections to the broadcast ephemeris in real-time or precise satellite three-dimensional Cartesian coordinates in post-processing. As well, satellite clock data can be either corrections to the broadcast satellite clock offsets or the absolute corrections to the GPS time. Atmospheric data are more complicated as the effects are location dependent. Usually, a grid-model is used where the corrections on the grid points with one-degree separation along the latitude and longitude are estimated, then users can calculate their localized corrections according to the surrounding four closest grid points [Abousalem, 1996].

In this section, the development of satellite orbit and clock products are discussed and some examples of networks and their products are presented.

### 3.2.1 Generating Precise GPS Data

Precise GPS data is estimated through a globally scaled network of carefully chosen reference stations, whose coordinates are precisely predetermined. Reference stations are usually a few thousand kilometres apart. Basically, such a system is made up of five components [Abousalem, 1996]:

- A Network of Reference Stations (RSs)
- Master Station(s) (MSs)
- Integrity Monitor Station(s) (IMSs)
- User Segment
- Communications Links

Reference stations are equipped with high-performance dual-frequency GPS receivers and communication devices, where code and carrier phase observations are collected and transmitted in real-time to the Master Station(s) via terrestrial communication links (usually leased telephone line) or satellite link. Then the Master Station(s) conduct computations with sophisticated algorithms to generate the precise satellite coordinates, precise satellite clock offset, and atmospheric parameters. Finally, the precise data is broadcast to users via geo-stationary communication satellites or wireless Internet. Integrity Monitor Station(s) check system integrity by simulating network users. If for any reason, an IMS detects intolerable system performance (e.g., latency of received corrections exceeds tolerance, position solution becomes worse than tolerance), then the system would alert users not to apply corrections.

In some cases, Virtual Reference Stations (VRSs) are also part of the system. The VRSs behave as reference stations but no GPS receiver is equipped on site. All they have are a communication equipment and a computing system where the precise data are received and localized into one set of pseudorange corrections which is then broadcasted for the users in the vicinity area via a terrestrial radio link (e.g., FM-subcarrier). Strictly speaking, these VRSs act as the radio beacon stations in conventional DGPS.

Currently, there are several GPS networks either in operation or under development. FAA's WAAS is a free DGPS service system designed primarily for airplane navigation and landing in the continental U.S and it is expected to be fully operational in 2003. The positioning accuracy with WAAS corrections is at the meter level. OmniSTAR and LandStar are two commercial services with reference stations covering many parts of the world. The positioning accuracy with their broadcast precise GPS data is similar to WAAS system focusing on meter level positioning service.

### 3.2.2 IGS Network and Products

The International GPS Service (IGS) is another large contributor towards the development of precise GPS data. After more than a decade of deployment through international collaborative efforts, IGS has established a global GPS reference network of 294 continuously operating dual-frequency GPS stations as of March 2002, with more than a dozen regional and operational data centres, three global data centres, seven analysis centres and a number of associate or regional analysis centres (see Figure 3.1). Through these global

stations, IGS collects, archives, and distributes GPS observation data sets of sufficient accuracy to meet the objectives of a wide range of scientific and engineering applications and studies. These data sets are used to generate the following major precise GPS products [http://igscb.jpl.nasa.gov]:

- GPS satellite ephemerides,
- Earth rotation parameters,
- IGS tracking station coordinates and velocities,
- GPS satellite and IGS tracking station clock information, and
- Zenith path delay estimates.

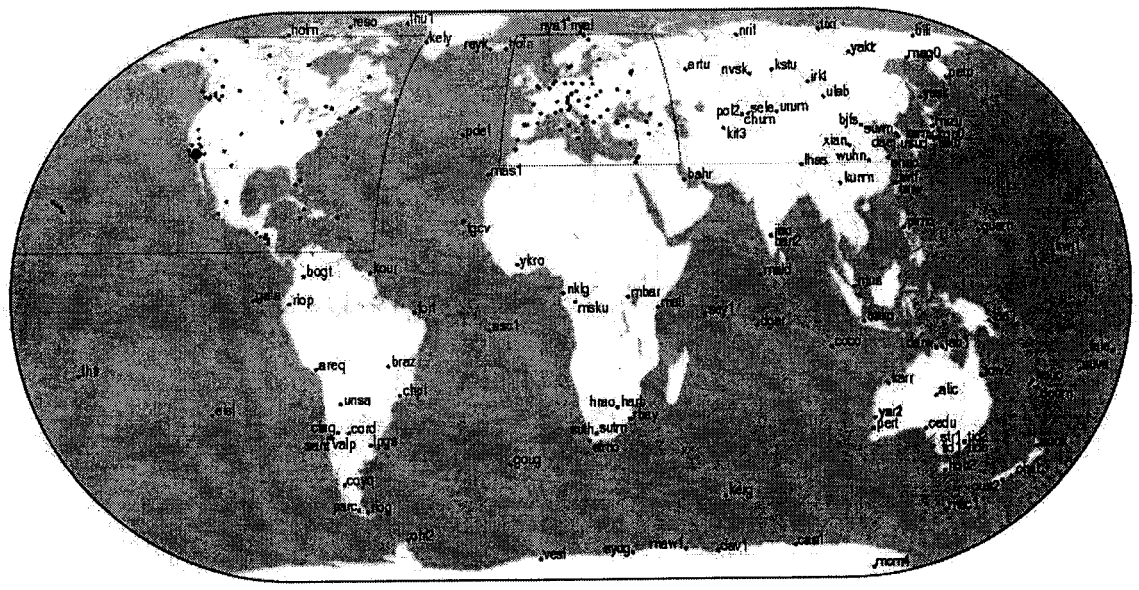


**Figure 3.1 IGS Reference Network [http://igscb.jpl.nasa.gov/network/map.html]**

Table 3.1 demonstrates the characteristics of different IGS precise satellite orbit and clock products with respect to different levels of time delays. These products have the potential to support SPP positioning accuracy ranging from meter level in real-time to a few centimetres in post-processing.

**Table 3.1 IGS Product of GPS Satellite Ephemerides/Satellite & Station Clocks**
[http://igscb.jpl.nasa.gov/components/prods.html]

| Product type | Accuracy | Latency | Updates | Sample Interval |
|---|---|---|---|---|
| Broadcast | ~260 cm/~7 ns | real time | -- | daily |
| Predicted (Ultra-Rapid) | ~25 cm/~5 ns | real time | twice daily | 15 min/15 min |
| Rapid | 5 cm/0.2 ns | 17 hours | daily | 15 min/5 min |
| Final | <5 cm/0.1 ns | ~13 days | weekly | 15 min/5 min |

The accuracy of IGS products suggested in the above table is based on comparisons with independent laser ranging results. The precision of Rapid and Final orbits is better. The precision of IGS Rapid and Final clocks are relative to the IGS timescale, which is linearly aligned to GPS time in one-day segments. The Broadcast and Ultra-rapid clocks refer only to the GPS satellites.

An additional aspect of IGS products is for the densification of the International Terrestrial Reference Frame (ITRF) at a more regional level. This is accomplished by some Analysis Centres (ACs) through the rigorous combination of regional or local network solutions utilizing the Solution Independent Exchange Format (SINEX) and a process defined in the

densification section. One example of such a kind is Canadian Active Control System (CACS).

### 3.2.3 CACS Network and Products

CACS is operated by the Geodetic Survey Division of Geomatics Canada, in partnership with Geological Survey of Canada. CACS network is composed of 12-station Active Control Points (ACPs) around Canada (see Figure 3.2). Each of these control stations is equipped with a dual frequency GPS receiver and an atomic frequency standard. The data of ACPs are transmitted to the Master Active Control Station (MACS) in Ottawa, where different forms of precise GPS data are calculated and finalized, which are:

- CACS final product for post-processing in the SP3 format for ephemeris and 30s format for satellite clock,
- CACS rapid product for post-processing in the SP3 format for ephemeris and 30s format for satellite clock, and
- CACS wide-area real-time DGPS corrections.

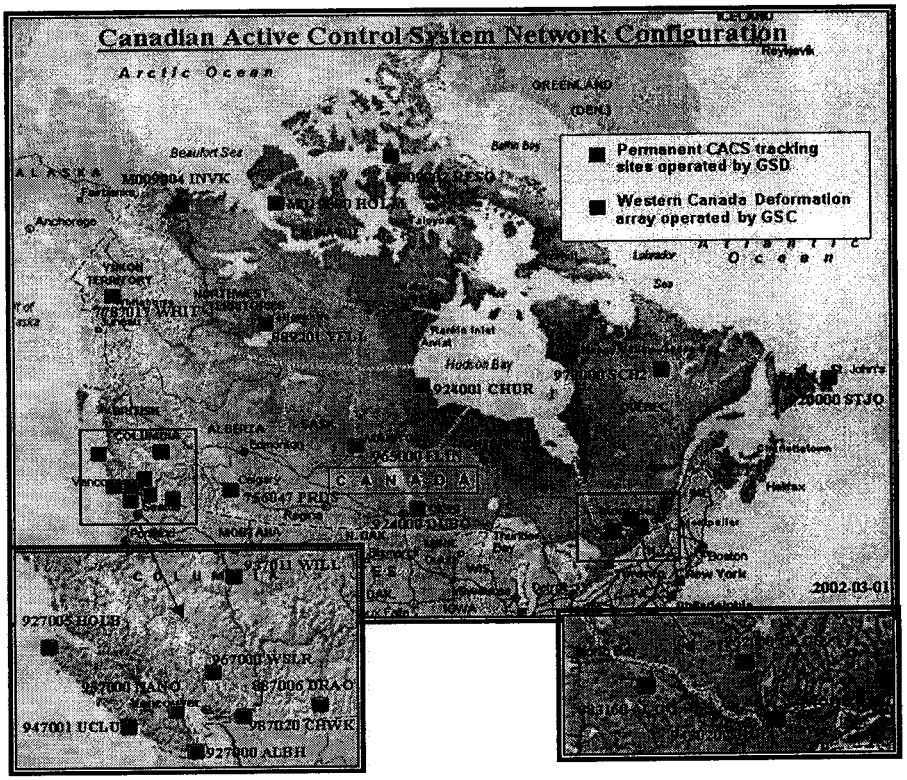


**Figure 3.2 Canada-wide CACS Network**
**[http://www.geod.nrcan.gc.ca/index_e/products_e/activeNetwork_e/acp_e.html]**

The CACS final GPS satellite ephemerides are computed from the data collected at the Canadian stations augmented by up to 24 globally distributed stations of the IGS network. They are available typically within 3 to 6 days following the observations. Based on IGS orbit comparisons, the CACS final GPS satellite ephemerides precision is better than 15 centimetres (one sigma) in each coordinate component. The rapid solution is computed at the end of the day using data available at the time. Normally data from 15 to 20 globally distributed stations are included in this solution and is available typically within 21 hours following the observations. Its accuracy is estimated at better than 30 cm (one sigma) in each

coordinate component. This degradation over the final solution in general has minor impact on the positioning accuracy for most GPS users. GPS satellite ephemerides are provided as daily files (0:00 to 23:45 GPS Time) in the internationally accepted NGS-SP3 format which contains X, Y, Z satellite positions and clock corrections at 15-minute intervals. They are available in the NAD83 (CSRS) reference frame as well as in the ITRF [http://www.geod.nrcan.gc.ca/site/index_e/products_e/cacs_e/eph_e/eph_e.html].

The CACS final GPS satellite clock corrections with respect to the CACS reference clock are computed from observational data and final GPS satellite ephemerides and are typically available 3 to 6 days after the observations. The clock corrections can be applied to pseudo-range (code) measurements from a single receiver and obtain positioning accuracy at the 1 metre level (depending on the GPS receiver characteristics). Rapid GPS satellite clock corrections are generated based on the CACS rapid orbit solution and made available typically within 21 hours after the end of the UT day. The GPS satellite clock corrections are archived in ASCII format at 30-second intervals and can be interpolated (e.g. 1-sec. data) without degrading positioning accuracies. They can be retrieved via the Canadian Spatial Reference System Database (CSRS_DB) for a full 24-hour period (0:00:00 to 23:59:30 GPS Time) or for one hour intervals [http://www.geod.nrcan.gc.ca/site/index_e/products_e/cacs_e /clock_e/clock_e.html].

Figure 3.3 shows the weighted orbit RMS of the IGS rapid and some AC final orbit solutions with respect to the IGS final orbit products (2000 IGS Annual Report, IGS Central Bureau). One can see that over the years from 1993 to 2000, the quality of the IGS Final orbits has

improved from about 30 cm to the 3-5 cm precision level currently realized by some of the AC's. However, over the period of 1997 to 2000, the improvement has started to become slower. This fact confirms the belief that increasing the number of global GPS tracking stations does not necessarily translate into higher orbit precision. Satellite clock estimates produced by different AC's agree within 0.1-0.2 nanoseconds RMS, or 3-6 cm, a level that is compatible with the orbit precision. The combination of precise GPS orbits and clocks weighted by their corresponding sigma is essential for PPP processing, given that the proper measurements are made at the user set and the observation models are correctly implemented.

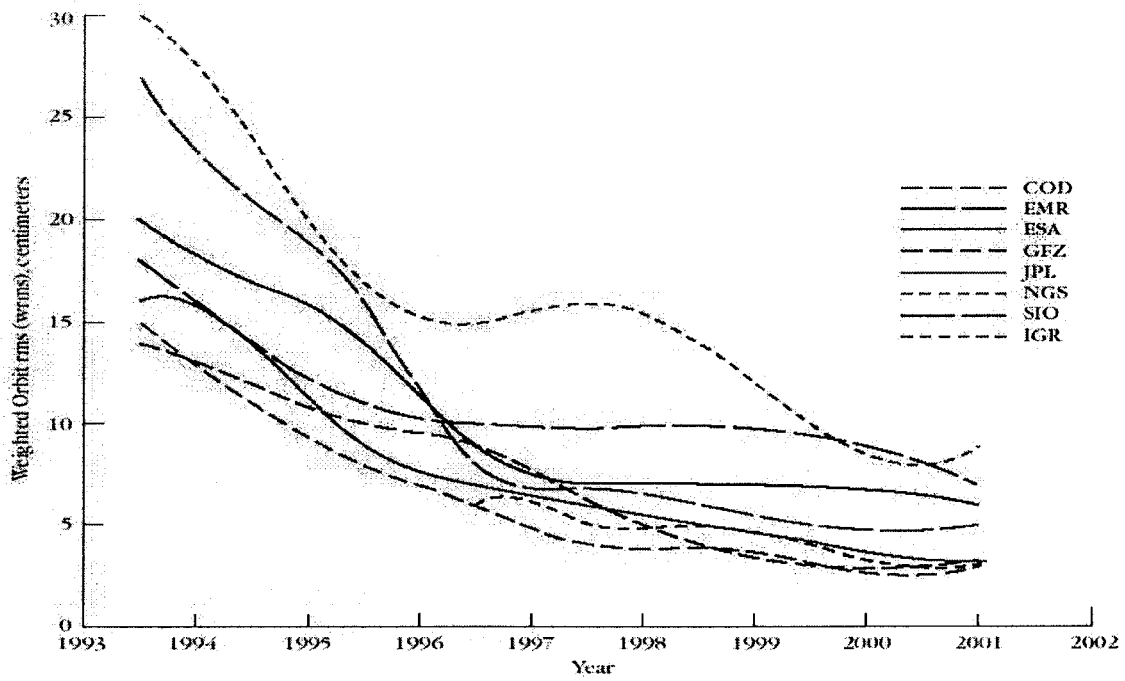


**Figure 3.3 Weighted Orbit RMS of IGS Rapid and AC Final Orbit Solutions**
(2000 IGS Annual Report, IGS Central Bureau)

CACS also supports Wide Area Differential GPS (WADGPS) development – Canadian Differential GPS (CDGPS) service – by initiating its own wide-area corrections, known as GPS·C for real-time applications. Currently GPS·C production system is reaching maturity in terms of robustness, and the CDGPS plans to distribute the real-time GPS·C corrections via the MSAT geo-stationary satellite by end of 2002. The CDGPS Service will develop the MSAT satellite distribution hub and radios required for GPS users to acquire the GPS·C corrections. The CDGPS radios will convert the corrections to the standard RTCM-104 serial format, which enables single-frequency pseudorange users to enhance their positioning precision. For the users equipped with dual-frequency receivers, CDGPS radios will also relay the GPS·C wide area corrections in the format defined in the GPS·C ICD, allowing the most demanding GPS·C users to achieve the highest possible accuracy.

Figure 3.4 shows position errors with GPS·C corrections over a 24-hour period using smoothed code observations on September 24, 2002 [Chen et al., 2002]. The 3D position errors, PDOP and satellite number values are also included. The basic observation is the ionosphere-free code combination from a high-end Rouge dual-frequency receiver. The RMS values for the whole day processing are 0.317 m, 0.097 m, 0.412 m for three coordinate components, indicating approximately 20 cm satellite orbit accuracy and 1 ns satellite clock for the real-time GPS·C corrections, which are much better than the accuracy values of the real-time products shown in Table 3.1.

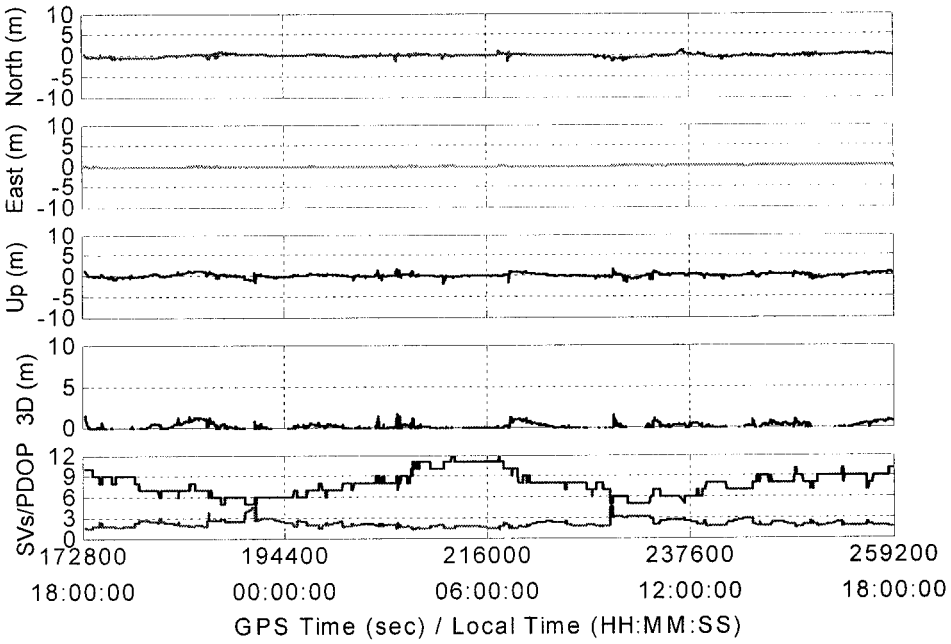


**Figure 3.4 Position Error with GPS·C Corrections [Chen et al., 2002]**

The availability of precise satellite ephemerides, precise satellite clock corrections and observational data from the ACPs offers significant benefits for Canadian users carrying out GPS surveys. These CACS products make it possible to position any point in Canada with a precision ranging from couple of centimetres to one metre in relation to the national spatial reference frame without actually occupying an existing control monument or base station [http://www.geod. nrcan.gc.ca /site/index_e/products_e/cacs_e/cacs_e.html].

## 3.3 More Error Considerations in PPP

Besides the error sources mentioned at section (2.3), another substantial error that has to be considered in PPP processing is the effects of special relativity. When computing satellite clock corrections from the broadcast coefficients, the effects of special relativity ($\Delta t_r$) have already taken into account as specified in GPS ICD-200 (http://www.spacecom.af.mil/usspace/gps_support/documents/ICD-GPS-200RC-004.pdf, p. 88). However, as relativistic effects are not counted in when generating precise clock corrections, such as SP3 satellite clocks, relativistic effects should be calculated and corrected into the pseudorange when using these products.

Besides relativistic effects, several other corrections need to be conducted to facilitate centimetre accuracy PPP positioning, which include [Kouba and Héroux, 2000]:

- Satellite Attitude Effect,
- Site Displacements Effect, and
- Compatibility Consideration.

### 3.3.1 Relativistic Effects

Relativity effects are so important to the GPS system that if they had not been applied, the whole system would have been useless. For a GPS user who is fixed at sea level on the Earth's surface, there are three primary consequences of relativity effects:

1) There is a fixed frequency offset in the satellite's clock rate when observed from Earth. Most of the effect is purposely removed by slightly offsetting the satellite clock in frequency prior to launch, the so-called "factory offset" of the clock.

2) The slight eccentricity of each satellite orbit causes an additional periodic clock error effect that varies with the satellite's position in its orbit plane. This additional effect is cancelled on the case of double differencing, while it would bring a maximum of 23ns for an eccentricity of .01 to single point positioning, an equivalent to 6.9 metres in distance.

3) There is also an effect – Sagnac effect – caused by the Earth's rotation during the time of transit of the satellite signal from satellite to ground. Dependent on the signal's trajectory, Sagnac effect cannot be removed in both double differencing and single point positioning.

Moving users on or near the Earth's surface or fixed users at an altitude above or below the geoid have additional relativistic effect caused by their velocity and height which is described by the Schwarzschild metric equation. This effect is usually merged into the receiver clock unknown.

***Special and General Relativity***

GPS signals exchanged by atomic clock at different altitudes are subject to general relativistic effects described by the Schwarzschild metric. Neglecting these effects would make the GPS useless.

The Schwarzschild metric describes space time on a stationary spherical shell. As the Earth rotates and is not perfectly spherical, strictly speaking, this expression does not describe space time above Earth's surface. But because Earth rotates slowly, the Schwarzschild metric is a good approximation for purposes of analyzing the GPS system. Under the assumption that the Earth is sphere and the satellites travel at constant radius around the Earth's centre, the Schwarzschild metric then has the following expression [Carroll O. Alley, 1983]:

$$d\tau^2 = \left(1 - \frac{2M}{r}\right)dt^2 - \frac{dr^2}{1 - \frac{2M}{r}} - r^2 d\phi^2 \tag{3.1}$$

where,

$d\tau$ is the time between ticks of a clock we intend for,

$M$ is the mass of the Earth,

$r$ is the radius of the clock around Earth's centre, and $dr = 0$ when assuming $r$ is constant,

$dt$ is a reference time, say, a standard clock at rest at infinity; or for GPS, a standard clock at rest on geoid,

$r \cdot d\phi / dt$ is the tangential velocity along the circular path of the same clock.

From the above equation, we see first that clocks run at different rates when they are at different distances form a centre of gravitational attraction. Second, clock rate is influenced by the speed of the moving clock. Therefore, both satellite motion and Earth rotation must be taken into account. Taking a closer look, we know "high clocks run fast and moving clocks

run slow." Imagine there are two clocks with the exact ticking time when manufactured in factory or more precisely when at rest on geoid: one is placed in the GPS satellite, the other on the ground, then the GPS satellite clock runs faster than the Earth clock by approximately 39,000 nanoseconds per day. That would cause 11.7 km in distance. Fortunately, most of this difference can be removed by implementing a frequency downward shift of clocks in orbit by 446.47 part of $10^{12}$ [Ashby, 1997]. This average frequency shift of clocks is a combination due to Earth's monopole and quadrupole moments, gravitational frequency shifts of the satellites clock, and second-order Doppler shifts from motion of satellite and Earth-fixed clocks.

However, as the satellite orbit is eccentric, an additional correction arises from a combination of varying gravitational and motional frequency shifts as the satellite's distance from Earth varies. This correction is periodic and is proportional to the orbit eccentricity. For an eccentricity of .01, the amplitude of this term is 23 ns [Ashby, 1997]. Due to a shortage of computer resources on satellites in the early days of GPS, it was decided that this additional correction was to be responsibility of software in GPS receivers. It is a correction that must be applied to the broadcast time of signal transmission, to obtain the coordinate time epoch of the transmission event in the ECI frame. This correction is calculated with the following dot (·) product expression [Parkinson and Ashby, 1996].

$$\Delta t_R = +\frac{2\boldsymbol{r}\cdot\boldsymbol{v}}{c^2} \tag{3.2}$$

where,

$r$ is the position of the satellite at the instant of transmission,

$v$ is the velocity of the satellite at the instant of transmission.

***Sagnac Delay***

Sagnac delay is caused by the Earth's rotation during the time of transit of the satellite signal to the ground user. It is proportional to the area swept out by the equatorial projection of a vector from Earth's centre to the light ray while it propagates from transmitter to receiver [Parkinson and Ashby, 1996].

$$\Delta t_S = +\frac{2\Omega_e \cdot A_e}{c^2} \tag{3.3}$$

where,

$\Omega_e$ is the Earth angular rotation rate (WGS-84), $7.2921151467\times10^{-5}$ rad/s,

$A_e$ is the total area swept out by the radius vector from the centre of the Earth to the light ray while it propagates from transmitter to receiver.

This equation can be expressed in another form if the user is fixed on Earth (vector cross ($\times$) product) [Parkinson and Ashby, 1996].

$$\Delta t_S = +\frac{2\Omega_e}{c^2} \cdot \frac{r_S \times r_R}{2} \tag{3.4}$$

where,

$r_S$ is the position vector of a satellite at the instant a signal is transmitted,

$r_R$ is the position vector of a receiver at the instant of signal transmission.

### 3.3.2 Satellite Attitude Effects

There are two corrections to the satellite attitude effects: one is satellite antenna offset because of the discrepancy of satellite mass centre and phase centre; the other is phase wind-up correction due to satellite rotation.

***Satellite Antenna offsets***

Satellite Antenna Offsets should be considered when IGS precise products are used. The reason for this satellite-based correction originates from the separation between the GPS satellite centre of mass and the phase centre of its antenna. Because the force models used by IGS community for satellite orbit modeling refer to the satellite centre of mass, their GPS precise satellite coordinates and clock products also refer to the same point. However, the broadcast ephemerides in the GPS navigation message and GPS measurements refer to the satellite antenna phase centre. As a result, users who apply the IGS products must know satellite phase centre offsets and the orientation of the offset vector in space as the satellite orbits the Earth. The phase centres for most satellites are offset both in the body z coordinate direction (towards the Earth) and in the body x coordinate direction which is on the plane containing the Sun (see Figure 3.5) [Kouba and Héroux, 2000].

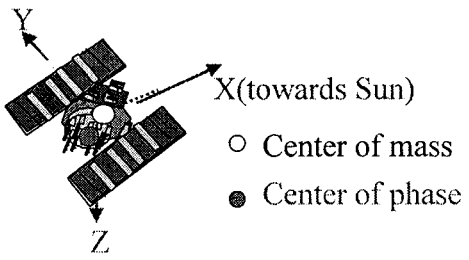


Antenna phase centre offsets
in satellite fixed reference frame (meters)

| | X | Y | Z |
|---|---|---|---|
| Block II/IIA: | 0.279 | 0.000 | 1.023 |
| Block IIR : | 0.000 | 0.000 | 0.000 |

**Figure 3.5: IGS Conventional Antenna Phase Centre in Satellite Fixed Reference Frame**
[Kouba and Héroux, 2000]

Not all satellites have antenna offset. Block IIR and satellites afterwards don't have to apply the correction as the two centres are consistent. For Block II/IIA satellites, the offset is a fixed value, whose influence on satellite coordinates in EFEC frame can be easily calculated once the orientation of the offset vector is known.

***Phase Wind-Up Correction***

GPS satellites transmit right circularly polarized (RCP) radio waves and therefore, the observed carrier-phase depends on the mutual orientation of the satellite and receiver antennas. A rotation of either receiver or satellite antenna around its bore axis will change the carrier-phase up to one cycle (one wavelength), which corresponds to one complete revolution of the antenna. This effect is called "phase wind-up" [Wu and et. al., 1993]. A receiver antenna, unless mobile, does not rotate and is oriented towards a reference direction (usually north). However, satellite antennas undergo slow rotations as their solar panels are being oriented towards the Sun and the station-satellite geometry changes. Besides, during

eclipsing seasons, satellites are also subjected to rapid rotations, the so-called "noon" and "midnight" turns, to reorient their solar panels towards the Sun. This can represent antenna rotations of up to one revolution within half an hour or less. During such noon or midnight turns, phase data needs to be corrected for this effect.

The phase wind-up correction has been generally neglected even in the most precise differential positioning software, as it is quite negligible for double difference positioning on baselines/networks spanning up to a few hundred kilometres. However, it has been shown that it can reach up to 4 cm for a baseline of 4000 km [Wu and et al., 1993]. For receiver antenna rotations (e.g. during kinematics positioning/navigation), phase wind-up is fully absorbed into station clock solutions (or eliminated by double differencing). However, this effect is quite significant for un-differenced point positioning when fixing IGS satellite clocks since it can reach up to one half of the wavelength. Since about 1994, most of the IGS Analysis Centres (and therefore the combined IGS orbit/clock products) apply this phase wind up correction. Neglecting it and fixing IGS orbits/clocks will result in position and clock errors at the dm level [Kouba and Héroux, 2000].

The phase wind-up correction can be evaluated from dot (·) and vector (×) products according to [Wu and at al., 1993] as follows:

$$\Delta\phi = sign(\zeta)\ \cos^{-1}(\vec{D}'\cdot\vec{D}/\left|\vec{D}'\right\|\vec{D}\right|) \tag{3.5}$$

where $\zeta = \hat{k}\cdot(\vec{D}'\times\vec{D})$, $\hat{k}$ is the satellite to receiver unit vector and $\vec{D}', \vec{D}$ are the effective dipole vectors of the satellite and receiver computed from the current satellite body

coordinate unit vectors ($\hat{x}', \hat{y}', \hat{z}'$) and the local receiver unit vectors ($\hat{x}, \hat{y}, \hat{z}$) [Wu and at al., 1993]:

$$\vec{D}' = \hat{x}' - \hat{k}(\hat{k} \cdot \hat{x}') - \hat{k} \times \hat{y}' \tag{3.6}$$

$$\vec{D} = \hat{x} - \hat{k}(\hat{k} \cdot \hat{x}) + \hat{k} \times \hat{y} \tag{3.7}$$

Continuity between consecutive phase observation segments must be ensured by adding full cycle terms of $\pm 2\pi$ to the correction (3.5).

### 3.3.3 Site Displacements Effects

In a global sense, a station undergoes real or apparent periodic movements reaching a few dm that are not included in the corresponding International Terrestrial conventional Reference Frame (ITRF) position. Consequently, if one is to obtain a precise station coordinate solution consistent with the current ITRF conventions, the above station movements must be modeled by adding the site displacement correction terms listed below to the conventional ITRF coordinates. Effects with magnitude of less than 1 centimetre such as atmospheric and antenna snow build-up loading have not been considered in the following.

***Solid Earth Tides***

The "solid" Earth is in fact pliable enough to respond to the same gravitational forces that generate the ocean tides. The periodic vertical and horizontal site displacements caused by

tides are represented by spherical harmonics of degree and order ($n \times m$) characterized by the Love number $h_{nm}$ and the Shida number $l_{nm}$. The effective values of these numbers weakly depend on station latitude and tidal frequency [Wahr, 1981] and need to be taken into account when an accuracy of 1 mm is desired in determining station positions (see e.g. IERS Conventions [IERS, 1996]). However, for 5 mm precision, only the second degree tides, supplemented with a height correction term are necessary.

For the site displacement vector in Cartesian coordinates $\Delta\vec{r}^{\,T} = |\Delta x, \Delta y, \Delta z|$ [IERS, 1989]:

$$\Delta\vec{r} = \sum_{j=2}^{3} \frac{GM_j}{GM} \frac{r^4}{R_j^3} \left\{ \left[ 3l_2 \left( \hat{R}_j \cdot \hat{r} \right) \right] \hat{R}_j + \left[ 3\left( \frac{h_2}{2} - l_2 \right) \left( \hat{R}_j \cdot \hat{r} \right)^2 - \frac{h_2}{2} \right] \hat{r} \right\} +$$

$$\left[ -0.025m \cdot \sin\phi \cdot \cos\phi \cdot \sin\left( \theta_g + \lambda \right) \right] \cdot \hat{r}, \qquad (3.8)$$

where,

$GM$, $GM_j$ are the gravitational parameters of the Earth, the Moon ($j=2$) and the Sun ($j=3$);

$r$, $R_j$ are geocentric state vectors of the station, the Moon and the Sun with the corresponding unit vectors $\hat{r}$ and $\hat{R}_j$, respectively;

$l_2$ and $h_2$ are the nominal second degree Love and Shida dimensionless numbers (0.609, 0.085);

$\phi$, $\lambda$ are the site latitude and longitude (positive east);

$\theta_g$ is Greenwich Mean Sidereal Time.

The tidal correction (3.8) can reach about 30 cm in the radial and 5 cm in the horizontal direction. It consists of a latitude dependent permanent displacement and a periodic part with predominantly semi diurnal and diurnal periods of changing amplitudes. The periodic part is largely averaged out for static positioning over a 24-hour period. However, the permanent part, which can reach up to 12 cm in mid latitudes (along the radial direction) remains in such a 24h average position. The permanent tidal distortion, according to the ITRF convention [IERS, 1996] has to be subtracted as well. In other words, the complete correction (3.8), which includes both the permanent and periodical tidal displacements, must be applied to be consistent with the ITRF convention. Even when averaging over long periods, neglecting the correction (3.8) in point positioning would result in systematic position errors of up to 12.5 and 5 cm in the radial and north directions, respectively. Note that for differential positioning over short baseline (<100km), both stations have almost identical tidal displacements so that the relative positions over short baselines will be largely unaffected by the solid Earth tides. If the tidal displacements in the north, east and vertical directions are required, they can be readily obtained by multiplying (3.8) by the respective unit vectors [Kouba and Héroux, 2000].

***Ocean Loading***

Ocean loading is similar to solid Earth tides as it is dominated by diurnal and semi diurnal periods, but it results from the load of the ocean tides. While ocean loading is almost an order of magnitude smaller than solid Earth tides, it is more localized and by convention it does not have a permanent part. For single epoch positioning at the 5 cm precision level, or

mm static positioning over 24h period and/or for stations that are far from the oceans, ocean loading can be safely neglected. On the other hand, for cm precise kinematics point positioning or precise static positioning along coastal regions over intervals significantly shorter than 24h, this effect has to be taken into account. Note that when the tropospheric zenith path delay (ZPD) or clock solutions are required, the ocean load effects also have to be taken into account even for a 24h static point positioning processing, unless the station is far (> 1000 km) from the nearest coast line. Otherwise, the ocean load effects will map into the tropospheric ZPD or clock solutions [Dragert, 2000], which may be significant particularly for coastal stations. The ocean load effects can be modeled in each principal direction by the following correction term [IERS, 1996]:

$$\Delta c = \sum_j f_j A_{cj} \cos\left(\omega_j t + \chi_j + u_j - \Phi_{cj}\right) \tag{3.9}$$

where,

$f_j$ and $u_j$ depend on the longitude of lunar node (at 1-3 mm precision $f_j$ =1 and $u_j$ =0);

$j$ represents the 11 tidal waves designated as $M_2$, $S_2$, $N_2$, $K_2$, $K_1$, $O_1$, $P_1$, $Q_1$, $M_f$, $M_m$ and $S_{sa.}$;

$\omega_j$ and $\chi_j$ are the angular velocity and the astronomical arguments at time $t=0h$, corresponding to the tidal wave component $j$; The arguments $\chi_j$ can be readily evaluated by a FORTRAN routine *ARG* available from the IERS Convention ftp site: *ftp://maia.usno.navy.mil/conventions/chapter7/arg.f*.

$A_{cj}$ and $\Phi_{cj}$ are the station specific amplitudes and phases for the radial, south (positive) and west (positive) directions.

$A_{cj}$ and $\Phi_{cj}$ are computed by convolution of Green functions utilizing the latest global ocean tide models as well as refined coastline database [Scherneck, 1991; Pagiatakis, 1992; Agnew, 1996]. A table of the amplitudes $A_{cj}$ and phases $\Phi_{cj}$ for most ITRF stations, computed by Scherneck (1993), is also available from the above ftp URL (*ftp://maia.usno.navy.mil/conventions/chapter7/olls25.bld*). Alternatively, software for evaluation of $A_{cj}$ and $\Phi_{cj}$ at any site is available from Pagiatakis (1992). Typically, the $M_2$ amplitudes are the largest and do not exceed 5 cm in the radial and 2 cm in the horizontal directions for coastal stations. For cm accuracy it is also necessary to augment the global tidal model with local ocean tides digitized, for example, from the local tidal charts. Future ITRF convention will likely also require a model for the geo-centre variation (at a cm level), which is also of tidal origin. Consequently the station specific amplitude $A_{cj}$ and phases $\Phi_{cj}$ would then include the geo-centre (tidal) variation. In fact the IERS tabulation at the above ftp site already includes the tidal geo-centre variation. One consequence of this new convention/approach is that for cm station position precision, the ocean load effect corrections must be included at all stations, even for those far from the ocean [Kouba and Héroux, 2000].

***Earth Rotation Parameters (ERP)***

The Earth Rotation Parameters (i.e. Pole position *Xp*, *Yp* and *UT1-UTC*), along with the conventions for sidereal time, precession and nutation facilitate accurate transformations between terrestrial and inertial reference frames that are required in global GPS analysis (see e.g. [IERS, 1996]). Then, the resulting orbits in ITRF, much like the IGS orbit products, imply, quite precisely, the underlying ERP. Consequently, IGS users who fix or heavily

constrain the IGS orbits and work directly in ITRF need not worry about ERP. However, when using software formulated in an inertial frame, the ERP corresponding to the fixed orbits are required.

For point positioning processing formulated within the terrestrial frame, with the IGS orbits held fixed, the sub-daily ERP model, which is also dominated by diurnal and sub-diurnal periods of ocean tide origin, is still required to attain sub-centimetre positioning precision. This results from the IERS convention for ERP, i.e. the IERS/IGS ERP series as well as ITRF positions do not include the sub-daily ERP variations, which can reach up to 3 cm at the surface of the Earth. However, the IGS orbits imply the complete ERP, i.e. the conventional ERP plus the sub-daily ERP model. In order to be consistent, in particular for precise static positioning over intervals much shorter than 24 h, this sub-daily effect needs to be taken into account. Note that much like the ocean tide loading, the sub-daily ERP are averaged out to nearly zero over a 24h period.

This effect can be modeled, like all the tidal displacements, as apparent corrections ($\Delta x$, $\Delta y$, $\Delta z$) to the conventional (ITRF) station coordinates ($x$, $y$, $z$), evaluated from the instantaneous sub-daily ERP corrections ($\delta Xp$, $\delta Yp$, $\delta UT1$) [IERS, 1996], i.e.

$$\Delta x = +y \cdot \delta UT1 + z \cdot \delta Y_P \tag{3.10}$$

$$\Delta y = -x \cdot \delta UT1 - z \cdot \delta X_P \tag{3.11}$$

$$\Delta z = -x \cdot \delta Y_P + y \cdot \delta X_P \tag{3.12}$$

where each of the sub-daily ERP component corrections *(δXp, δYp, δUT1)* is obtained from the following approximation form, e.g. for the *Xp* pole component [IERS, 1996]:

$$\delta X_P = \sum_{j=1}^{8} (F_j \sin \xi_j + G_j \cos \xi_j) \tag{3.13}$$

where,

$\xi_j$ is the astronomical argument at the current epoch for the tidal wave component *j;*

$j$ represents the eight diurnal tidal waves considered ($M_2$, $S_2$, $N_2$, $K_2$, $K_1$, $O_1$, $P_1$, $Q_1$), augmented with $n \cdot \pi/2$ ( $n$= *0, 1* or –1);

$F_j$ and $G_j$ are the tidal wave coefficients derived from the latest global ocean tide models for each of the three ERP components.

The above (conventional) Fortran routine, evaluating the sub-daily ERP corrections can also be obtained at the [IERS, 1996] ftp site: *ftp://maia.usno.navy.mil/conventions/chapter8/ray.f.*

### 3.3.4 Compatibility Considerations

Positioning and GPS analyses that constrain or fix any external solutions/products need to apply consistent orbit/clock weighting, models and conventions. This is particular true for precise point positioning and clock solutions/products. However, even for cm differential positioning, consistency with the IGS global solutions needs to be considered. This includes issues such as the respective version of ITRF, the IGS ERP, the IGS orbit and station

solutions used, the station logs (antenna offsets) and the adopted antenna calibration table (*IGS_01.pcv*) available at the IGS Central Bureau (http://igscb.jpl.nasa.gov).

The GPS System already has some well developed conventions, e.g. that only the periodic special relativity correction [ION, 1980]:

$$\Delta T_{rel} = -2\vec{X}s \cdot \vec{V}s / c^2 \tag{3.14}$$

is to be applied by all GPS users [ION, 1980]. Here $\vec{X}s, \vec{V}s$ are the satellite position and velocity vectors and $c$ is the speed of light. The same convention has also been adopted by IGS, i.e. all the IGS satellite clock solutions are consistent with this convention.

By agreed convention, there are no group delay calibration corrections applied for the station and satellite (L2-L1) biases in all the IGS AC analyses, thus no such calibrations are to be applied when the IGS clock products are held fixed or constrained in dual frequency point positioning. Furthermore, a specific set of pseudorange observations consistent with the IGS clock products needs to be used even for point positioning utilizing phase observations, otherwise the clock solutions are significantly affected. This is a result of significant satellite dependent differences between L1 C/A ($P_{C/A}$) and P ($P_1$) code pseudoranges which can reach up to 2 ns (60 cm). IGS has been using the following conventional pseudorange observation set, which needs to be enforced when using the IGS orbit/clock products (*IGS Mail #2744*):

Up to April 02, 2000 (GPS Week 1056): $\boldsymbol{P_{C/A}}$ and $\boldsymbol{P'_2 = P_{C/A} + (P_2 - P_1)}$

After April 02, 2000 (GPS Week 1056): $\boldsymbol{P_1}$ and $\boldsymbol{P_2}$

Note that in case of C/A and P code carrier phase observations there is no such problem and no need for any such convention. The GPS system specifications state the difference between the two types of code observation on L1 is the same for all satellites and it is equal to a constant fraction of the L1 wavelength. This difference is fully absorbed into an insignificant offset of the station clock solutions. For more information on this convention and how to form the above pseudorange observation set for receivers, which do not give all the necessary observation types, see *IGS Mail #2744* available from the IGS CB Archives: *http://igscb.jpl.nasa.gov/mail/igsmail/2000/.*

## 3.4 PPP Processing Method: the Traditional Model

In this section, a traditional ionosphere-free combination and its characteristics are first discussed. Based on the combination, the observation model is addressed, followed by its error descriptions.

### 3.4.1 Traditional Ionosphere-Free Combination

The ionosphere-free combination is also known as "L3" combination. The ionospheric refraction bias is eliminated by constructing a combined ionosphere-free phase or pseudo-range observable from the L1 and L2 data. It has two special forms in the unit of cycle, one with L1 wavelength, and the other of L2 wavelength.

Equation (3.15) shows the combination with L1 wavelength.

$$\begin{aligned}\phi(L3)_1 &= \alpha_1\phi(L1)+\alpha_2\phi(L2)=\left(\phi(L1)-\frac{f_2}{f_1}\cdot\phi(L2)\right)\cdot\frac{f_1^2}{f_1^2-f_2^2}\\ &=\left(\frac{f_1}{c}\right)\cdot\rho+\left(\frac{f_1}{c}\right)\cdot c(dt-dT)+\left(\frac{f_1}{c}\right)\cdot d_{orb}+\left(\frac{f_1}{c}\right)\cdot d_{trop}+\\ &\quad N_{3,a}+\left(\frac{f_1}{c}\right)\cdot(d_{mult/\phi(L3)}+\varepsilon(\phi(L3)))\end{aligned} \tag{3.15}$$

$$N_{3,a}=\alpha_1 N_1+\alpha_2 N_2 \tag{3.16}$$

$$\alpha_1=\frac{f_1^2}{f_1^2-f_2^2}\approx 2.546 \quad \alpha_2=\frac{-f_1 f_2}{f_1^2-f_2^2}=-1.984 \tag{3.17}$$

Equation (3.18) shows the combination with L2 wavelength.

$$\begin{aligned}\phi(L3)_2 &= \beta_1\phi(L1)+\beta_2\phi(L2)=\left(\phi(L2)-\frac{f_1}{f_2}\cdot\phi(L1)\right)\cdot\frac{f_2^2}{f_1^2-f_2^2}\\ &=\left(\frac{f_2}{c}\right)\cdot\rho+\left(\frac{f_2}{c}\right)\cdot c(dt-dT)+\left(\frac{f_2}{c}\right)\cdot d_{orb}+\left(\frac{f_2}{c}\right)\cdot d_{trop}+\\ &\quad N_{3,b}+\left(\frac{f_2}{c}\right)\cdot(d_{mult/\phi(L3)}+\varepsilon(\phi(L3)))\end{aligned} \tag{3.18}$$

$$N_{3,b}=\beta_1 N_1+\beta_2 N_2 \tag{3.19}$$

$$\beta_1=\frac{f_1 f_2}{f_1^2-f_2^2}\approx 1.984 \quad \beta_2=\frac{-f_2^2}{f_1^2-f_2^2}=-1.54 \tag{3.20}$$

When expressed in the metric unit, Equations (3.15) and (3.18) have the same form as follows:

$$\begin{aligned}\Phi_{IF} &= \frac{f_1^2 \cdot \Phi(L1) - f_2^2 \cdot \Phi(L2)}{f_1^2 - f_2^2} \\ &= \rho + c(dt - dT) + d_{orb} + d_{trop} + \frac{cf_1 N_1 - cf_2 N_2}{f_1^2 - f_2^2} + d_{mult/\Phi(L1+L2)} \\ &\quad + \varepsilon\,(\Phi(L1 + L2))\end{aligned} \tag{3.21}$$

No matter which wavelength is used, as the ambiguity terms $N_{3,a}$ and $N_{3,b}$ are the linear combination of L1 and L2 with non-integer coefficients, the resulted combined ambiguity can only be estimated as a float value.

The equivalent pseudo-range L3 combination can be written as:

$$\begin{aligned}P(L3) &= \frac{f_1^2 \cdot P(L1) - f_2^2 \cdot P(L2)}{f_1^2 - f_2^2} \\ &= \rho + c(dt - dT) + d_{orb} + d_{trop} + d_{mult/P(L3)} + \varepsilon(P(L3))\end{aligned} \tag{3.22}$$

Using L3 combinations could have some disadvantages. First, the combinations are not totally ionosphere-free. They cannot remove the higher-order of the ionospheric effects as the Equation (2.6) is just the approximation to the first-order. Although the high-order ionospheric effects usually cover less than 0.1% of the total effects, they can still be several tens of centimetres of range error during times of high TEC [Parkinson and Klobuchar, 1996]. Second, the noise level of L3 combination increases by nearly a factor of three as compared to the noise level of the corresponding original code and carrier phase observables.

### 3.4.2 Observation Model

The PPP Traditional Model uses the traditional ionosphere-free code and phase combinations as expressed in Equation (3.21) and (3.22) and rewritten in the following:

$$P_{IF} = \frac{f_1^2 \cdot P(L1) - f_2^2 \cdot P(L2)}{f_1^2 - f_2^2} = \rho + c(dt - dT) + d_{orb} + d_{trop} + d_{mult\,/\,P(L1+L2)} + \varepsilon\ (P(L1 + L2)) \tag{3.23}$$

$$\Phi_{IF} = \frac{f_1^2 \cdot \Phi(L1) - f_2^2 \cdot \Phi(L2)}{f_1^2 - f_2^2} = \rho + c(dt - dT) + d_{orb} + d_{trop} + \frac{cf_1N_1 - cf_2N_2}{f_1^2 - f_2^2} + d_{mult\,/\,\Phi(L1+L2)} + \varepsilon\ (\Phi(L1 + L2)) \tag{3.24}$$

Applying the precise orbit and clock corrections to Equations (3.23) and (3.24) results in the following equations:

$$P_{IF}^{'} = \rho - c \cdot dT + d_{trop} + \varepsilon^{'}(P_{IF}) \tag{3.25}$$

$$\Phi_{IF}^{'} = \rho - c \cdot dT + d_{trop} + N^{'} + \varepsilon^{'}(\Phi_{IF}) \tag{3.26}$$

where,

$P_{IF}^{'}$ is the corrected ionosphere-free code observable in meters,

$\Phi_{IF}^{'}$ is the corrected ionosphere-free phase observable in meters,

$N^{'}$ is the combined ambiguity term in unit of meters, and

$\varepsilon'(\ )$ is the random noise part, including residual errors of precise orbit and clock data, multipath and noise.

The model unknowns include three dimension components, receiver clock offset, tropospheric effects, and the combined ambiguity parameters for each observed satellite.

This model has been applied into the PPP software implementation by several research institutes, including NRCan of Canada and JPL of United States. Some of their results were presented in the papers of [Kouba and Héroux, 2000] and [Muellerschoen, 2001], which showed a sub-meter positioning accuracy in real-time kinematics mode with smoothed code and several-centimetre accuracy in post-processing static mode with code and phase observations. In both cases, the processing time before a convergence value can be reached is usually more than half hour.

Three weaknesses need to be pointed out for this traditional PPP processing method. First, the combined ambiguity term in the new phase suggested by Equation (3.24) can only be estimated as a single float unknown. Therefore, the ambiguity integer characteristics can't be exploited, which indicates estimation convergence of parameters can only be gradually made with the observations' accumulation and geometry change. Second, the measurement noise terms in Equations (3.23) and (3.24) are three times greater than the original corresponding code and phase observations. Finally, the traditional ionosphere-free combination cannot remove the higher-order ionospheric effects, which, although covering less than 0.1% of the

total effects, can be several tens of centimetres of range error during times of high TEC [Parkinson and Klobuchar, 1996].

The higher-order ionospheric effects and any other unmodeled errors are usually merged into the measurement noise term. The higher the noise, the bigger the converged position error and the longer the convergence time will be. Generally, with the PPP Traditional Model, approximately 30 minutes is required before a converged position solution can be reached at a decimetre accuracy level in a static processing.

### 3.4.3 Residual Error Budget in Traditional Model

After different kinds of error mitigations with the PPP Traditional Model, residuals still exist in the centimetre level to many GPS errors. Table 3.2 lists the main error residuals. With the PPP Traditional Model, the residual errors for the ionosphere-free code and phase observations are approximately 32 cm and 9 cm respectively without considering multipath. Code and phase observations play different roles in PPP processing, usually the size of code error residual is the key element on determining the amount of time for position to converge, and the phase counterpart weighs more on the converged positioning accuracy. In the numerical results and analysis chapters, these relations will be discussed in detail between two PPP processing models.

**Table 3.2 PPP Traditional Model Residual Error Budget (One-sigma)**

| | |
|---|---|
| Satellite orbit | < 5 cm |
| Satellite clock | < 3 cm |
| Troposphere | < 5 cm (1) |
| Ionosphere | < 5 cm (2) |
| Noise | $3\sigma$ (3) |
| Multipath | -- (4) |
| Others | < 1~2 cm |
| **Total** | **< 32 cm (for Code)**<br>**< 9 cm (for Phase)** |

(1): 5 cm is an average value of the mapping function error scaled by the zenith path delay;

(2): 5 cm is a typical high-order value of ionospheric effects in a comparatively TEC stable condition;

(3): $\sigma$ is the measurement noise of either code or phase observations. With high-end GPS receivers, the code and phase noise levels are approximately 10 cm and 0.3 cm respectively, therefore, the ionosphere-free combinations have approximately 30 cm and 1 cm noise for code and phase respectively;

(4): The multipath effect is environment dependent and therefore, is not listed here.

# CHAPTER 4

# DEVELOPMENT OF A NEW PPP PROCESSING METHOD

Although the PPP Traditional Model presented in the previous chapter is simple to implement, it has several disadvantages. First, the measurement noise in the Traditional Model is three times bigger than the corresponding original measurement noise. Second, the traditional ionosphere-free combination cannot remove higher-order ionospheric effects, resulting in bigger error residuals. Third, the ambiguity term is a combined single unknown from $N_1$ and $N_2$ on two carriers, only a float solution can be obtained as this combined term does not preserve the integer characteristics of carrier phase ambiguity. Generally, the convergence of the ambiguity parameters, along with the convergence of the position parameters, is a function of the number of unknowns and the total level of measurement noise and unmodeled errors. With the Traditional Model, over 30 minutes is required before a converged position solution is obtained in a post-processing static mode [Gao and Shen, 2001]. To reduce the required convergence time, either fewer unknowns or a lower measurement noise level should be applied.

In this chapter, a new observation model P1-P2-CP is proposed which is able to reduce the noise level and residual error, and to allow ambiguity-fixing approach to decrease the number of unknowns.

## 4.1 P1-P2-CP Model

This section first describes a code-phase combination and its characteristics. Based on the combination, the observation model is discussed, followed by its error description and the model comparison with the PPP Traditional Model.

### 4.1.1 Code-Phase Combination

The code and phase observables on the same frequency suffer the same amount of ionospheric effect but with opposite sign, therefore, their sum is ionosphere-free. A new observable constructed from the combination of the code and phase observations has a form as follows.

$$\begin{aligned} P_i &= 0.5(P(L_i)+\Phi(L_i)) \\ &= \rho + c(dt-dT) + d_{orb} + d_{trop} + 0.5d_{mult/P(L_i)} + 0.5\varepsilon(P(L_i)+\Phi(L_i)) - 0.5\lambda_i N_i \end{aligned} \tag{4.1}$$

where $i$ represents either L1 or L2. The using of 0.5 makes the combination to be scaled back to the satellite-receiver range.

The code-phase combination is more than ionosphere-free. It reduces the noise level by half compared with the original code observations. This is very important as the smaller the sum of noise and unmodeled error residuals, the faster the convergence and the more accurate the converged positioning estimation will be. Table 4.1 displays the size of error residuals of the ionosphere-free code and code-phase combinations. The error residuals from satellite orbit,

satellite clock, and troposphere are the same for both combinations, while the code-phase combination has much smaller noise compared to the traditional ionosphere-free code combination, which, as a result, generate much smaller total error residual error level. In the numerical analysis section, the relations between the error residual and the convergence time as well as the converged positioning accuracy will be discussed in detail through the comparison of results with different processing methods.

**Table 4.1 Residual Error Comparison between Two Code Combinations**

| | Ionosphere-free Code Combination | Code-Phase Combination |
|---|---|---|
| Satellite orbit | < 5 cm | < 5 cm |
| Satellite clock | < 3 cm | < 3 cm |
| Troposphere | < 5 cm | < 5 cm |
| Ionosphere | < 5 cm | < 5 cm |
| Noise | $3\sigma$ ** | $\frac{1}{2}\sigma$ ** |
| Multipath* | -- | -- |
| Others | < 1~2 cm | < 1~2 cm |
| **Total** | **< 32 cm** | **<10 cm** |

*: The multipath effect is environment dependent and therefore, is not listed here.

**: $\sigma$ is the measurement noise of either code or phase observations. With high-end GPS receivers, the code and phase noise levels are approximately 10 cm and 0.3 cm

respectively, therefore, the ionosphere-free combinations have approximately 30 cm and 1 cm noise for code and phase respectively.

### 4.1.2 Observation Model

The P1-P2-CP observation model includes the code-phase combinations on both L1 and L2 frequencies, together with the traditional ionosphere-free phase combination, which have the following expressions:

$$\begin{aligned} P_{IF,L1} &= 0.5(P(L1)+\Phi(L1)) \\ &= \rho + c(dt-dT) + d_{orb} + d_{trop} + 0.5\lambda_1 N_1 + \\ &\quad 0.5d_{mult/P(L1)} + 0.5\varepsilon\ (P(L1)+\Phi(L1)) \end{aligned} \tag{4.2}$$

$$\begin{aligned} P_{IF,L2} &= 0.5(P(L2)+\Phi(L2)) \\ &= \rho + c(dt-dT) + d_{orb} + d_{trop} + 0.5\lambda_2 N_2 + \\ &\quad 0.5d_{mult/P(L2)} + 0.5\varepsilon\ (P(L2)+\Phi(L2)) \end{aligned} \tag{4.3}$$

$$\begin{aligned} \Phi_{IF} &= \frac{f_1^2\cdot\Phi(L1)-f_2^2\cdot\Phi(L2)}{f_1^2-f_2^2} \\ &= \rho + c(dt-dT) + d_{orb} + d_{trop} + \frac{cf_1}{f_1^2-f_2^2}\cdot N_1 + \frac{cf_2}{f_1^2-f_2^2}\cdot N_2 + \\ &\quad d_{mult/\Phi(L1+L2)} + \varepsilon\ (\Phi(L1+L2)) \end{aligned} \tag{4.4}$$

Applying the precise orbit and clock corrections to Equations (4.2) through (4.4) results in the following equations:

$$P'_{IF,L1} = \rho - c\cdot dT + d_{trop} + 0.5\lambda_1 N_1 + \varepsilon\left(P'_{IF,L1}\right) \tag{4.5}$$

$$P'_{IF,L2} = \rho - c \cdot dT + d_{trop} + 0.5\lambda_2 N_2 + \varepsilon\left(P'_{IF,L2}\right) \tag{4.6}$$

$$\Phi'_{IF} = \rho - c \cdot dT + d_{trop} + \frac{f_1^2}{f_1^2 - f_2^2} \cdot \lambda_1 N_1 + \frac{f_2^2}{f_1^2 - f_2^2} \cdot \lambda_2 N_2 + \varepsilon\left(\Phi'_{IF}\right) \tag{4.7}$$

where,

$P'_{IF,Li}$ is the corrected code observable ($i$ = 1, or 2) in meters,

$\Phi'_{IF}$ is the corrected phase observable in meters, and

$\varepsilon(\ )$ is the random noise part, including residual errors of precise orbit and clock data, unmodeled higher-order ionospheric effects, multipath and noise.

This observation model, compared with the one applied in the Traditional Model, has lower noise and error residual level. But the biggest gain is the feasibility of the fixed ambiguity estimation as both L1 and L2 ambiguities can be estimated separately. Therefore, ambiguity searching and fixing technique can be implemented to further improve positioning convergence, which is a result of the reduction of unknown parameters.

The model unknowns include three coordinate components, receiver clock offset, tropospheric wet zenith path delay, and the L1 and L2 ambiguity parameters for each observed satellite.

Table 4.2 summarizes the characteristics of the two PPP processing models and their differences are highlighted. First, P1-P2-CP Model has three observations for each observed satellite with one more code observation than the Traditional Model, which, as a trade-off,

adds a doubled number of ambiguities to be estimated in P1-P2-CP Model. Second, the separate estimation of ambiguities on L1 and L2 with P1-P2-CP Model makes it feasible to carry out both float and fixed ambiguity solutions, while the Traditional Model has only float solution. Third, P1-P2-CP Model has a smaller noise level, resulting in a smaller error residual than the Traditional Model.

**Table 4.2 Comparison between the Traditional Model and P1-P2-CP Model**

| | **Traditional Model** | **P1-P2-CP Model** |
|---|---|---|
| **Observations** | Two per satellite, one code and one phase | Three per satellite: two codes and one phase |
| **Noise** | Three times of the original code noise level | Approximately half of the original code noise level |
| **Ambiguity** | Combined L1/L2 ambiguity, float value | L1 and L2 ambiguity, pseudo-integer, both the fixed and float solutions can be carried out |
| **Unknown Parameters** | Three-dimension coordinates,<br>Tropospheric wet zenith delay,<br>Receiver clock offset,<br>N ambiguities | Three-dimension coordinates,<br>Tropospheric wet zenith delay,<br>Receiver clock offset,<br>2×N ambiguities |

## 4.2 Variance Adjustment Procedure for P1-P2-CP

The noise term in the observation equations is the sum of the measurement noise and any un-modeled errors and error residuals. Compared with the code combination in the Traditional Model, the noise level of the new code is much smaller.

The influence of measurement noise should be stochastically and correctly modeled in the parameter estimation process. Inappropriate stochastic information could not only degrade the estimation solution to sub-optimal estimates, but also provide false statistical results critical for data quality control and analysis. To ensure more precise stochastic data for the filter to start with, a stochastic modeling procedure has been proposed with the P1-P2-CP Model. This procedure contains two parts: a two-step variance-estimation procedure to be used at the initial epoch and a variance adjustment to be used at the subsequent epochs.

Based on the theory that "even poor quality data provides some information, and should thus increase the precision of the filter output" [Maybeck, 1979], the two-step variance-estimation procedure is designed to derive the initial variance data for the filter, including the appropriate estimates for all the unknown parameters and the reliable stochastic information for the observations:

a) First, only the traditional ionosphere-free code combinations are used to calculate the initial estimations of unknown parameters, whose precision is described by the corresponding variance-covariance matrix. Using a single type of observable can give a better calculation of the a posteriori variance for unit weight $\hat{\sigma}_0^2$, which aided by the a priori variance for unit weight $\sigma_0^2$, is used to scale the pre-defined code observation standard deviation. These results are then used as the a priori information for the least-squares estimation to be conducted in the second step.

b) Second, the new P1-P2-CP observation model is used to derive the final estimations of position, receiver clock, station tropospheric wet zenith path delay, as well as the ambiguity parameters.

A detailed implementation of two-step procedure is given in the following.

At the first step, the PPP Traditional Model with only code observations is used. The variance factor (the a priori variance for unit weight) $\sigma_0^2$ and the ionosphere-free code combination variance $\sigma_{P_{IF}}^2$ are both set to one.

$$\sigma_0^2=\sigma_{P_{IF}}^2=1.0 \tag{4.8}$$

After processing with least-squares estimation, the a posteriori variance for unit weight $\hat{\sigma}_0^2$ is calculated based on the following equation:

$$\hat{\sigma}_0^2=\frac{V^T C_l^{-1} V}{r} \tag{4.9}$$

where,

$V$ is the observation residual vector,

$C_l$ is the observation variance-covariance matrix, and

$r$ is the system redundancy, which usually equals to the number of observations minus the number of unknowns. But a more precise way is to sum up the redundancy number $r_i$ for each observation, which is the function of geometry

and the observation precision and has the following expression [Mackenzie,1985; also see the Appendix A] ($[\ ]_{ii}$ in the equation represents the diagonal element on row $i$):

$$r_i = \left[(C_l - A(A^T C_l^{-1} A)^{-1} A^T) C_l^{-1}\right]_{ii} \tag{4.10}$$

Based on the a posteriori variance $\hat{\sigma}_0^2$ and the a priori variance $\sigma_0^2$, a more precise estimate of the code observation variance $\sigma_{P_{IF}}^2$ can be obtained with the following expression:

$$\hat{\sigma}_{P_{IF}}^2 = \sigma_{P_{IF}}^2 \cdot \frac{\hat{\sigma}_0^2}{\sigma_0^2} = \sigma_{P_{IF}}^2 \cdot \hat{\sigma}_0^2 \tag{4.11}$$

According to the error propagation theory, the $\sigma_{P_{IF}}^2$, which represents the variance of the ionosphere-free code combination, can also be expressed with the following equation [Abidin, 1993]:

$$\sigma_{P_{IF}}^2 = \left(\frac{f_1^2}{f_1^2 - f_2^2}\right)^2 \sigma_{P(L1)}^2 + \left(\frac{f_2^2}{f_1^2 - f_2^2}\right)^2 \sigma_{P(L2)}^2 = 2.39\sigma_{P(L1)}^2 + 6.48\sigma_{P(L2)}^2 \tag{4.12}$$

where $\sigma_{P(Li)}^2$ is the variance of the original code observations on the $L_i$ ($i$=1 or 2) frequency. Assuming the code precision is the same on both L1 and L2: $\sigma_{P(L1)} = \sigma_{P(L2)} = \sigma_P$, gives

$$\hat{\sigma}_P^2 = \hat{\sigma}_{P_{IF}}^2 / 8.87 = \sigma_{P_{IF}}^2 \hat{\sigma}_0^2 / 8.87 \tag{4.13}$$

As a result, the variance of the code-phase ionosphere-free combination described in Equations (4.2) and (4.3), can be determined as:

$$\hat{\sigma}^2_{P(IF,L1)} = \hat{\sigma}^2_{P(IF,L2)} = \frac{1}{4}\hat{\sigma}^2_P = \sigma^2_{P_{IF}}\hat{\sigma}^2_0 / 35.5 \tag{4.14}$$

The variance for the traditional ionosphere-free phase combination described in Equation (4.4) has a similar expression as Equation (4.12).

$$\hat{\sigma}^2_{\Phi_{IF}} = 2.39\sigma^2_{\phi(L1)} + 6.48\sigma^2_{\phi(L2)} \tag{4.15}$$

where $\sigma^2_{\Phi(Li)}$ is the variance of the original phase observations on the $L_i$ ( $i$ =1 or 2) frequency.

The numerical difference between code and phase observations is equivalent to the phase ambiguity if all the errors are corrected. Although GPS errors cannot be removed completely, the difference can still be a good approximation to the phase ambiguity. The following equation gives the approximate initialization of $L_1$ ambiguity with the ionospheric effect calculated from the dual frequency code observations.

$$\begin{aligned}
\lambda_1 N_1' &= P(L_1) - \Phi(L_1) - 2\cdot d_{ion,1} \\
&= P(L_1) - \Phi(L_1) - 2\cdot\left(P(L_1) - P(L_2)\right)/\left(1 - \frac{f_1^2}{f_2^2}\right) \\
&= \left(1 + \frac{2\cdot f_2^2}{f_1^2 - f_2^2}\right)\cdot P(L_1) - \frac{2\cdot f_2^2}{f_1^2 - f_2^2}\cdot P(L_2) - \Phi(L_1)
\end{aligned} \tag{4.16}$$

The corresponding variance for $L_1$ initial ambiguity, after neglecting phase measurement noise, can then be determined by

$$\hat{\sigma}^2_{N_1'} = (1+\frac{2\cdot f_2^2}{f_1^2-f_2^2})^2\cdot\sigma_P^2 + (\frac{2\cdot f_2^2}{f_1^2-f_2^2})^2\cdot\sigma_P^2 = 26.30\cdot\sigma_P^2 = 2.97\cdot\sigma^2_{P_{IF}}\hat{\sigma}_0^2 \qquad (4.17)$$

Similarly, the initial value for $L_2$ ambiguity can be calculated as Equation (4.16) and the corresponding variance is given by

$$\hat{\sigma}^2_{N_2'} = 42.67\cdot\sigma_P^2 = 4.80\cdot\sigma^2_{P_{IF}}\hat{\sigma}_0^2 \qquad (4.18)$$

In summary, after conducting the least-squares adjustment in the first epoch, more precise stochastic information for both the observations and the unknown parameters can be derived, which are beneficial for the processing at subsequent epochs.

After the first epoch, the precision of code observation may still vary due to the phase-smoothing procedure. As a result, observation variance should be adjusted accordingly at each epoch. This adjustment can be made by scaling with the a posteriori variance of unit weight. For different observation type, the a posteriori variance of unit weight is different and can be expressed as [Mackenzie, 1985]:

$$\hat{\sigma}^2_{0,j} = \frac{v_j^T C_l^{-1} v_j}{\sum_j r_i} \qquad (4.19)$$

where j denotes the observation type.

## 4.3 Ambiguity Initialization

As discussed in the previous section, initial ambiguities and their variance can be estimated with the use of Equations (4.16) through (4.18). For the sake of convenience, they are repeated once again:

$$\lambda_i N_i = P(L_i) - \Phi(L_i) - 2 \cdot d_{ion,i} \tag{4.20}$$

$$\hat{\sigma}^2_{N_1} = 26.3 \cdot \sigma^2_P = 3 \cdot \sigma^2_{P_{IF}} \hat{\sigma}^2_0 \tag{4.21}$$

$$\hat{\sigma}^2_{N_2} = 42.667 \cdot \sigma^2_P = 4.8 \cdot \sigma^2_{P_{IF}} \hat{\sigma}^2_0 \tag{4.22}$$

where the ionospheric effect is calculated based on dual-frequency code observations.

Although the initialized value based on the above equation is only an approximation with standard deviation of couple of meters, it is still important and has a positive effect for processing convergence.

## 4.4 Ambiguity Pseudo-Fixing and Fixing Criteria

The ambiguity estimation on both L1 and L2 with P1-P2-CP Model brings the possibility of fixed ambiguity resolution. However, this is the concept of pseudo-fixing as L1 and L2 ambiguity terms include a non-zero initial phase resulted from the un-synchronization of satellite-transmitted and receiver-generated signals [Teunissen, 1998]. The magnitude of the

non-zero initial phase is always less than one cycle. Since errors of the ambiguity estimation in PPP could range from several cycles up to more than ten cycles from their true value before convergence is reached, an ambiguity searching process can be developed to speed up the ambiguity and position convergence. The fixed ambiguities, which are the results of the searching process, only have an error of a fraction of one cycle if they are successfully found. Therefore, they are of much better precision than the float ambiguity estimates in the early-stage processing, and a better positioning solution can be ensured. But in the long period of processing, the converged float ambiguity estimation can be very accurate when the information accumulates. The pseudo-fixed solution, being a truncated estimation and not as accurate as the converged float solution, can only reach decimetre level accuracy. Therefore, the pseudo-fixing approach is only useful for kinematics and fast static applications that only need decimetre-level positioning accuracy.

Just as the residual threshold criterion used in the double-differenced ambiguity resolution, the main criterion to validate ambiguity pair in pseudo-fixing is to look for the smallest a posteriori variance factor.

$$\hat{\sigma}_0^2 = \frac{\hat{v}^T C_l^{-1} \hat{v}}{r} \tag{4.23}$$

where

$\hat{v}$ is the residual vector,

$C_l$ is the observation variance matrix, and

$r$ is the redundancy of the adjustment system.

$\hat{\sigma}_0^2$ is an important factor in least-squares adjustment as the least-squares estimation is based on the minimization of the weighted squared residual sum $\hat{v}^T C_l^{-1} \hat{v}$. Theoretically, the a posteriori variance factor with the correct integer should have the smallest value.

As the ambiguity is originally non-integer value, two integers – the upper bound and lower bound of float-valued ambiguity – could theoretically generate the smallest and second smallest $\hat{\sigma}_0^2$. Once the searching results show the ambiguity pairs with the smallest and second smallest $\hat{\sigma}_0^2$ are $n$ and $n \pm 1$, then the ambiguity is fixed to their average – a float value:

$$N = \frac{N_1 + N_2}{2} \tag{4.24}$$

where $N_1, N_2$ are the integer ambiguities with the smallest and second smallest a posteriori variance factor, and they have the relation of $N_1 = N_2 \pm 1$.

In order to increase the reliability of ambiguity searching, another criterion – the observation residual check – can be combined with the weighted squared residual sum check and has the following expression.

$$\begin{aligned} R &= P_{IF,L1} - P_{IF,L2} + \left(\frac{\lambda_1 N_1}{2} - \frac{\lambda_2 N_2}{2}\right) \\ &= d_{multipath}\left(\sum P_{IF,Li}\right) + \varepsilon\left(\sum P_{IF,Li}\right) \end{aligned} \tag{4.25}$$

With the right ambiguity pair, the remaining part $R$ equals to the sum of multipath effect and measurement noise. Therefore, the observation residual check cannot be used in a strong multipath and noise environment. But with phase smoothing, the code measurement noise can be reduced significantly, therefore, it can be a good indicator.

# CHAPTER 5

# NUMERICAL RESULTS AND ANALYSIS: STATIC PROCESSING

To assess the performance of the proposed P1-P2-CP Model in a static processing mode, numerical computations for both P1-P2-CP Model and the Traditional one were conducted and their results are presented in this chapter. A performance comparison between the two models was made in terms of solution/ambiguity convergence and positioning accuracy.

Section 5.1 gives a description of the testing data. The sequential filter and its PPP implementation are introduced in Section 5.2. Result analyses on float solutions are given in Sections 5.3 and 5.4. Then the chapter concludes with ambiguity pseudo-fixing results in Section 5.5.

## 5.1 Data Description

Data used for the numerical computation were collected on August 15, 2001 from eight CACS permanent stations, which are ALBH, DRA2, PRDS, YELL, CHUR, ALGO, NRC1 and STJ0 (see Figure 3.2). AOA BENCHMARK ACT dual-frequency receivers or similar were used at those stations. The data-sampling rate was 1 Hz. The number of visible satellites was between 5 and 10 during the most of test period.

The IGS final ephemerides in the SP3 format at a sampling interval of 15 minutes and the CACS precise satellite clock corrections in an NRCan proprietary format at an interval of 30 seconds were used to correct the satellite orbital and clock errors. In order to have a 1 second of estimation output rate in agreement with the observation data rate, an interpolation technique based on Chebychev polynomials was applied to calculate the satellite's positions and clock corrections at every epoch, and this interpolation technique has reportedly no degradation effect to the positioning accuracies [http://www.geod.nrcan.gc.ca/site/index_e/ products_e/cacs_e/clock_e/ clock_e.html].

The unknown parameters to be estimated include three position coordinates, a receiver clock offset, a tropospheric wet zenith path delay, and the ambiguity parameters of all visible satellites.

A sequential filter is used, where the parameters' information is carried on from epoch to epoch through the variance-covariance matrix.

## 5.2 Sequential Filter and its Implementation in PPP Processing

Different parameters have different varying characteristics between epochs. When applying sequential filter in PPP processing, an adjustment should be made on the parameter variance-covariance matrix to reflect this change.

Sequential filter in the least-squares process requires the treating of the parameters as pseudo-observables with the corresponding variance-covariance matrix as the observation

precision. The parameters, or the states of a system, are typically a vector of scalar random variables, and their variance-covariance matrix expresses the states' uncertainty. Each diagonal term of the matrix is the variance of a pseudo-observable, or the variable's mean squared deviation from its mean, and the square root is its standard deviation. The matrix's off-diagonal terms are the covariances that describe any correlations between pairs of variables. Then, the parametric observation equations for the real observables and the weighted parameters at epoch $i$ are represented as:

$$l_i = f(X);\ C_{li} \tag{5.1}$$

$$l_{X,i} = \hat{X}_{i-1};\ C_{l_{X,i}} = C_{\hat{X}_{i-1}} \tag{5.2}$$

where,

$l_i$ is the observation vector,

$C_{li}$ is the observation variance-covariance matrix,

$l_{X,i}$ is the vector of pseudo-observations of the parameters at epoch $i$,

$\hat{X}_{i-1}$ is the vector of parameter estimations at epoch $i-1$, and

$C_{l_{X,i}}, C_{\hat{X}_{i-1}}$ are the variance-covariance matrix of the pseudo-observations $l_{X,i}$ and parameter estimations $\hat{X}_{i-1}$ respectively.

The estimated parameters $\hat{X}_i$ at the epoch $i$ are then computed from

$$\hat{X}_i = \hat{X}_{i-1} - \left(A^T C_{l,i}^{-1} A + C_{l_{X,i}}^{-1}\right)^{-1} A^T C_{l,i}^{-1} w \tag{5.3}$$

where,

$A$ is the design matrix, which is expressed by

$$\mathrm{A} = \left.\frac{\partial f}{\partial X}\right|_{X=\hat{X}_{i-1}} \tag{5.4}$$

$w$ is the misclosure vector and has the following expression

$$w = f\left(X^0\right) - l \Big|_{\substack{X^0=\hat{X}_{i-1} \\ l=l_i}} = f\left(\hat{X}_{i-1}\right) - l_i \tag{5.5}$$

The corresponding variance-covariance matrix of the parameters is given as

$$C_{\hat{X}_i} = \left(A^T C_{l,i}^{-1} A + C_{l_{X,i}}^{-1}\right)^{-1} \tag{5.6}$$

And the residual vectors for real and pseudo observables respectively are:

$$\hat{V} = A\hat{\delta} + w \tag{5.7}$$

$$\hat{V}_X = \hat{\delta} \tag{5.8}$$

Treating the weighted station parameters as observables results in the computation of the a posteriori variance for the unit weight through the following equation:

$$\hat{\sigma}_0^2 = \frac{V^T C_{l_i}^{-1} V + V_X^T C_{l_{X,i}}^{-1} V_X}{r} \tag{5.9}$$

where $r$ is system redundancy.

### 5.2.1 Parameters' Variance Adjustment between Epochs

PPP post-processing usually includes four types of unknown parameters: the three-dimensional station coordinates, receiver clock offset, tropospheric wet zenith path delay, and carrier phase ambiguities. Therefore, to propagate the parameters' variance-covariance information from epoch $i$-1 to $i$, process noise $C\varepsilon_{\Delta t}$ as expressed in Equation (5.10) should be added according to the user's dynamics, receiver clock behaviour and atmospheric activity, which are shown in Equation (5.11).

$$C_{l_{X,i}} = C_{\hat{x}_{i-1}} + C\varepsilon_{\Delta t} \tag{5.10}$$

$$C\varepsilon_{\Delta t} = \begin{bmatrix} C\varepsilon(x)_{\Delta t} & 0 & 0 & 0 & 0 & 0 \\ 0 & C\varepsilon(y)_{\Delta t} & 0 & 0 & 0 & 0 \\ 0 & 0 & C\varepsilon(z)_{\Delta t} & 0 & 0 & 0 \\ 0 & 0 & 0 & C\varepsilon(dt)_{\Delta t} & 0 & 0 \\ 0 & 0 & 0 & 0 & C\varepsilon(zpd)_{\Delta t} & 0 \\ 0 & 0 & 0 & 0 & 0 & C\varepsilon(N^{j}_{(j=1,nsat)})_{\Delta t} \end{bmatrix} \tag{5.11}$$

In all instances ambiguity process noise $C\varepsilon(N^{\,j}{}_{(j=1,nsat)})_{\Delta t}$ equals to zero since the carrier-phase ambiguities remain constant over time when there is no cycle slip. In static mode, the user position is also constant and consequently $C\varepsilon(x)_{\Delta t} = C\varepsilon(y)_{\Delta t} = C\varepsilon(z)_{\Delta t} = 0$. In kinematics mode, it is increased as a function of user dynamics. The receiver clock process noise can vary as a function of frequency stability but is usually set to white noise with a large $C\varepsilon(dt)_{\Delta t}$ value to accommodate the unpredictable occurrence of clock resets. A random walk process

noise of $5mm/\sqrt{hour}$ is assigned to the zenith path delay $C\varepsilon(zpd)_{\Delta t}$ [Kouba and Héroux, 2000].

### 5.2.2 Model Performance Criteria

To evaluate the performance of two aforementioned PPP methods processed in a sequential filter, three criteria: model stability, estimation variance, and time of convergence, need to be analyzed separately. Each criterion demonstrates one aspect of a model's performance, and the combination of the three gives a whole picture of how well a model works.

Model stability refers to the estimation variation of unknown parameters between consecutive epochs due to the participation of new observations into the least-squares adjustment. Therefore, it measures how the chosen measurement variance influences the unknown parameters' determination (see Figure 5.1). A smaller variation in estimation over time would reflect greater stability of the estimation process. Model stability is a function of two stochastic parameters: the standard deviation (sigma value) for measurement precision, and the variance-covariance matrix for the unknown parameters. The disproportionate relationship between the two stochastic parameters would bring false variation to parameter estimation. In static processing, model stability can be investigated by comparing the estimations between the neighbouring epochs, and their statistic data can demonstrate how a model works in terms of model stability.

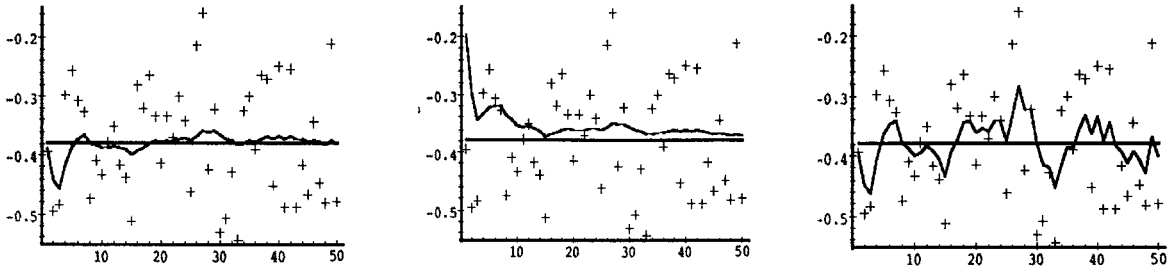


$\sigma^2 = (0.1)^2 = 0.01$ $\sigma^2 = 1$ $\sigma^2 = 0.0001$

The true value of the random constant $X = -0.37727$ is given by the solid line, the noisy measurements by the cross marks, and filter estimate by the remaining curve. The true measurement noise has a 0.1 RMS.

**Figure 5.1 Model Stability Simulation [Welch and Bishop, 2001]**

Estimation variance shows how big difference the estimates would be from the "true" value once the filter converges. It can be measured by the mean and variance of the converged values of a group of processing samples. Estimation variance can be described as positioning accuracy.

Time of convergence shows how long it takes a filter to reach a stable condition. In GPS kinematics applications with less demand for high accuracy, this factor can be the most important as such applications usually require a quick convergence in the beginning and quick re-convergence during the operation to overcome mechanical problems or loss of satellite lock.

The performance of an ideal model processed in a sequential filter would have fast convergence in the beginning of processing and stable estimates once convergence is reached. However, this good performance relies on the combination of several factors: high-precision measurements, the correct standard-deviation values depicting the precision of

measurements, and the correct variance-covariance information depicting the precision of unknown parameters.

## 5.3 Numerical Results: Model Stability Analysis

To test the stability of the proposed P1-P2-CP and the Traditional Models, and demonstrate their behaviour, a short processing period of 10 minutes is used for all the datasets collected at the eight CACS stations. After each 10 minutes, the filter is reset. Therefore, the generated plots can well demonstrate how both models work in term of model stability.

The following plots show the information related to station NRC1, where, during the testing period, the number of observed satellites ranges from 5 to 8, and the corresponding PDOP value varies from 0.6 to 1.1 as shown in Figure 5.2.

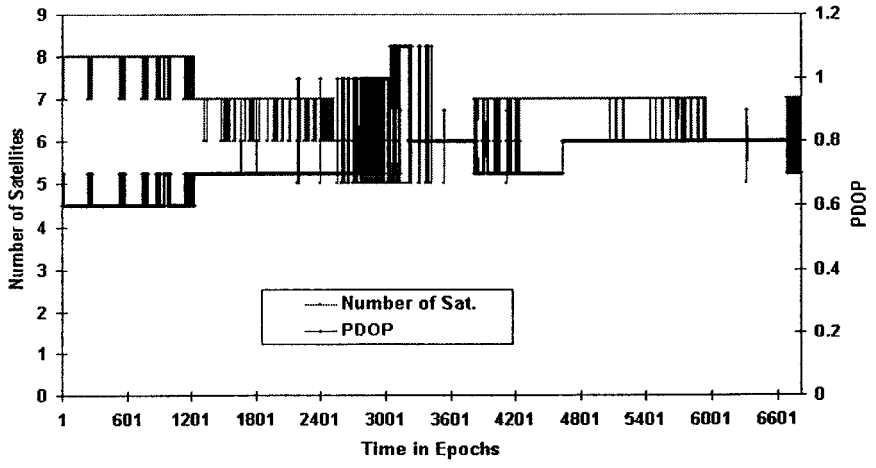


**Figure 5.2 Number of Observed Satellites and PDOP at NRC1**

Shown in Figures 5.3 through 5.5 are error variations in latitude, longitude, and height in twelve 10-minute processing samples for the station NRC1. The light (pink) colour lines represent the error change with the Traditional Model, while the dark lines (blue) are for the new P1-P2-CP Model. It can be clearly observed that the light colour lines have more frequent and larger variations. This less stable behaviour is indicative of the disproportional stochastic information of the Traditional Model while the variance adjustment procedure in P1-P2-CP Model can generate better stochastic information.

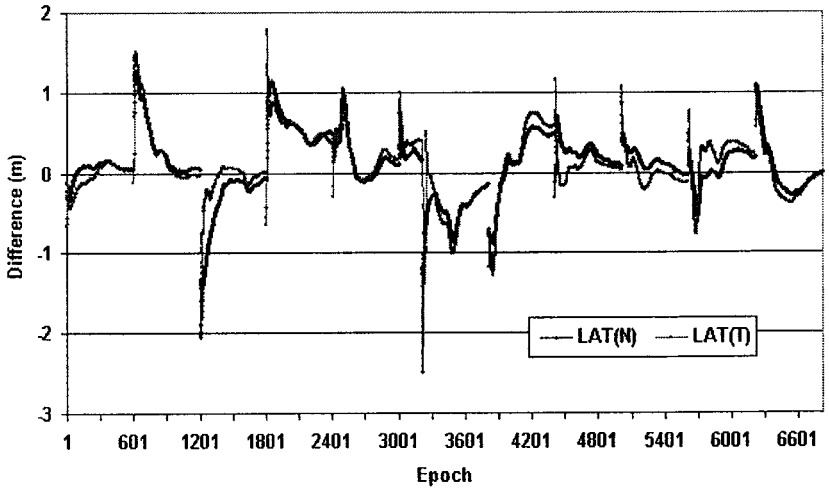


**Figure 5.3 Latitude Error of Twelve 10-minute Processing at NRC1**

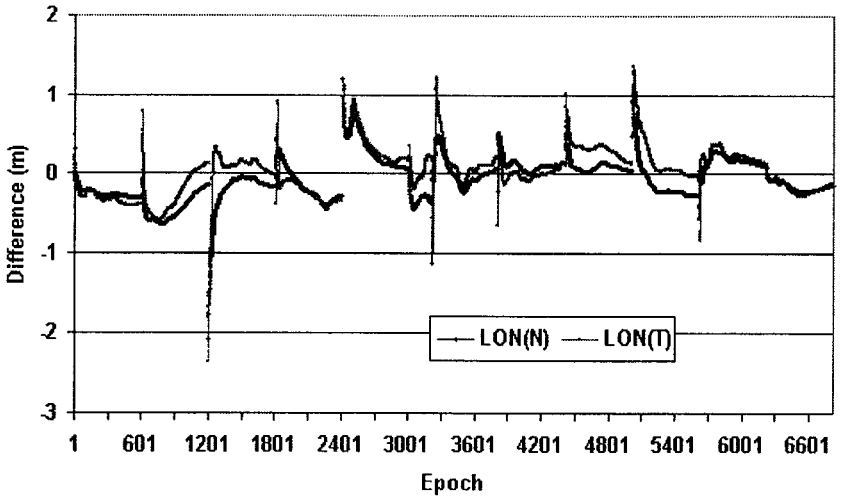


**Figure 5.4 Longitude Error of Twelve 10-minute Processing at NRC1**

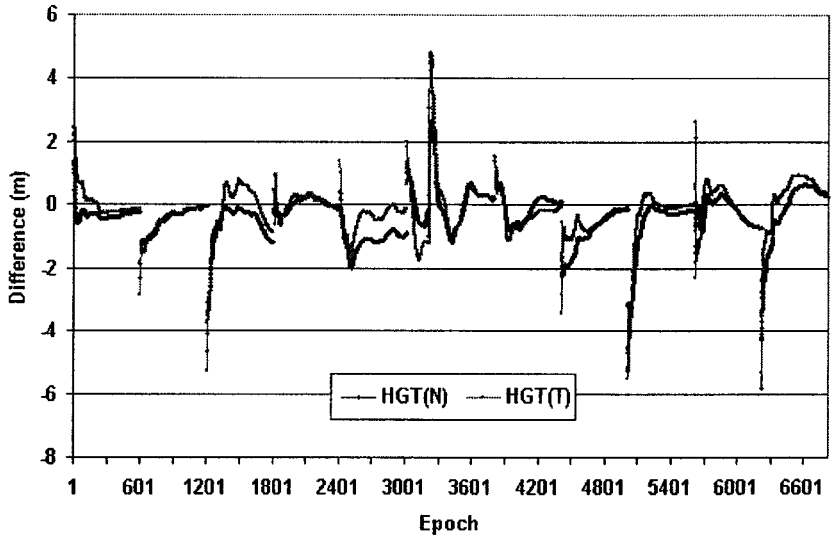


**Figure 5.5 Height Error of Twelve 10-minute Processing at NRC1**

Figure 5.6 shows the L1 and L2 ambiguity estimations for satellite PRN1. Compared with the positioning estimations in the above figures, the ambiguity estimations have similar variations. As the processing only includes the ten minutes' period, both position and

ambiguity estimations could not fully converge for some processing samples. However, it can be demonstrated from the results that the true value of PRN01 L1 ambiguity is within 130129308 and 130129310 cycles, and the L2 ambiguity is within 101399422 and 101399424 cycles.

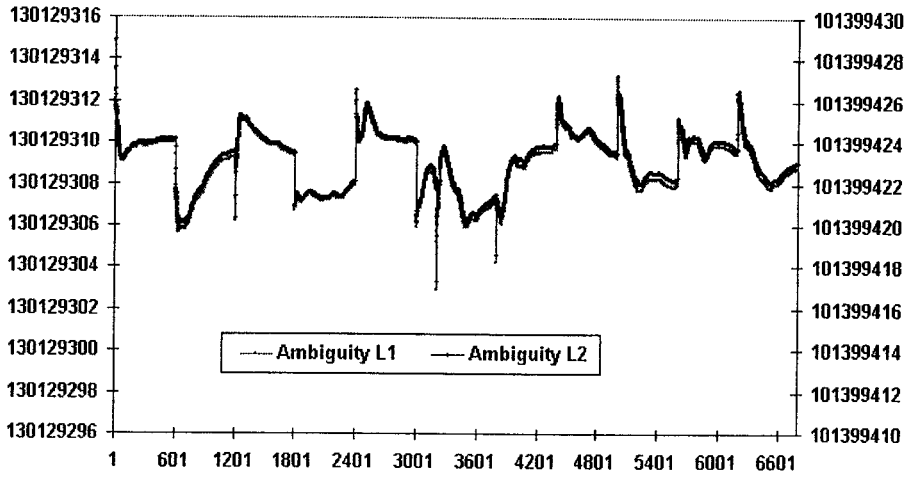


**Figure 5.6 Ambiguity Estimation of PRN01**

Model stability in static sequential filter processing can be investigated by comparing the positioning estimates between the neighbouring epochs. The variation mean and standard-deviation values can demonstrate how a model works in terms of model stability. Shown in Figure 5.7 are the differences in height from the 8 stations with a 10-minute sample for each station. The light-colour (pink) line represents the results with the new model, while the dark one (blue) refers to the traditional one. At the commencement of processing the measurement has too much weight on the parameters' estimation, the filter is more sensitive to the measurement noise, resulting in a bigger estimation variation. In order to reduce the influence of such big variation in the beginning of processing on the final calculation of the

mean and standard-deviation values, the first 100 epochs were removed from each sample, and the revised plots are shown in Figures 5.8 and 5.9 for the Traditional Model and the P1-P2-CP Model respectively.

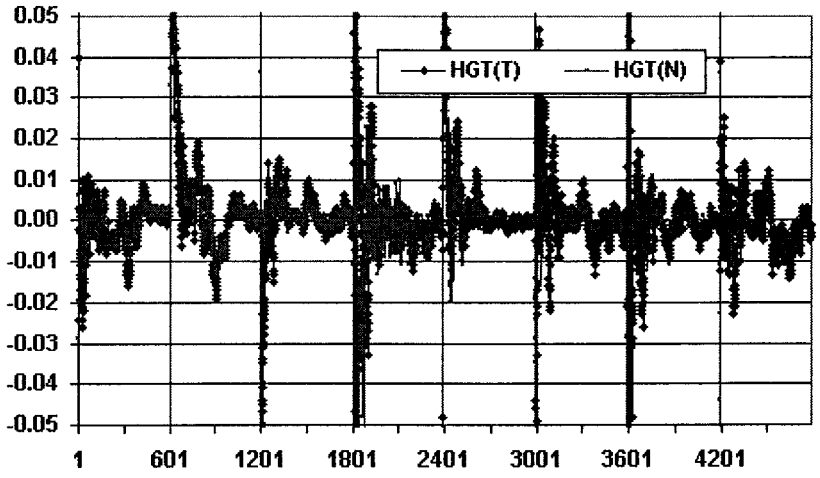


**Figure 5.7 Variation of Height Error between Neighbouring Epochs**

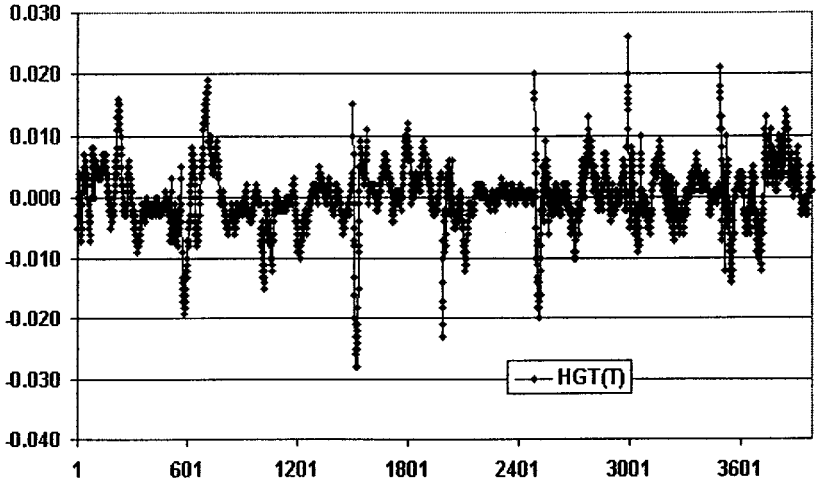


**Figure 5.8 Height Error Variation between Neighbouring Epochs with Traditional Model**

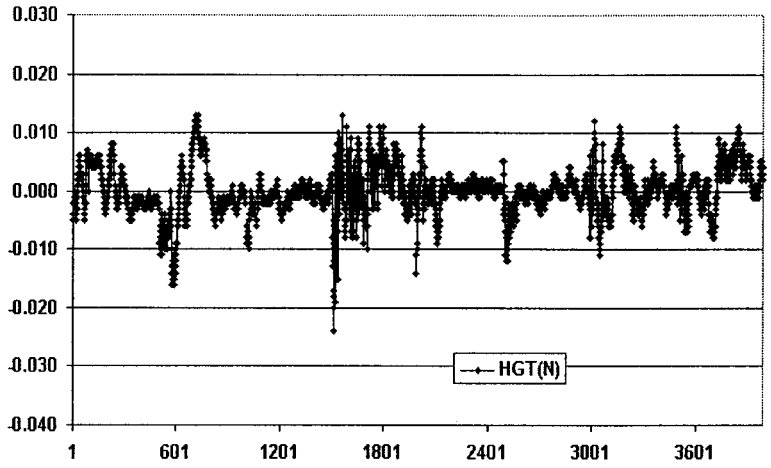


**Figure 5.9 Height Error Variation between Neighbouring Epochs with New Model**

Table 5.1 shows the mean and RMS values of the variations suggested in Figures 5.8 and 5.9. Absolute variation values are used. The results demonstrate the new model has smoother results and smaller variations.

**Table 5.1 Mean and RMS of Variation between Neighbouring Epochs**

| Statistics | Position Component | P1-P2-CP Model | Traditional Model |
|---|---|---|---|
| **Mean (meter)** | Latitude | 0.001 | 0.002 |
| | Longitude | 0.001 | 0.001 |
| | Height | 0.003 | 0.004 |
| **RMS (meter)** | Latitude | 0.002 | 0.002 |
| | Longitude | 0.001 | 0.001 |
| | Height | 0.004 | 0.005 |

## 5.4 Estimation Variance and Time of Convergence Analysis

Estimation variance shows how big difference the estimate is from the "true" value once the filter converges. It can be measured by the mean and RMS of the convergence values of a group of processing samples. Time of convergence shows how long it takes a filter to reach a stable condition.

To display these two features, one-hour processing is necessary as an average of half an hour convergence time is a common occurrence for precise point positioning. A total of 36 one-hour datasets from the eight stations were processed. For the analysis of the estimation variance between the two models, the last-epoch error results of each one-hour sample are treated as the converged coordinate errors, and the mean and RMS of the total 36 samples are calculated. Similarly, the mean and RMS for the time of convergence are calculated and compared between the two models.

The following plots show the results related to the station PRDS. Figure 5.10 displays the number of observed satellites and its changes over the testing period. The maximum satellite number is nine, but in some epochs, there is only one valid satellite for the least-squares adjustment. The corresponding PDOP value also shows large variations. In order to better observe the satellite number change over time, Figure 5.11 shows the information of the first-hour – a zoomed plot of Figure 5.10. The number of observed satellites in the first hour ranges mostly from 5 to 7. In some epochs, the number drops to 4, resulting in a big increase

of the PDOP value. The number of valid satellites equals to one in only one epoch for this first hour data sample.

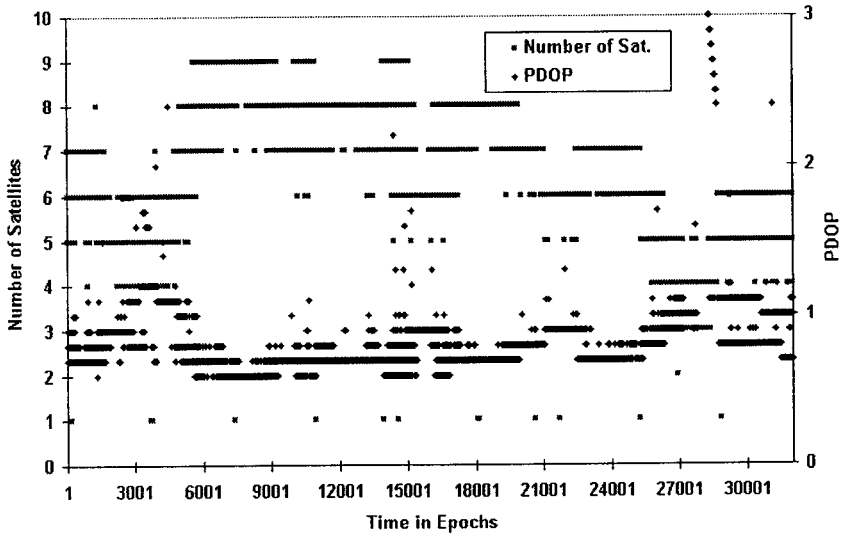


**Figure 5.10 Number of Observed Satellites and PDOP at PRDS**

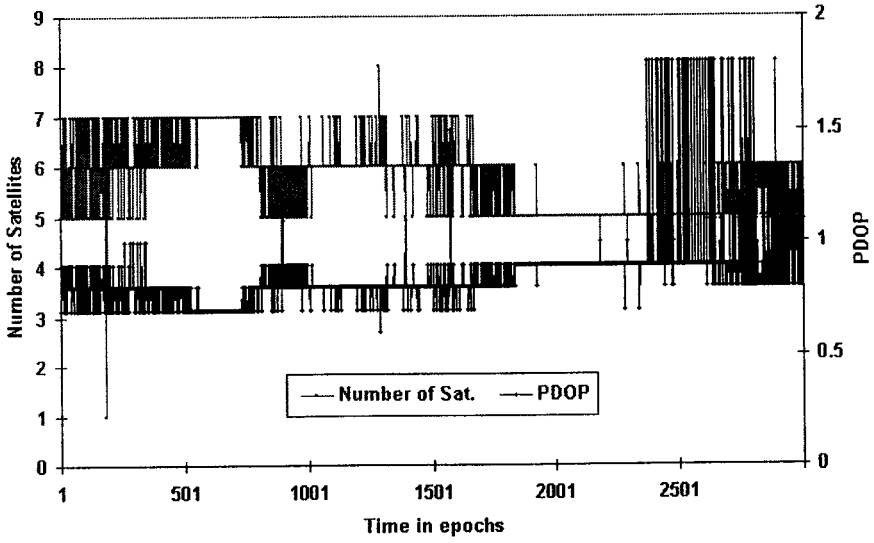


**Figure 5.11 Number of Observed Satellites and PDOP in 1st Hour**

Shown in Figures 5.12 through 5.14 are error trends in latitude, longitude, and height in 9 one-hour processing samples for the station PRDS. The light-colour (pink) lines represent the error changes with the Traditional Model, while the dark ones (blue) refer to the new P1-P2-CP Model. Most samples perform fairly well with small convergence errors, but the 8$^{th}$ and 9$^{th}$ samples converge to comparatively large non-zero values for both models. And with the Traditional Model, the 2$^{nd}$ sample hour also converges to a large value, especially in the longitude component. The reason for large non-zero converging will be discussed later in this section. In order to demonstrate positioning error changes after one-hour processing, Figure 5.15 shows the coordinate errors in a 9-hour processing using the same dataset with P1-P2-CP Model, which are used as reference results. The final converged coordinate errors are – 0.009m, -0.102m, and 0.029m for latitude, longitude and height respectively, which are in agreement with the PPP error budget as discussed in the PPP processing methods.

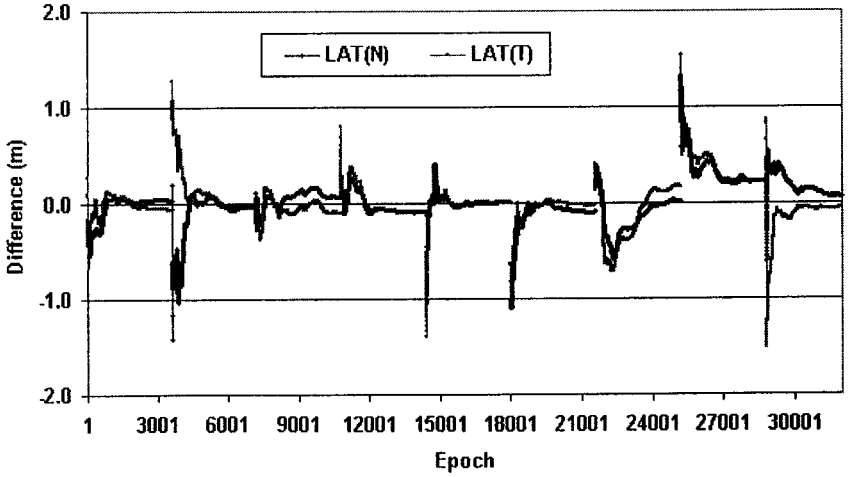


**Figure 5.12 Latitude Error of Nine 1-hour Processing at PRDS**

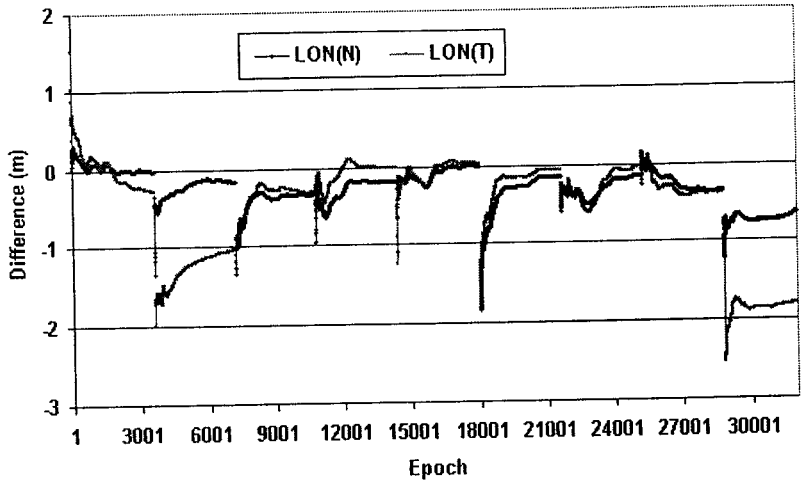


**Figure 5.13 Longitude Error of Nine 1-hour Processing at PRDS**

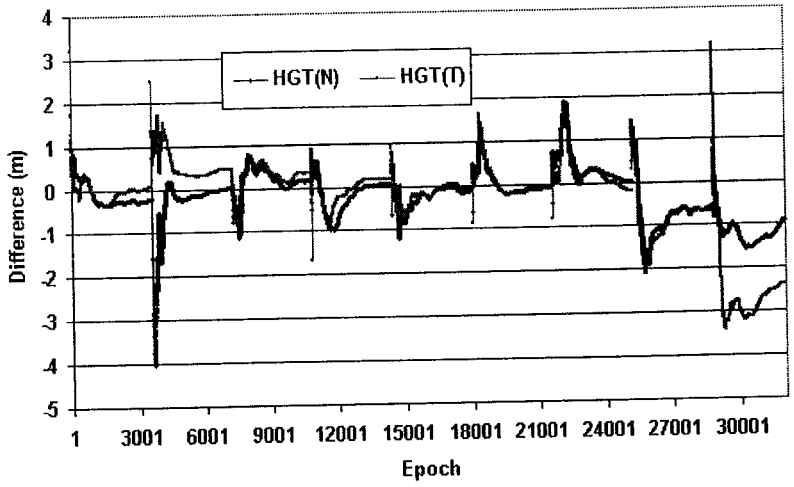


**Figure 5.14 Height Error of Nine 1-hour Processing at PRDS**

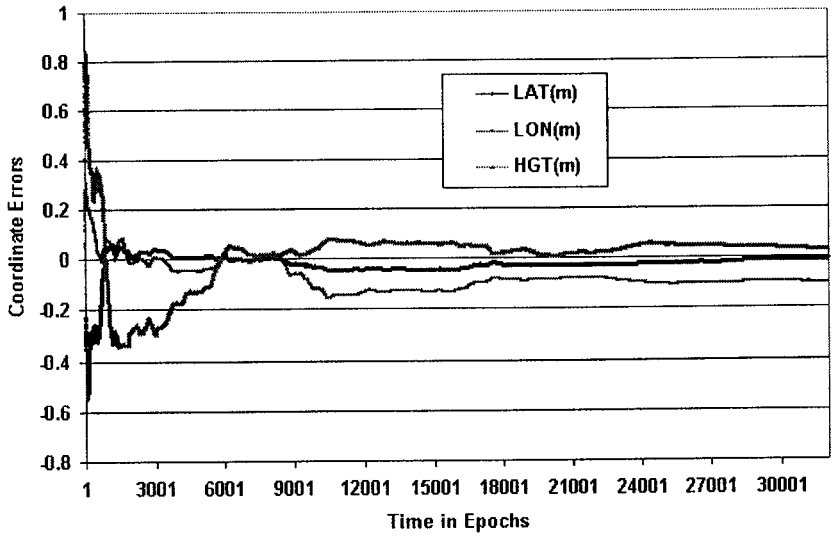


**Figure 5.15 Coordinate Errors of a 9-hour' Processing at PRDS**

Figures 5.16 shows the receiver clock-offset estimation with P1-P2-CP Model in 9 one-hour processing samples for the station PRDS, where an atomic clock was installed. Usually atomic clock offset is in a very stable variation, such as linear change. For comparison, Figure 5.17 shows the receiver clock-offset estimation with P1-P2-CP Model in a 9-hour processing, which can be treated as the receiver clock true variation. Comparison between these two figures demonstrates that the clock-offset estimations in the one-hour samples 8 and 9 went away from the supposed-to-be track. This irregular change matches the wrong convergence of positioning estimations for these two processing samples.

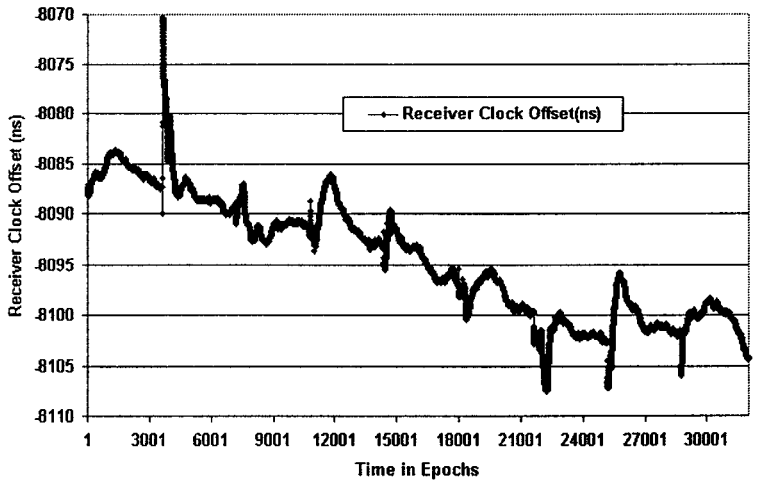


**Figure 5.16 Receiver Clock Offset Estimation in Nine 1-hour Processing**

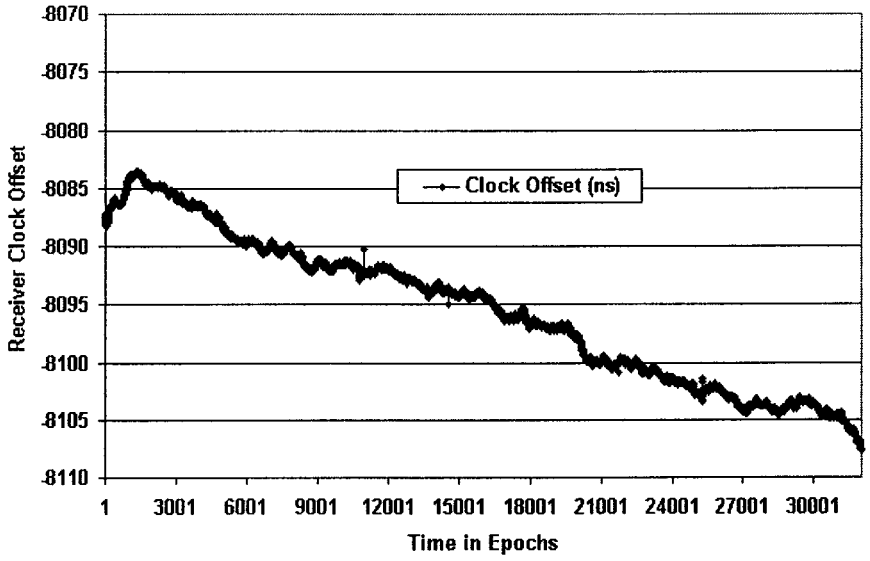


**Figure 5.17 Receiver Clock Offset Estimation of a 9-hour' Processing at PRDS**

In order to find out what causes the incorrect convergence, results from hour 9 are analyzed. Figure 5.18 shows the number of observed satellites and the corresponding PDOP values. An average of 5.3 satellites contributes to the least-squares adjustment for this one-hour processing. With the new P1-P2-CP Model, fifteen observations can be obtained when five

satellites are observed. However, the number of unknowns is 15 too, including the five fundamental parameters (X, Y, Z, Trop and receiver clock offset), and the 10 ambiguities. With the Traditional Model, the number of unknowns and the number of observations are both 10 when five satellites are observed. Therefore, the unmodeled errors cannot be compensated through the least-squares adjustment, and fully absorbed into the parameters' estimation. As seen in Figure 5.10, compared with the sample hours 8, 9, other samples have a higher average number of observed satellites.

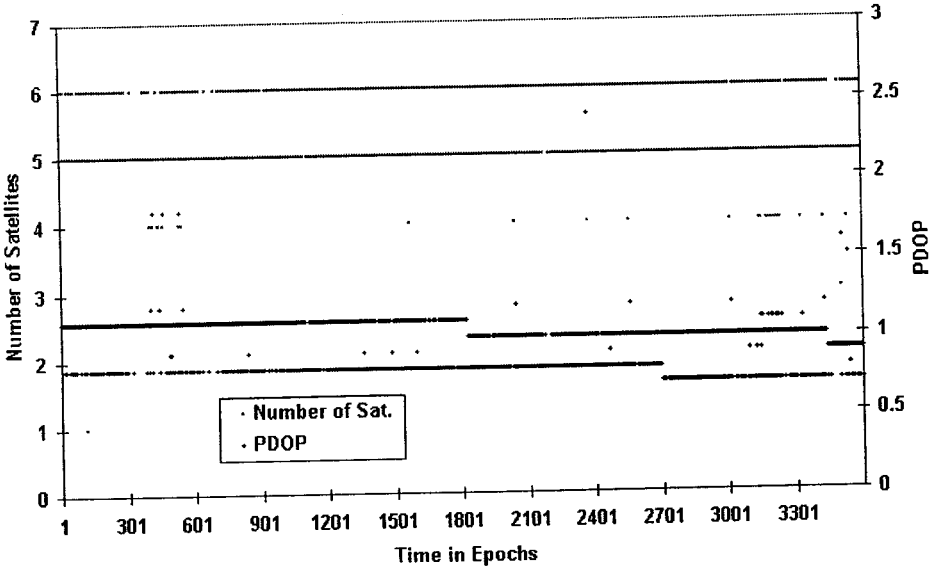


**Figure 5.18 Number of Observed Satellites and PDOP in 9th Hour**

Figures 5.19 and 5.20 display the converged errors in latitude, longitude, and height of all the 36 samples for the traditional and the new models respectively. There are four out of 36 samples converging to the comparatively large non-zero values when the Traditional Model is used, while only one sample fails when the new model is applied.

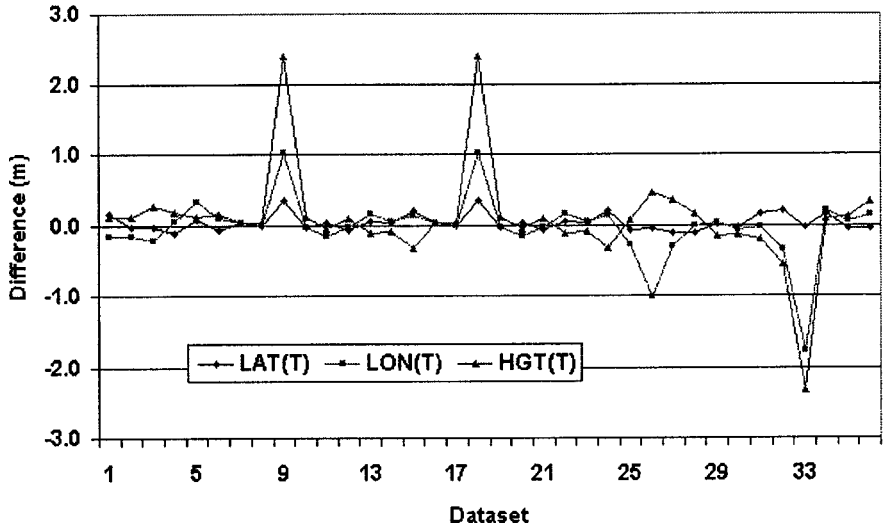


**Figure 5.19 Converged Position Errors with Traditional Method in 1-hour Processing**

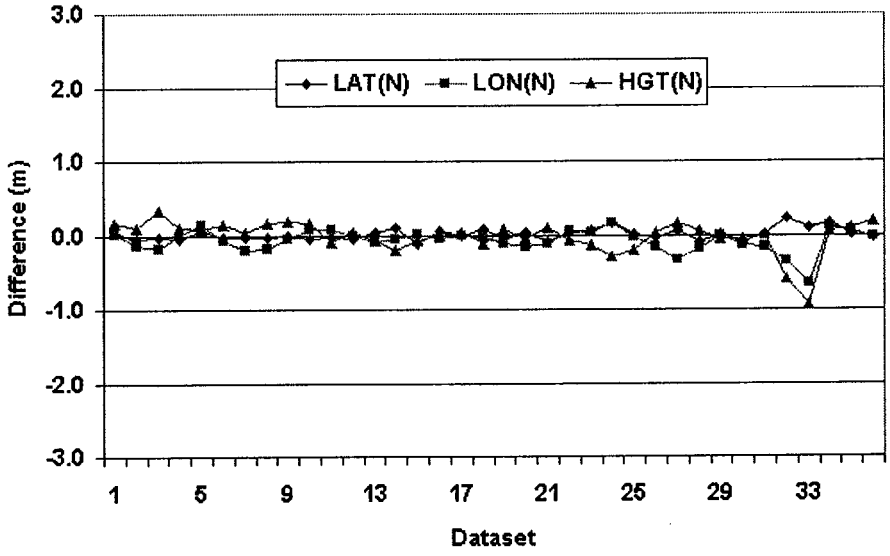


**Figure 5.20 Converged Position Errors with P1-P2-CP Method in 1-hour Processing**

Table 5.2 gives the MEAN, SIGMA, RMS of the errors shown in Figures 5.19 and 5.20. Absolute error values are used to calculate the MEAN. As for the estimation variance, the new model has smaller values on mean, sigma, and RMS than the Traditional Model. The improvements on the mean factor are 33%, 49%, and 57% for the latitude, longitude, and height respectively.

**Table 5.2 Mean, STD, and RMS of Position Error after 1-Hour Processing**

| Parameter | Position Component | P1-P2-CP | Traditional | Improvement Ratio |
|---|---|---|---|---|
| Mean (m) | Latitude | 0.059 | 0.088 | 33% |
| | Longitude | 0.121 | 0.237 | 49% |
| | Height | 0.147 | 0.346 | 57% |
| Sigma (m) | Latitude | 0.046 | 0.082 | 44% |
| | Longitude | 0.122 | 0.373 | 67% |
| | Height | 0.172 | 0.622 | 72% |
| RMS (m) | Latitude | 0.074 | 0.120 | 38% |
| | Longitude | 0.172 | 0.442 | 61% |
| | Height | 0.226 | 0.711 | 68% |

To define convergence time for a filter may vary from user to user. It largely depends on what accuracy is required. In this paper, the convergence time is defined as when the coordinate converged errors are less than 40cm, and is described in the unit of seconds or epochs. Figure 5.21 shows the convergence time in the unit of epochs for all the 36 processing samples, whose mean and RMS values are given in Table 5.3. There is a slight

improvement for the P1-P2-CP Model over the traditional one in terms of the convergence time factor.

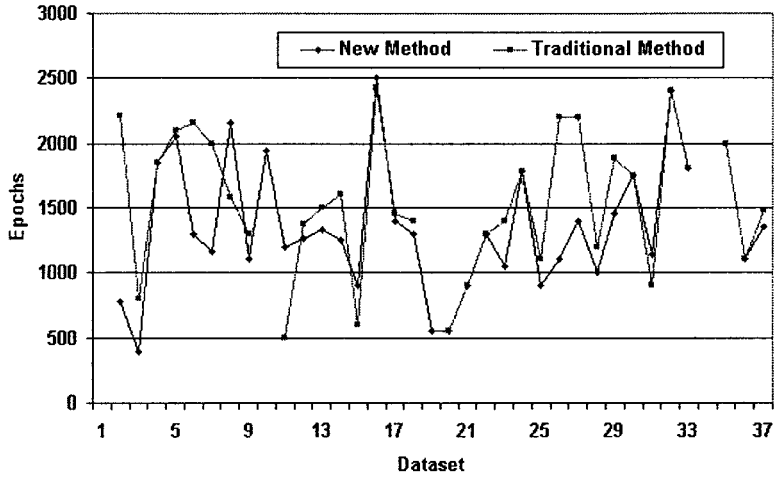


**Figure 5.21 Convergence Time of 36 1-hour Sample Datasets**

**Table 5.3 Mean and Variance of Convergence Time with Two Methods**

| Parameter | New | Traditional |
|---|---|---|
| Mean | 1350 | 1550 |
| Variance | 500 | 530 |

Processing convergence can also be observed through ambiguity estimations. Figures 5.22 to 5.24 demonstrate ambiguity estimations with the P1-P2-CP Model for satellites PRN1, PRN27, and PRN28 over one-hour processing samples. Usually after approximately half an hour, ambiguity estimation can reach a convergence value. Also clearly seen is that those one-hour samples in the centre of the plots perform much better. That is because the error

residual of tropospheric effects due to the mapping function error is smaller during that period with high satellite elevation angle. Figures 5.25 and 5.26 show the variation of elevation angle for satellites PRN 27 and 28, indicating a bigger elevation angle in the middle of satellite visibility period. As a result, a conclusion can be made that low-elevation angle still brings big uncertainty to the tropospheric estimation due to the mapping function error although the tropospheric wet zenith path delay is treated as an unknown parameter. Figures 5.27 to 5.29 also demonstrate ambiguity estimation with the P1-P2-CP Model for satellites PRN1, PRN27, and PRN28 over several hours of processing.

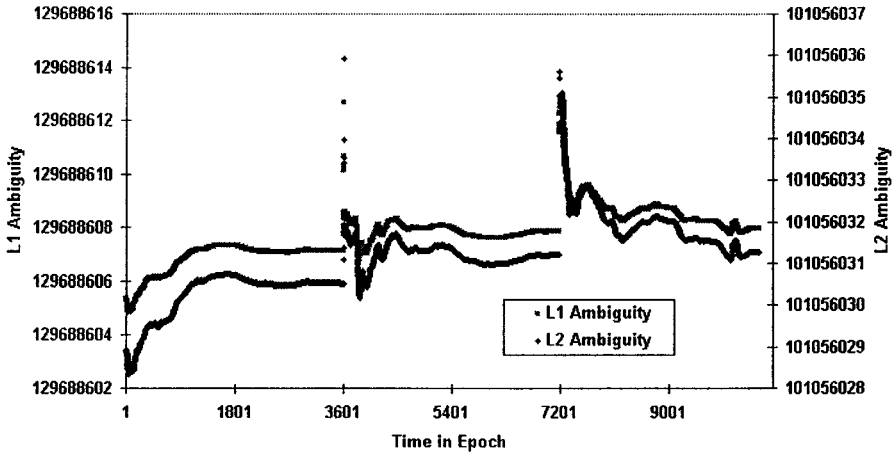


**Figure 5.22 Ambiguity Estimation of PRN01 from Hour 1 to Hour 3**

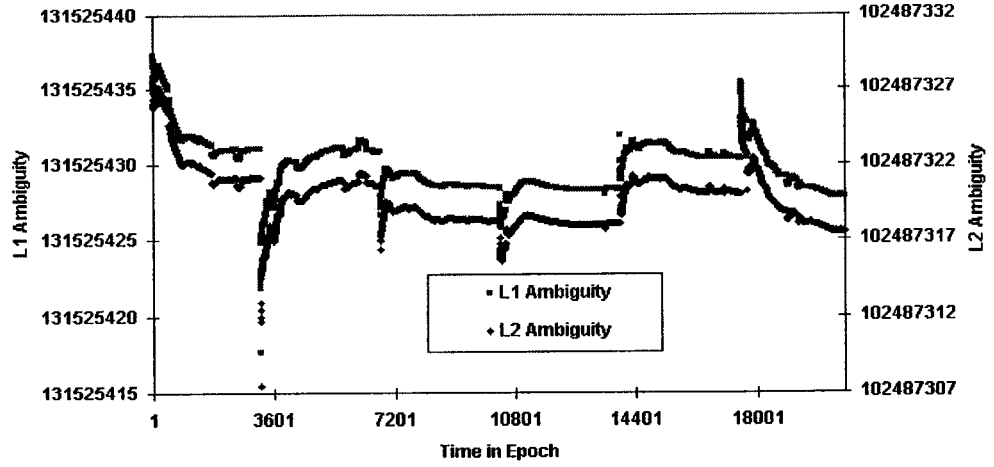


**Figure 5.23 Ambiguity Estimation of PRN27 from Hour 1 to Hour 6**

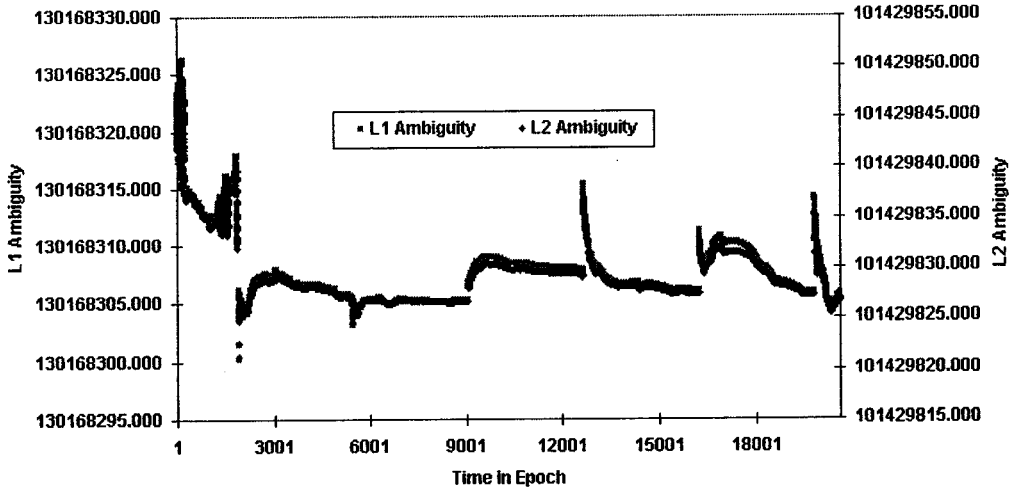


**Figure 5.24 Ambiguity Estimation of PRN28 from Hour 2 to Hour 8**

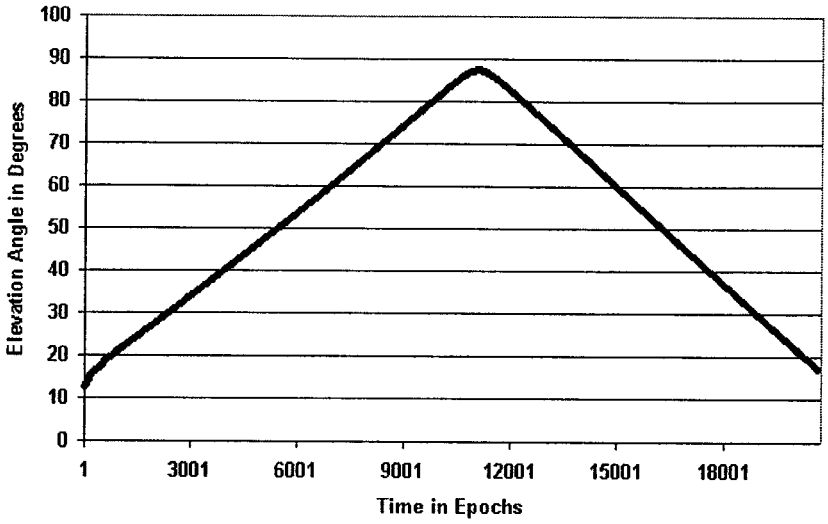


**Figure 5.25 PRN27 Elevation Angle from Hour 1 to Hour 6**

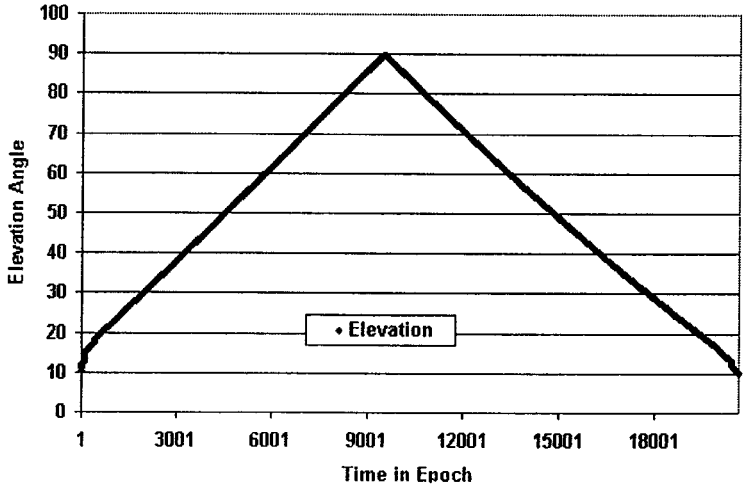


**Figure 5.26 PRN28 Elevation Angle from Hour 2 to Hour 8**

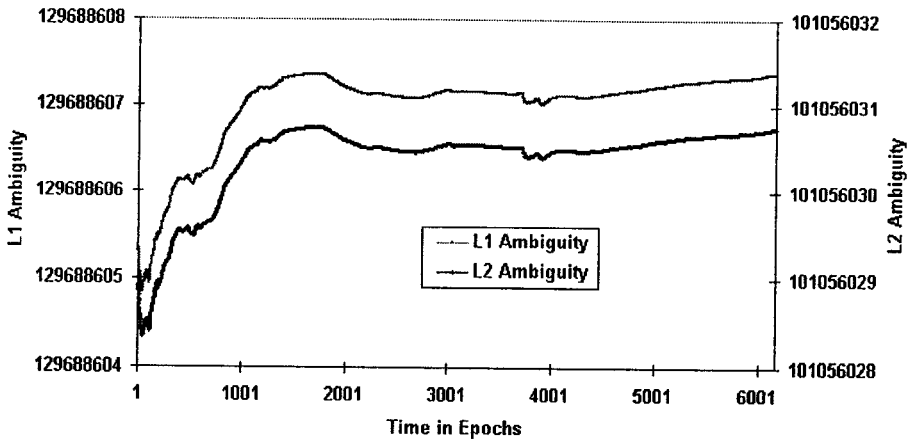


**Figure 5.27 Ambiguity Estimation of PRN01**

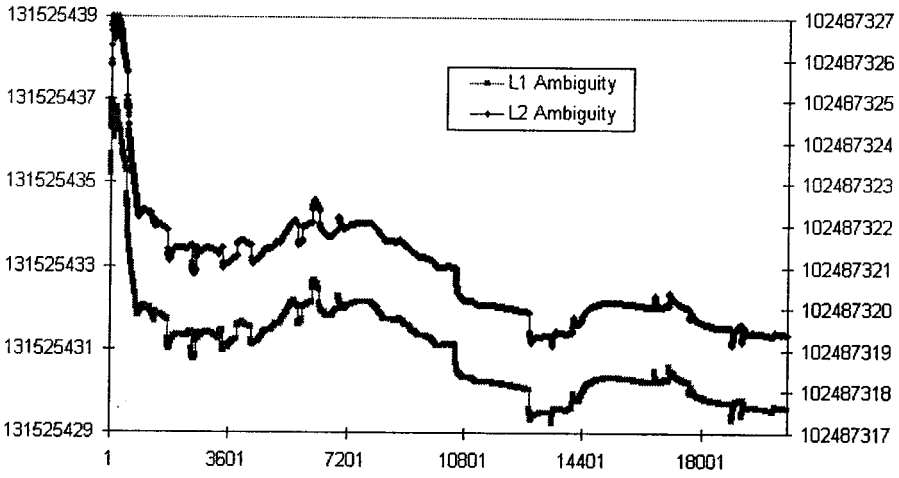


**Figure 5.28 Ambiguity Estimation of PRN27**

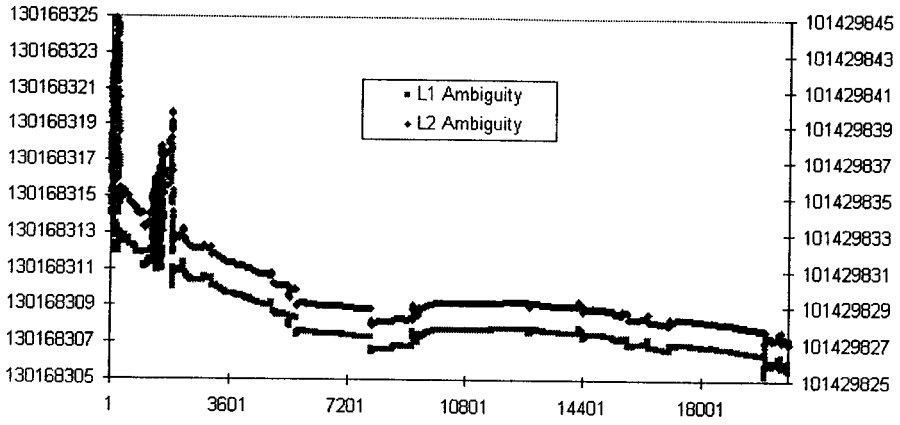


**Figure 5.29 Ambiguity Estimation of PRN28**

For comparison, Figures 5.30 and 5.31 demonstrate ambiguity estimations with the Traditional Model for satellites PRN1 and PRN27 over one-hour processing samples. The Y-axis is in the unit of metres instead of cycles as shown in the plots for the P1-P2-CP Model. The ambiguity estimation in these plots represents the correction to the initial value that is calculated from code and phase observations. After each one-hour processing, the initial value is reset. Approximately 30 minutes is needed for the ambiguities to converge to within 1 cycle with the Traditional Model, which is in agreement with the positioning results.

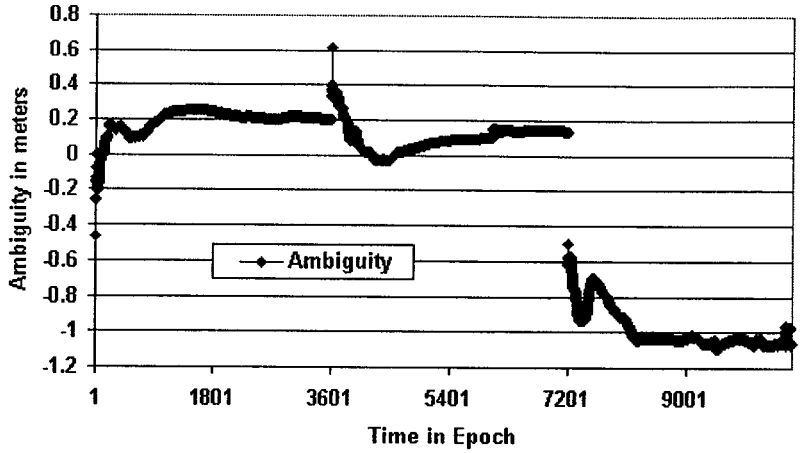


**Figure 5.30 Ambiguity Estimation of PRN01 from Hour 1 to Hour 3**

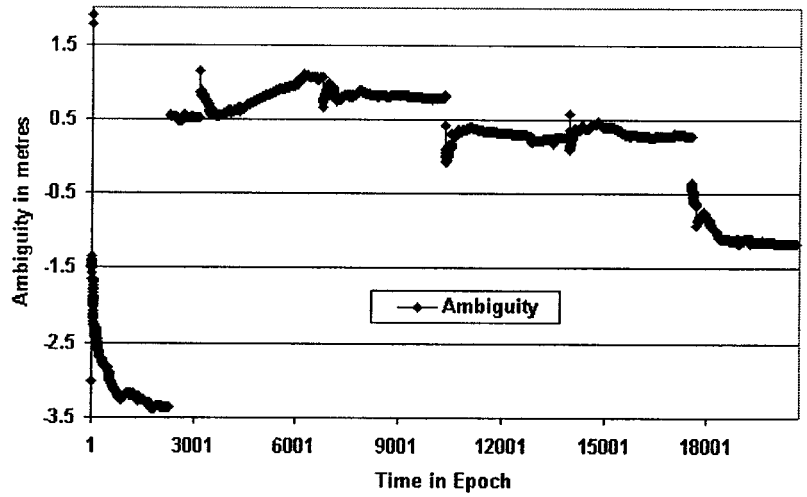


**Figure 5.31 Ambiguity Estimation of PRN27 from Hour 1 to Hour 6**

To summarize, the proposed P1-P2-CP Model has smoother results, smaller estimation variance, and slightly faster convergence, and as a result, has better overall performance than the Traditional Model.

## 5.5 Numerical Results of Ambiguity Partial-Fixing

One conclusion from the static processing is that there is not much improvement on the convergence time with the use of P1-P2-CP Model as compared to the Traditional Model. That is because the accumulation of variance-covariance information does require a specific period of time. However, the convergence time may be the most important factor that many GPS users care about when carrying out their positioning or navigation tasks. A method that can significantly decrease convergence time will be more advantageous. Just like the ambiguity searching and fixing approach used in the double differential GPS (DDGPS) for faster convergence, ambiguity searching can also be carried out with the new P1-P2-CP Model in precise point positioning to achieve a faster converged positioning solution.

A partial ambiguity fixing method was investigated in this research, where ambiguity searching focuses only on one satellite with the smallest variance at a time. The first step to carry out this procedure was to check the smallest ambiguity variance, if the variance falls below a predefined threshold value, a partial ambiguity searching for the satellite with that variance is activated. Second, several criteria discussed in the previous chapter are used to check if there is a fixed solution. Third, if there is no valid solution for all the ambiguity pairs, the searching process ends with the float estimates moving onto the next epoch. In the case that a partial fixing is made, the corresponding ambiguities will keep the fixed value in subsequent epochs.

The numerical computations are based on the data collected at an IGS reference station CHUR on August 15, 2001.

First, one-hour non-stop processing was made, where the converged results were used as the reference value. Figures 5.32 and 5.33 show the processing coordinate errors and receiver clock offset respectively. The converged positioning errors in three dimensions are within one decimetre. The precision of clock offset was maintained within one nanosecond as receiver was aided by an outer accurate atomic clock.

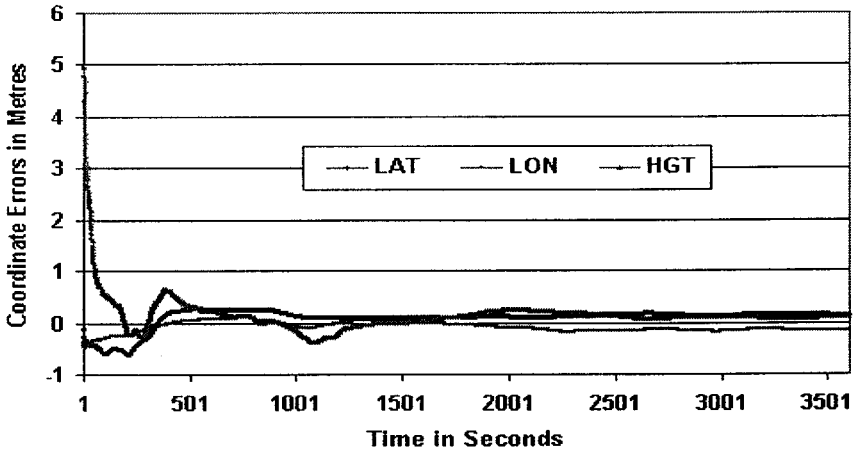


**Figure 5.32 Coordinate Errors in a 1-hour Processing**

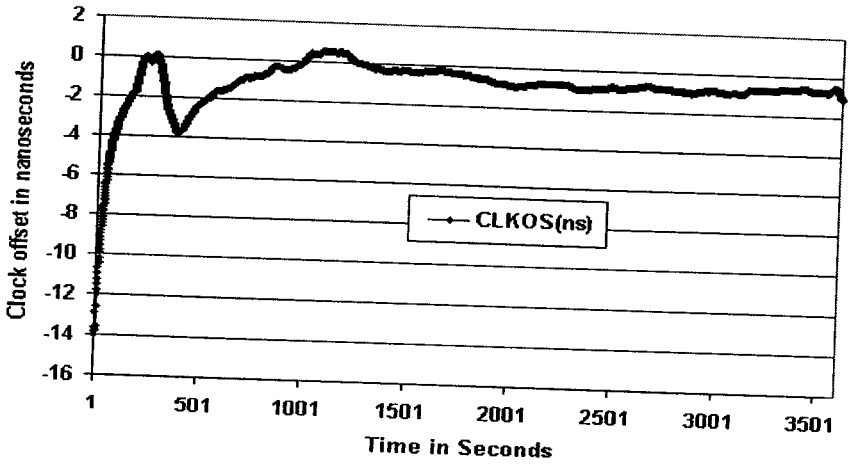


**Figure 5.33 Receiver Clock offset in a 1-hour Processing**

Second, short-period float-solution processing with 3-minute each was made in order to demonstrate the convergence performance of float-solution. Shown in Figures 5.34 and 5.35 are coordinate errors and receiver clock offset respectively in six processing samples. Ambiguity estimations for three satellites are shown in Figures 5.36 through 5.38.

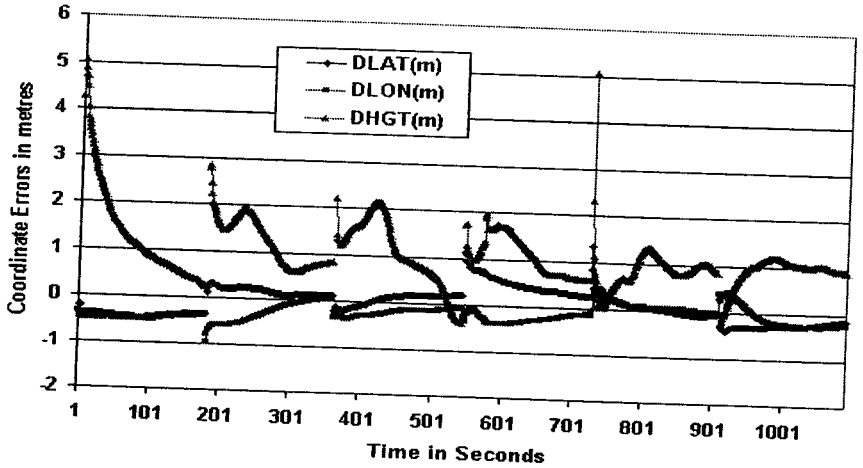


**Figure 5.34 Coordinate Errors in Six 3-minute Processing**

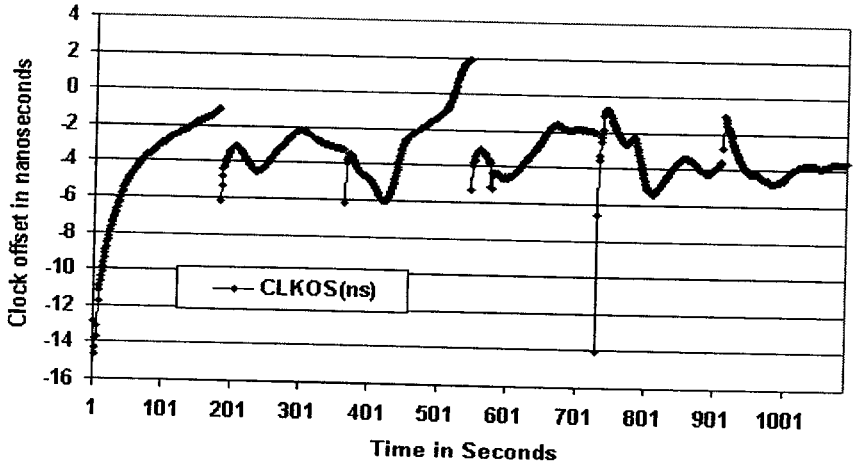


Figure 5.35 Receiver Clock Offset in Six 3-minute Processing

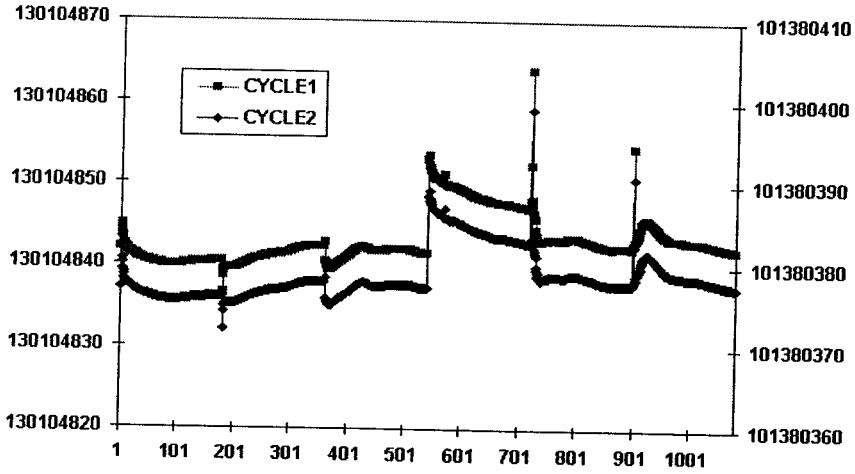


Figure 5.36 PRN01 Ambiguity Estimation

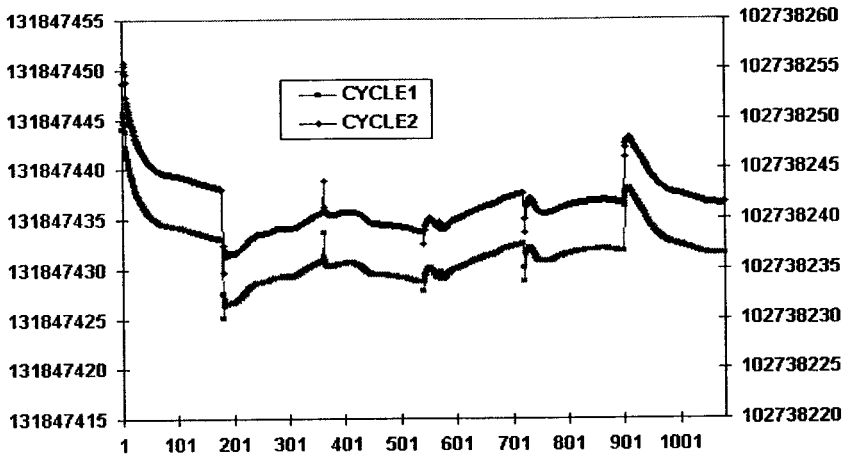


**Figure 5.37 PRN27 Ambiguity Estimation**

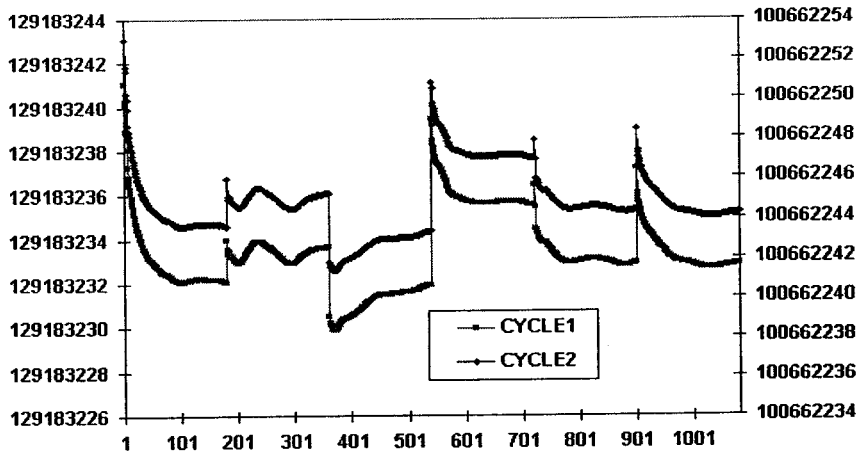


**Figure 5.38 PRN31 Ambiguity Estimation**

The objective of showing the 3-minute float-solution processing samples is to compare it with the pseudo-fixing results shown in the following. As in Figure 5.34, the height errors are usually still around one metre after three minutes, which is in accordance with 3 ~ 4 nanoseconds clock error in Figure 5.35. Ambiguity estimates between different processing might be apart from 5 cycles as shown in Figures 5.36 through 5.38.

Third, the partial pseudo-fixing method was applied to the same six 3-minute datasets and their results are shown in the following plots. The ambiguity sigma threshold value was set to 0.5 in order to reduce the searching range. Shown in Figures 5.39 and 5.40 are the position errors and receiver clock offset respectively. Results show that after approximately 60 epochs, the partial ambiguity fixing process was activated. Ambiguities for six satellites were searched and fixed in the subsequent six consecutive epochs. There is a clear change with coordinate errors and clock-offset estimations when the ambiguities start to fix, and the estimations are converged once the fixing is complete. The fixed solution has a precision of several decimetres for all coordinate components. As compared with Figures 5.34 and 5.35, it is clear that pseudo-fixing can accelerate convergence, but in the long run the float solution has a better positioning accuracy as shown in Figure 5.32.

Figures 5.41 through 5.43 show the ambiguity estimations for three observed satellites. It is clearly observed that ambiguities for each processing are not fixed to the same value. In some cases, the difference could be up to 5 cycles. That indicates that the criterion of using the a posteriori variance factor is not enough to determine the correct fixed ambiguity, other criteria should be developed in order to make ambiguity fixing more successful.

Although ambiguity is not fixed to the correct value, the fixed solutions are still improved. How far the fixed ambiguity is from the true value is reflected by the positioning errors.

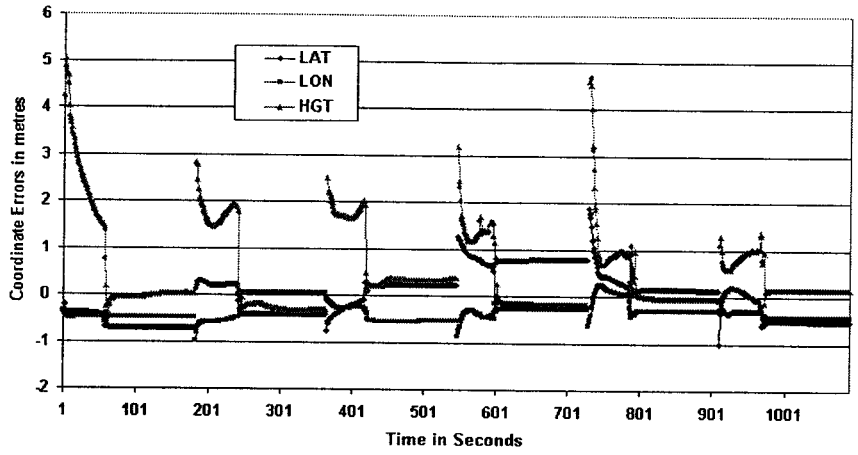


**Figure 5.39 Coordinate Errors in Six 3-minute Processing**

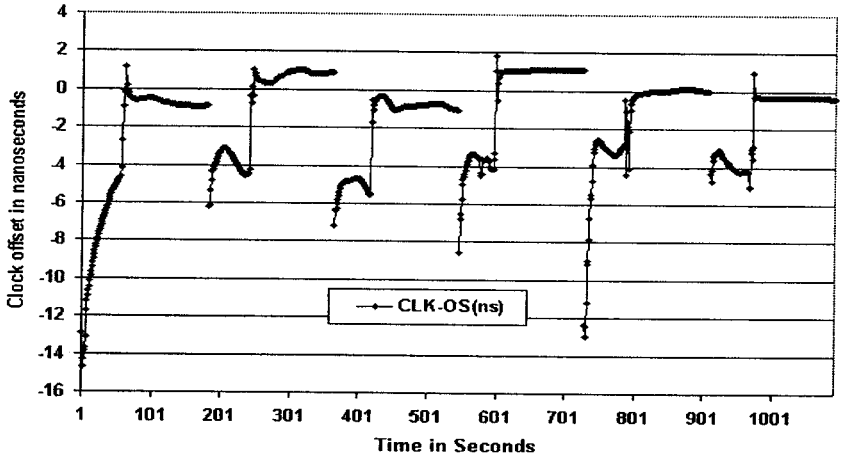


**Figure 5.40 Receiver Clock Offset in Six 3-minute Processing**

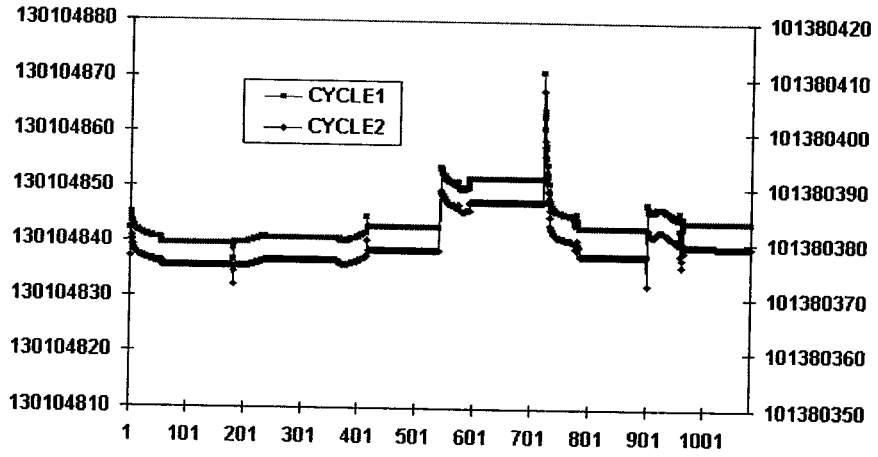


**Figure 5.41 PRN01 Ambiguity Estimation**

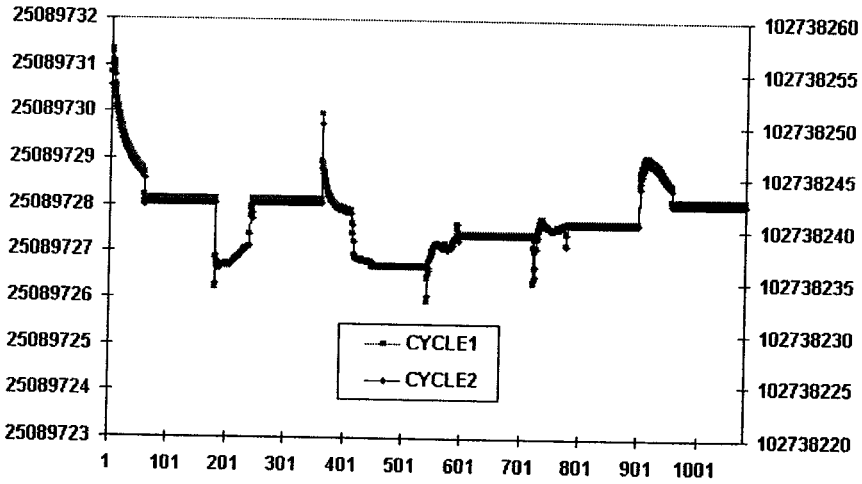


**Figure 5.42 PRN27 Ambiguity Estimation**

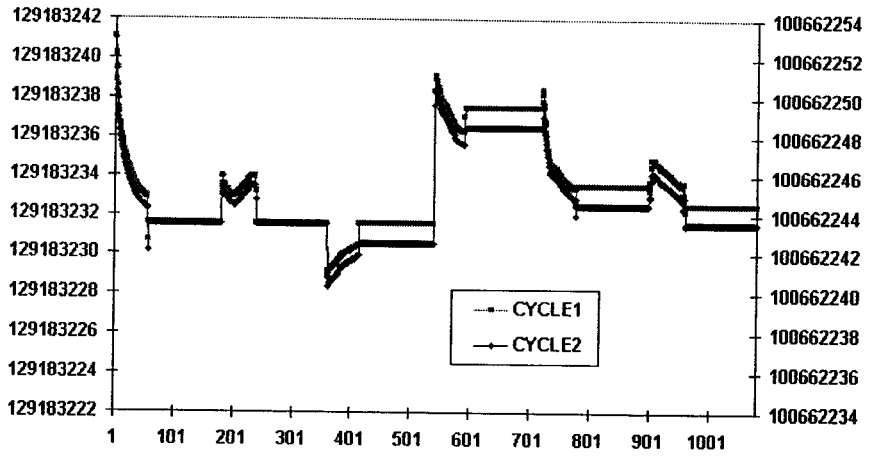


**Figure 5.43 PRN31 Ambiguity Estimation**

# CHAPTER 6

# NUMERICAL RESULTS AND ANALYSIS: KINEMATICS PROCESSING

The objectives of PPP kinematics processing are two-fold: 1) to assess the convergence time in the pure kinematics mode, and 2) to assess the obtainable kinematics positioning accuracy.

Section 6.1 gives data description while the kinematics results and their analyses are presented in Section 6.2.

## 6.1 Data Description

In this research, tests in kinematics processing were made with the same datasets collected at six CACS stations. Sequential filter was applied, where the positioning solution was determined at 1Hz without any constraints on the receiver's motion to simulate a pure kinematics situation. Therefore, such processing is completely insensitive to the dynamics of the user. Information for ambiguity unknowns was accumulated and carried on from epoch to epoch through the variance-covariance matrix as ambiguity maintains constant if no cycle-slip occurs.

The processing result analyses include the position error and the estimation of tropospheric effects. Analysis on model performance is made with regards to the time of convergence, and model estimation stability expressed by mean, variance, and RMS values once convergence is reached.

## 6.2 Analysis of Float Solutions

The following plots demonstrate the variations of position errors in latitude, longitude, and height for the six stations. A non-stop processing is carried out with several hours of continuous data in order to evaluate the model's stability in kinematics situation.

The following processing all includes 8~10 hours of results. The x-axis is the processing time in unit of hours. The starting time of all processing is set to hour 0, but only the converged results are displayed. The RMS values of three coordinate components are also shown in the plots. Shown in Figure 6.1 is a 9-hour long processing for the station CHUR, where the first hour is the estimation converging period and therefore, not shown in the plot. The converged results (from hour 2 to hour 9) have RMS values of 5 cm, 3 cm, and 8 cm for latitude, longitude, and height respectively. Similarly, Figures 6.2 to 6.6 shows the results for the other five stations.

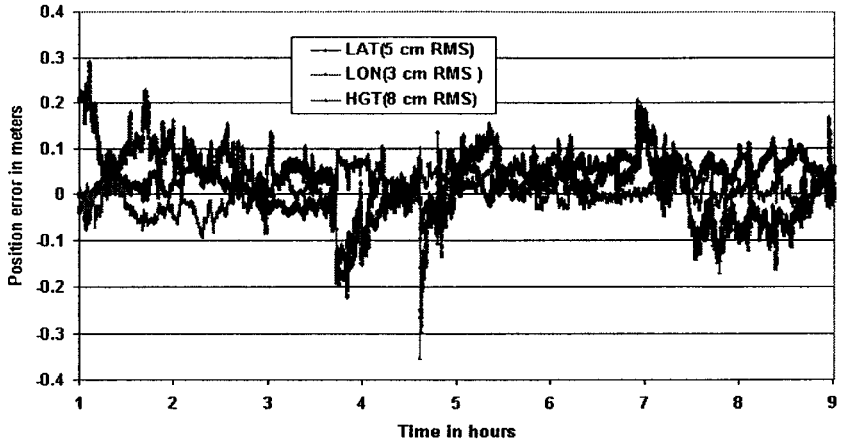


**Figure 6.1 Results of a 9-hour 1-Hz Kinematics Processing at Station CHUR**

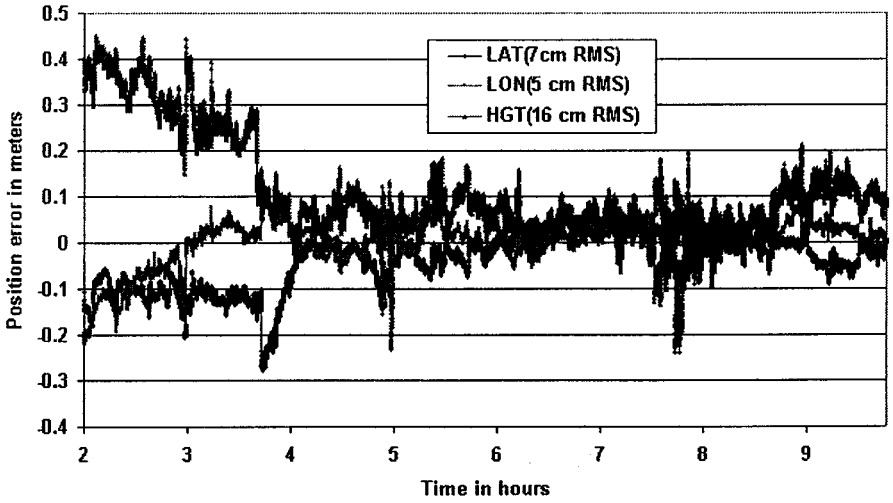


**Figure 6.2 Results of a 10-hour 1-Hz Kinematics Processing at Station DRA2**

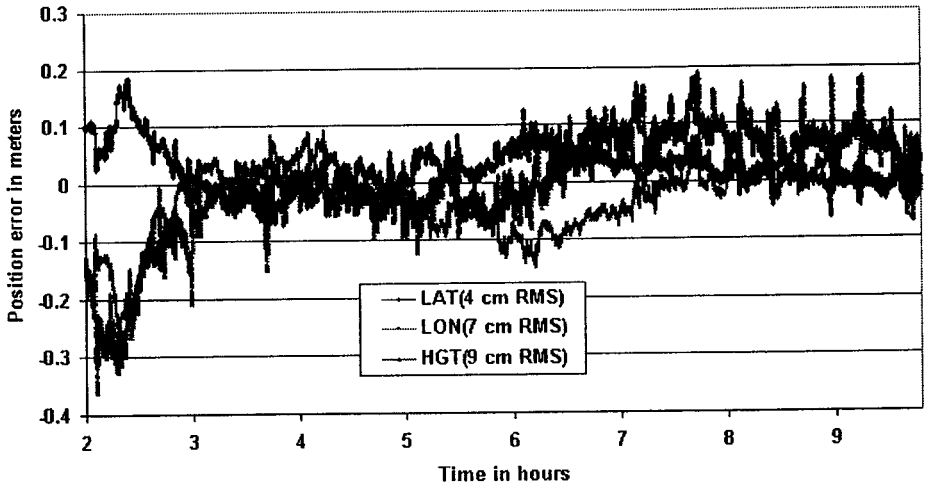


**Figure 6.3 Results of a 10-hour 1-Hz Kinematics Processing at Station NRC1**

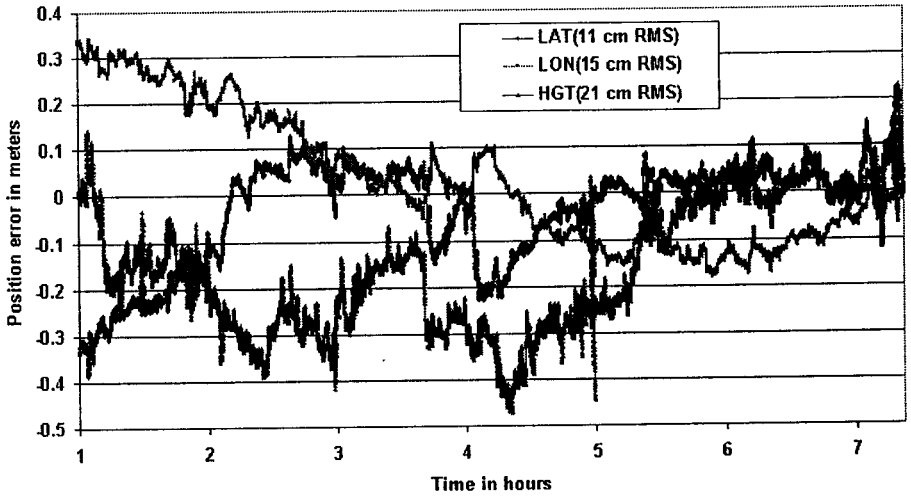


**Figure 6.4 Results of a 8-hour 1-Hz Kinematics Processing at Station PRDS**

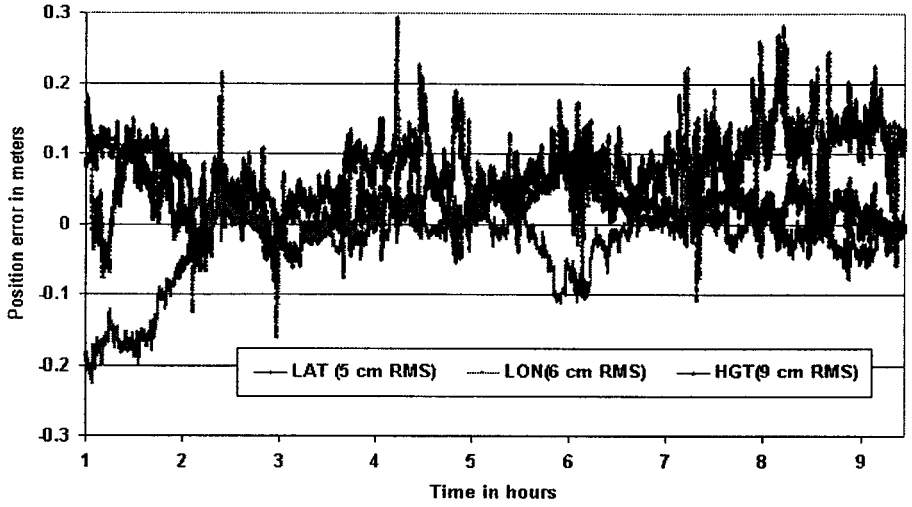


**Figure 6.5 Results of a 10-hour 1-Hz Kinematics Processing at Station STJO**

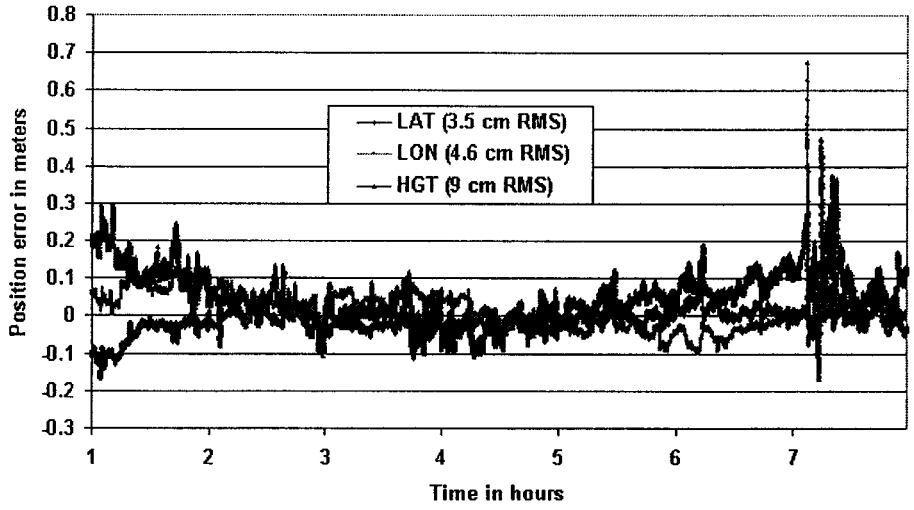


**Figure 6.6 Results of a 8-hour 1-Hz Kinematics Processing at Station YELL**

The position errors in the above figures display randomness with a changing range from approximately -10 cm to 10 cm centred at approximately 0. Spikes occur in some processing, which indicate the occurrence of ambiguity reset of some satellite due to the failure of residual check at the previous epoch. This reset brings an information decrease in the

variance-covariance matrix of the unknown parameters. For analysing convenience, Table 6.1 lists the mean, sigma, and root mean square (RMS) values of the position errors in latitude, longitude, and height for all the above six processing. The mean values in horizontal direction for all six stations are usually several centimetres, and there are bigger mean values in height with two cases exceeding 10 centimetres. Several reasons might account for the existence of this bias, among which is the processing time window. Averaging over a 24-hour processing period should reduce the mean values in latitude and longitude to below one centimetre. But for height, due to the clock and atmospheric residual, a bias of several centimetres is always normal.

Table 6.2 summarizes the RMS values shown in Table 6.1, listing the maximum, minimum, and average values for the six stations. An average 12 cm RMS vertical error and less than 10 cm horizontal error can be achieved in kinematics processing. This accuracy, similar to the static processing discussed in the previous chapter, is in agreement with the PPP error budget of 1~2 decimetres, which is the combination of the tropospheric mapping function error, the error residual of the precise ephemeris (3~5 cm RMS) and clock correction (0.1~0.2 nanosecond RMS, or 3~6 cm) [Kouba, 2000], plus receiver noise and multipath.

**Table 6.1 Statistics of Converged Position Errors in Kinematics Processing**

| | | Latitude | Longitude | Height |
|---|---|---|---|---|
| CHUR (Average satellite number: 7.7) | MEAN | 0.019 | 0.004 | 0.030 |
| | SIGMA | 0.052 | 0.032 | 0.075 |
| | RMS | 0.055 | 0.032 | 0.081 |
| DRA2 (Average satellite number: 7.0) | MEAN | -0.036 | -0.001 | 0.114 |
| | SIGMA | 0.065 | 0.050 | 0.114 |
| | RMS | 0.074 | 0.050 | 0.161 |
| NRC1 (Average satellite number: 6.8) | MEAN | 0.023 | -0.031 | 0.001 |
| | SIGMA | 0.038 | 0.06 | 0.091 |
| | RMS | 0.044 | 0.067 | 0.091 |
| PRDS (Average satellite number: 7.3) | MEAN | -0.038 | 0.029 | -0.155 |
| | SIGMA | 0.107 | 0.146 | 0.140 |
| | RMS | 0.114 | 0.149 | 0.209 |
| STJO (Average satellite number: 7) | MEAN | 0.033 | -0.025 | 0.076 |
| | SIGMA | 0.040 | 0.054 | 0.055 |
| | RMS | 0.052 | 0.060 | 0.094 |
| YELL (Average satellite number: 8.2) | MEAN | -0.011 | 0.011 | 0.053 |
| | SIGMA | 0.033 | 0.045 | 0.072 |
| | RMS | 0.035 | 0.046 | 0.090 |

**Table 6.2 RMS of the Converged Position Errors in Kinematics Processing**

| RMS | Latitude | Longitude | Height |
|---|---|---|---|
| Maximum | 0.114 | 0.149 | 0.209 |
| Minimum | 0.035 | 0.032 | 0.081 |
| Average | 0.062 | 0.067 | 0.121 |

Another finding from the statistical data is the mean values of coordinate errors ranges from several centimetres to over 10 centimetres. In order to find out the reason that causes these

non-zero mean values, another test was made which includes six 4-hour static processing samples from a 24-hour continuous dataset observed at station CHUR. As similarity is demonstrated among the converged position errors from all six processing samples, a conclusion can be made that the converged static position error, which reflects the mean value in the kinematics processing, mostly comes from the systematic error – the discrepancy between the used reference coordinates and their true value. The results in Table 6.3 also support this.

**Table 6.3 Comparison of Kinematics RMS and Converged Static Position Error (m)**

| | **Latitude** | **Longitude** | **Height** |
|---|---|---|---|
| **Converged Static Position Error** | 0.023 | -0.002 | 0.050 |
| **Mean Error (Kinematics processing)** | 0.019 | 0.004 | 0.030 |

Figure 6.7 shows the complete positioning error variation of Figure 6.1 in a nine-hour 1-Hz kinematics processing at station CHUR. It can be clearly seen that approximately 50 minutes is needed for the position estimation to reach convergence in this processing. If all six samples are considered, an average of approximately 2 hours is required for the position estimation to converge to 10 centimetres (1 sigma) in each coordinate component in the kinematics mode (see Table 6.4).

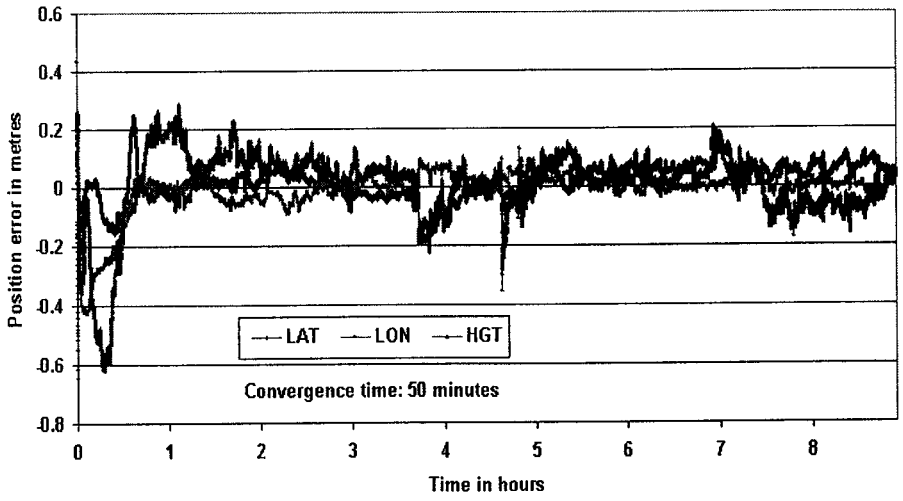


**Figure 6.7 Position Error of a 9-hour 1-Hz Kinematics Processing at CHUR**

**Table 6.4 Convergence Time in Kinematics Processing (Unit: Hour)**

| CHUR | DRA2 | NRC1 | PRDS | STJO | YELL | AVERAGE |
|---|---|---|---|---|---|---|
| 0.8 | 3.5 | 2.8 | 1.2 | 1.5 | 1.0 | **1.8** |

Figures 6.8 to 6.10 demonstrate ambiguity estimations for satellites PRN1, PRN8, and PRN22 over the nine-hour processing at Station CHUR. Approximately half an hour is required for ambiguity to converge, which is shorter than the positioning convergence time. That is because coordinate estimation has high correlations with tropospheric effect and receiver clock offset.

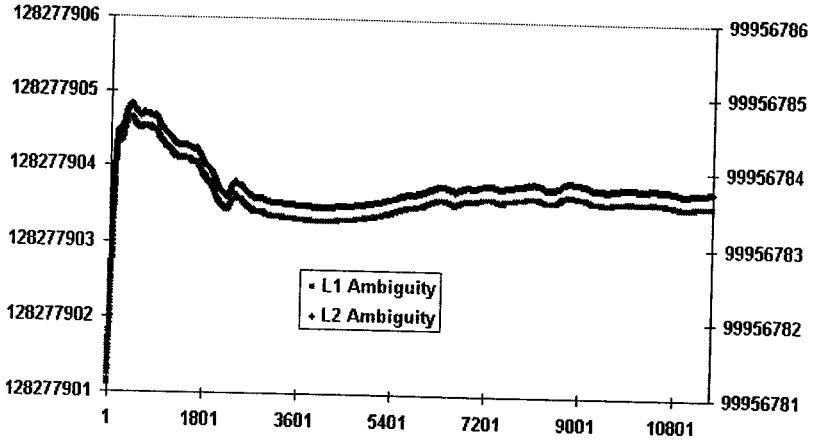


**Figure 6.8 Ambiguity Estimation of PRN22**

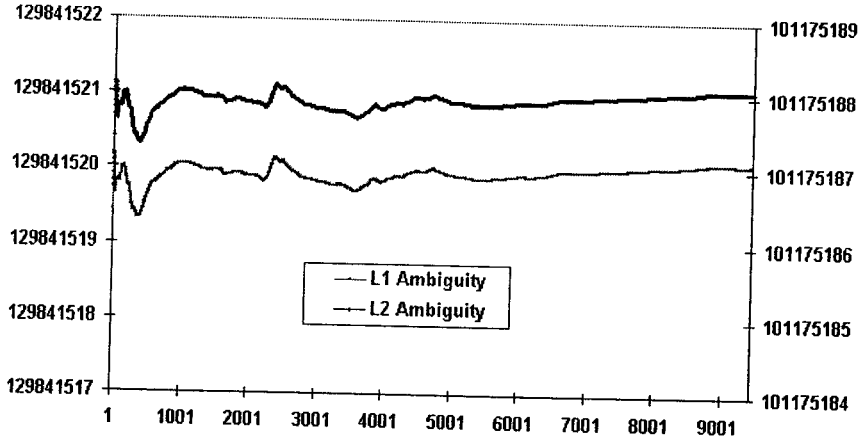


**Figure 6.9 Ambiguity Estimation of PRN01**

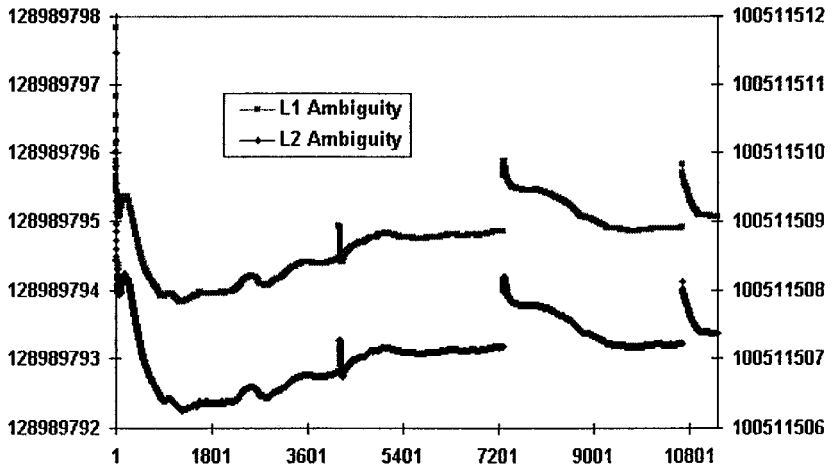


**Figure 6.10 Ambiguity Estimation of PRN08**

Tropospheric effects were also studied, whose result is showed in Figure 6.11 below. The y-axis indicates the values of tropospheric zenith path delay in metres. TROP-S represents the static results which act as the reference tropospheric effects, while TROP-K is for the kinematics. A nine-hour processing at Station CHUR shows a 0.4 cm RMS is achievable.

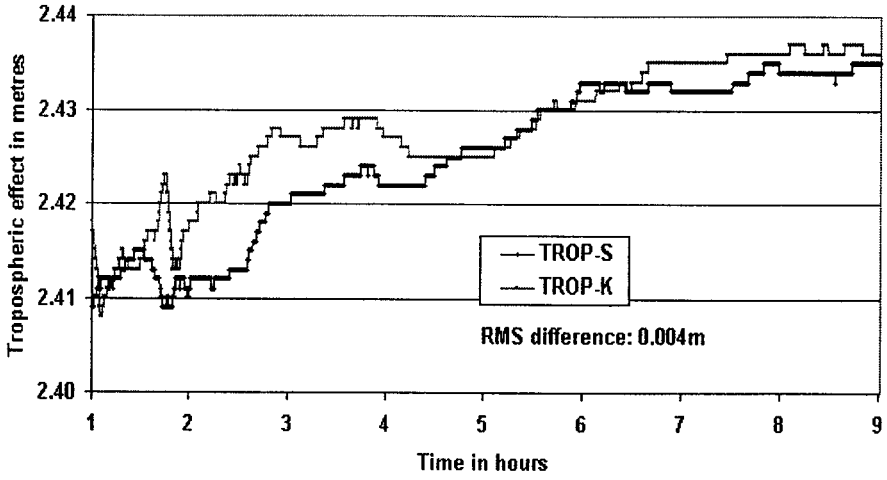


**Figure 6.11 Comparison of Kinematics and Static Tropospheric Estimation**

# CHAPTER 7

# CONCLUSIONS

This thesis systematically investigated a new GPS processing approach: Precise Point Positioning (PPP). Several aspects of PPP processing were discussed, including different precise GPS data products, PPP processing methods and their comparisons. Two PPP processing models were addressed in this thesis: the PPP Traditional Model, and P1-P2-CP Model. The latter one is a new PPP processing method proposed in this research. Tests were made in both static and kinematics post-processing modes. The precise GPS data used in the tests were the IGS final ephemerides available at a sampling interval of 15 minutes and the CACS precise satellite clock corrections at an interval of 30 seconds.

Several conclusions from the investigation have been made and are provided in the following:

1) Precise Point Positioning (PPP) is a new processing approach aimed at high positioning accuracy with the use of only a single GPS receiver. The major advantages of PPP lie in two aspects: system simplicity at the user's end, and the globally consistent positioning accuracy. The PPP concept has become possible with important developments such as the advent of precise GPS data, including precise satellite orbit

and clock corrections, and model construction technology with carrier phase observations from more advanced dual-frequency receiver.

2) Code and phase observables are the basic observations in PPP processing but play different roles. Usually the size of the code error residual is the key factor in the time required for position estimation to converge, while the phase counterpart weighs more on the converged positioning accuracy.

3) The unknown parameters in PPP processing include three coordinate components, receiver clock offset, tropospheric wet zenith path delay, and ambiguity parameters for each observed satellite. As the deterministic tropospheric mapping function cannot fully reflect the highly variable real atmosphere, the uncertainty for the tropospheric estimations, especially with low-elevation angle satellites, remains fairly large.

4) The PPP Traditional Model uses the traditional ionosphere-free code and phase combinations to mitigate the ionospheric effects. However, this method has several disadvantages. First, the measurement noise in the Traditional Model grows three-fold as compared to the original measurement noise. Second, the traditional ionosphere-free combination cannot remove higher-order ionospheric effects, which could be several centimetres, resulting in a bigger error residual. Third, the ambiguity term is a combined single unknown from $N_1$ and $N_2$ on two frequencies. Only a float solution can be obtained as this combined term does not preserve the integer characteristics of carrier phase ambiguity. With the Traditional Model, over 30 minutes is required before a converged position solution is obtained in a post-processing static mode.

5) A new observation model, named as P1-P2-CP, has been developed in this research. Similar to the Traditional Model, the new observation system also applies ionosphere-free combinations from dual-frequency observations but in a different form. This difference brings about a much lower measurement noise level and smaller error residuals. A stochastic estimation approach was also developed for precise stochastic modeling of the observations through the use of a variance adaptive procedure. Moreover, the new observation system allows for a simultaneous estimation of both L1 and L2 ambiguities and fixed ambiguity resolution becomes possible.

6) Different processing was carried out with both the Traditional and the P1-P2-CP Models using data collected at eight IGS stations across Canada. Analyses were made in terms of model stability, estimation variance, and time of convergence. Model stability refers to the estimation variation of unknown parameters between consecutive epochs due to the participation of new observations into the least-squares adjustment, and it measures how the chosen measurement variance influences the unknown parameters' determination. Estimation variance shows how big difference estimates are from the "true" values once filter converges. Time of convergence shows how long it takes a filter to reach a stable condition. Each criterion demonstrates one aspect of a model's performance, and the combination of the three gives a whole picture of how well a model works.

7) Numerical results with both PPP processing methods in a static processing mode have shown that centimetre positioning accuracy can be reached after approximately 30

minutes of processing. For a 40-centimetre positioning accuracy, an average of 4~5 minutes is required with the P1-P2-CP Model, a 20% time improvement compared to the Traditional Model. Considering the static processing results, the proposed new model has more stable results, smaller estimation variance, and faster convergence than the Traditional Model.

8) Kinematics processing was also conducted with the P1-P2-CP Model in which no constraint was imposed on the position parameters. The objectives of kinematics tests are first to assess the convergence time of the new model in the pure kinematics mode, and then to assess the obtainable kinematics positioning accuracy. Results have shown an average RMS value of 12 cm vertical positioning error and less than 10 cm horizontal positioning error. An average of 2 hours is needed for position to converge to an accuracy of a few centimetres indicating the importance for the development of fixed ambiguity resolution for PPP processing.

9) Finally, a pseudo-fixed ambiguity technique was investigated. Ambiguity-searching criteria based on the sum of weighted squared residual were implemented. Results from a partial fixing procedure have indicated that a positioning accuracy of several decimetres can be achieved once the fixing is completed, and ambiguity convergence time can be significantly reduced. The importance of pseudo-fixing is the fixed ambiguities are of much better precision than the float ambiguity estimations during the early-stages of processing, and a better positioning solution can be ensured, which is

useful for kinematics and fast static applications that only need decimetre-level positioning accuracy.

Based on the research in this thesis, the following recommendations can be made:

1) It is clear that the ambiguity pseudo-fixing approach can significantly accelerate convergence. But as the current results show that the ambiguity estimations are usually fixed to different values among processing samples with different starting time inside the same dataset, the criteria for determining fixed-ambiguity in the current implementation need further investigation.

2) The accuracy of real-time GPS precise products has reportedly improved to 10 cm and 1~2 ns precision level for the orbit and clock products, which are currently realized by some IGS Analysis Centres. PPP implementation in real-time applications will be in great demand in the future. Tests need to be done at a fixed station or on the road with precise GPS data input from wireless Internet or a radio beacon broadcasting system.

3) Least-squares sequential filter can generate the optimal results for static processing, but for real-time kinematics processing with Doppler observations, Kalman filter has more advantages. Therefore, tests with P1-P2-CP Model processed in Kalman Filter should also be made.

# REFERENCES

Abousalem, M.A (1996). Development and Analysis of Wide Area Differential GPS Algorithms. UCGE Reports Number 20083, Department of Geomatics Engineering, The University of Calgary, AB, Canada.

Abidin, H.Z. (1993). "Computational and Geometrical Aspects of On-The-Fly Ambiguity Resolution", Department of Geodesy & Geomatics Engineering, University of New Brunswick, Canada, Technical Report No.164.

Agnew, D.C. (1996). SPOTL: Some programs for ocean-tide loading, SIO Ref. Ser. 96-8, Scripps Inst. of Oceanography, La Jolla, California.

Ashby, Neil, "General Relativity in the Global Positioning System," in Gravitation and Relativity at the Turn of the Millennium, *Proceedings of the GR-15 conference* held at IUCAA, Pune, India, December 16-21, 1997, Naresh Didhich and Jayant Narlikar, editors, Inter-University Centre for Astronomy and Astrophysics, Pune, India, 1998, pages 231-258.

Carroll O. Alley, "Proper Time Experiments in Gravitational Fields With Atomic Clocks, Aircraft and Laser Light Pulses". in *Quantum Optics, Experimental Gravity, and Measurement Theory*, edited by Pierre Meystre and Marlan O. Scully, Plenum Publishing, New York, 1983, pages 421-424.

Chen, K., Gao Y., and Shen, X. (2002) "An Analysis of Single Point Positioning with Real-Time Internet-based Precise GPS Data". *Proceedings of 2002 International Symposium on GPS/GNSS*, Wuhan, China.

Dragert, H., T.S. James, and A. Lambert (2000). *Ocean Loading Corrections for Continuous GPS: A Case Study at the Canadian Coastal Site Holberg*, Geophysical Research Letters, Vol. 27, No. 14, pp. 2045-2048, July 15, 2000.

Forstner, W., On internal and external reliability of Photogrametric coordinates. Presented paper ASP-ASCM Convention, Washington, D.C., 1979.

Gao, Y. and Shen, X. (2001). "Improving Ambiguity Convergence in Carrier Phase-Based Precise Point Positioning", *Proceedings of ION GPS-2001*, Salt Lake City, USA, September 11-14, 2001.

Graybill, F.A., *Theory and Application of the Linear Model*. Duxbury Press, Mass., U.S.A, 1976.

Horvath, T. (2002). Performance Comparison of Wide Area Differential GPS System. Technical Report No. 212, Department of Geodesy and Geomatics Engineering, The University of New Brunswick, NB, Canada.

Hofmann-Wellenhof, B., Lichtenegger, H. & Collins, J., (1998). *GPS Theory and Practice*. Springer-Verlag, Vienna New York, 4th ed.

IERS (1989). *IERS Standards* (1989), IERS Technical Note 3, (ed. D.D. McCarthy)

IERS (1996). *IERS Conventions* (1996), IERS Technical Note 21, (ed. D.D. McCarthy)

ION (1980). *Global Positioning System, Vol. I*, Papers published in NAVIGATION, ISBN:0-936406-00-3.

Janes, H.W., Langley, R.B., and Newby, S.P., (1991) "Analysis of Tropospheric Delay Prediction Models", *Bulletin Geodesique*, Vol.65,

Kouba, J And Héroux, P. (2000). "Precise Point Positioning Using IGS Orbit Products", *GPS Solutions*, Vol.5, No.2, Fall, pp12-28.

IGS Analysis Activities (2000). *IGS Annual Report*, IGS Central Bureau, Jet Propulsion Laboratory, Pasadena, CA, pp. 15-16.

Krakiwsky, E.J., A synthesis of recent advances in the method of least squares. Division of Surveying Engineering, Publication 10003, University of Calgary, Calgary, AB, Canada, 1981.

Krakiwsky, E.J. (1990). "The Method of Least-squares: a Synthesis of Advances." Department of Surveying Engineering, The University of Calgary.

Lachapelle, G., Klukas, R., D. and Qiu, W. (1995). One-Meter Kinematics Point Positioning Using Precise Orbits and Satellite Clock Corrections. *Proceedings of ION GPS-96*, Salt Lake City, Utah, September 20-23.

Levy, L. J. (1997). The Kalman filter: Navigation's integration workhorse. *GPS World*, September, Vol. 8, No. 9, pp. 65-71.

Maybeck, P.S. (1979). *Stochastic Models, Estiamtion, and Control (Vol. 141)*. Academic Press Inc. New York. 1979.

Mackenzie, A.P. (1985). Design and Assessment of Horizontal Survey Networks, M. Sc. Thesis, Department of Civil Engineering Division of Surveying Engineering, University of Calgary, 1985.

Muellerschoen, RJ. Y.E. Bar-Sever, W.I. Bertiger, D.A. Stowers (2001). "NASA's Global DGPS for High Precision Users", *GPS World*, Vol. 12, No. 1, pp.14-20.

Pagiatakis,S.D. ( 1992). Program LOADSDP for the calculation of ocean load effects, Man. Geod., 17, 315-320.

Parkinson, B.W., "GPS Error Analysis", *Global Positioning System: Theory and Applications Volume I*, Volume 163, Progress in Astronautics and Aeronautics, The American Institute of Aeronautics and Astronautics, Washington, 1996, pp. 469-483

Parkinson, B.W., Ashby, N., "Introduction to Relativistic Effects on the Global Positioning System", *Global Positioning System: Theory and Applications Volume I*, Volume 163, Progress in Astronautics and Aeronautics, The American Institute of Aeronautics and Astronautics, Washington, 1996, pp. 679-682

Parkinson, B.W., and Klobuchar, J.A., "Ionospheric Effects on GPS", *Global Positioning System: Theory and Applications Volume I*, Volume 163, Progress in Astronautics and Aeronautics, The American Institute of Aeronautics and Astronautics, Washington, 1996, pp. 491-493

Parkinson, B.W., Spilker, J.J., "Tropospheric Effects on GPS", *Global Positioning System: Theory and Applications Volume I*, Volume 163, Progress in Astronautics and Aeronautics, The American Institute of Aeronautics and Astronautics, Washington, 1996, pp. 517-546

Pope, A.J., The statistics of residuals and the detection of outliers. NOAA Technical Report NOS 65 NGS 1, US Department of Commerce, Rockville, Md., USA, 1976.

Rizos, C. (1999). "Satellite Ephemeris Bias." Principles and Practice of GPS Surveying. The University of New South Wales, Sydney, Australia. http://www.gmat.unsw.edu.au/snap /gps/gps_survey/chap6/6212.htm (last updated: 18 January 2000)

Rizos, C. (1999). "Multipath Disturbance & Signal Interference." Principles and Practice of GPS Surveying. The University of New South Wales, Sydney, Australia. http://www.gmat.unsw.edu.au/snap/gps/gps_survey/chap6/623.htm (last updated: 18 January 2000)

Rizos, C. (1999). "Tropospheric Delay." Principles and Practice of GPS Surveying. The University of New South Wales, Sydney, Australia. http://www.gmat.unsw.edu.au/snap/gps/gps_survey/chap6/628.htm (last updated: 18 January 2000)

Scherneck, H.G. (1991). A parameterized Solid Earth Tide Model and Ocean Tide Loading Effects for global geodetic baseline measurements, Geophs. J. Int. 106, pp. 677-694.

Scherneck, H.G. (1993). Ocean Tide loading: Propagation errors from ocean tide into loading coefficients, Man. *Geodetica*, 18, pp.59-71.

Seeber, G., (1993). *Satellite Geodesy: Foundations, Methods & Applications*. Walter de Gruyter, Berlin New York, 531pp.

Shen, X. and Gao, Y. (2002). "Kinematics Processing Analysis of Carrier Phase-based Precise Point Positioning", *Proceedings of FIG XXII International Congress*, Washington, D.C. USA, April 19-26 2002.

Wahr, J.M. (1981). The forced nutation of an elliptical, rotating, elastic, and oceanless Earth, Geophys. J. Roy. Astron. Soc., 64, pp. 705-727.

Welch G., Bishop G. (2001) An Introduction to the Kalman Filter. TR 95-041, Department of Computer Science, University of North Carolina at Chapel Hill, 2001

# APPENDIX A: REDUNDANCY NUMBER

Redundancy r of the adjustment system is usually computed through the number of observations minus number of unknowns as suggested in the above table. However, using this simple deduction may cause the incorrect system redundancy, and then result in an incorrect estimation of the important index – the a posteriori variance for unit weight $\hat{\sigma}_0^2$. A more precise way to calculate redundancy is by calculating redundancy numbers of each contributing observation via the variance-covariance matrix of the adjusted observables and has the following theoretical procedure.

In least-squares adjustment, the correction vector and the residual vector are expressed by

$$\hat{\delta} = -\left(A^T C_l^{-1} A\right)^{-1} A^T C_l^{-1} w \tag{A.1}$$

$$\hat{v} = A \cdot \hat{\delta} + w \tag{A.2}$$

Substituting $\hat{\delta}$ in Equation (A.2) with the right-hand side in Equation (A.1), the estimated residual vector has the expanding form:

$$\hat{v} = -A\left(A^T C_l^{-1} A\right)^{-1} A^T C_l^{-1} w + w \tag{A.3}$$

Collecting terms of $w$ and $C_l^{-1}$ in equation and rearranging results in

$$\hat{v} = \left[C_l - A\left(A^T C_l^{-1} A\right)^{-1} A^T\right] C_l^{-1} w \tag{A.4}$$

Which simplifies to

$$\hat{v} = \left[C_l - C_{\hat{l}}\right] C_l^{-1} w \tag{A.5}$$

Where $C_{\hat{l}}$ is the variance-covariance matrix of the adjusted observables, given as

$$C_{\hat{l}} = AC_X A^T = A\left(A^T C_l^{-1} A\right)^{-1} A^T \tag{A.6}$$

Further simplification of equation may be arrived at through consideration of the equation for the covariance matrix of the estimated residuals $C_{\hat{r}}$ given as [Krakiwsky, 1981]

$$C_{\hat{r}} = C_l - C_{\hat{l}} \tag{A.7}$$

Substitution of equation into equation gives

$$V = C_{\hat{r}}\, C_l^{-1} w \tag{A.8}$$

The matrix product $C_{\hat{r}} C_l^{-1}$ is symmetric and idem-potent. Two of the properties of a symmetric idem-potent matrix H of size n by n and rank p are as follows [Graybill, 1976]:

(i) HH=H; and (A.9)

(ii) Rank{H} = tr{H} = p (A.10)

In light of the second property, it reveals that the trace of matrix H is equal to the redundancy of the system, due to the fact that the rank of $C_{\hat{l}}$ is equal to $r$, the system redundancy. Each diagonal element of $C_{\hat{l}}C_l^{-1}$, given as $r_i$, then represents the contribution of the i'th observation to the system redundancy [Forstner, 1979]. The amount of contribution of an observation to the system redundancy is a function of geometry and observational accuracy. The size of such contribution cannot be greater than one, nor can its contribution have a negative effect giving [Pope, 1976]:

$$0 \le r_i \le 1 \tag{A.11}$$

and the redundancy of the system $r$ is

$$r = \sum r_i \tag{A.12}$$

A posteriori variance for unit weight $\hat{\sigma}_0^2$, or in other words, the estimated variance factor, is a very important index for measuring and adjusting the observation standard deviation. Another important index for least-square adjustment is a priori variance of unit weight $\sigma_0^2$, a preset value without any meaning by its own.

Before carrying out a least-squares adjustment, users may have only limited knowledge from previous experiences about observation precision, and therefore use an approximate value representing its standard deviation $\sigma$. This value might not be accurate enough. Once a posteriori variance $\hat{\sigma}_0^2$ is estimated, an updated observation precision can be expressed as:

$$\hat{\sigma} = \sigma \cdot \frac{\hat{\sigma}_0^2}{\sigma_0^2} \tag{A.13}$$

which would more reflect the observation precision.

# APPENDIX B: DUAL-FREQUENCY GPS OBERVATION COMBINATIONS

For simplicity and readability, the frequency-independent terms in the GPS observations equations, including $dt$, $dT$, $d_{orb}$, and $d_{trop}$, are removed from the observation equations and merged into the geometry-range $\rho$ term. Multipath $d_{mult}$ and observation noise $\varepsilon(.)$ are removed as well, but their influences to different combinations are different and are discussed and shown in the following table in this Appendix.

**Geometry-Free Ionosphere Combination (L4)**

This is also referred to as the "L4" combination. It has the following expression.

$$\begin{aligned}\Phi(L4) = \Phi(L1) - \Phi(L2) &= \lambda_1 N_1 - \lambda_2 N_2 - d_{ion(L1)} + d_{ion(L2)} \\ &= \lambda_1 N_1 - \lambda_2 N_2 + 0.646 \cdot d_{ion(L1)}\end{aligned} \tag{B.1}$$

The geometry part $\rho$ is gone after the deduction. Hence, any variation in the L4 represents entirely the variation in L1 ionosphere effect unless there is a cycle slip on L1 or L2. The ionospheric delay changes slowly and any sudden "jumps" could be interpreted as cycle slip on L1 and/or L2.

The equivalent pseudo-range L4 combination therefore is:

$$P(L4) = P(L1) - P(L2) = -0.646 \cdot d_{ion(L1)} \tag{B.2}$$

The above equation implies that the ionospheric delay can be measured directly with the two P code pseudo-range observations. This is not entirely correct because what is missing from the observation model is the data "noise" and multipath, both of which can have serious impact at the decimetre level or better.

**Wide-Lane combination (L5)**

This combination is commonly used because its longer wavelength is better for ambiguity searching and estimation. It is expressed as follows.

$$\Phi(L5) = \rho + \frac{f_1}{f_2} \cdot d_{ion(L1)} + \lambda_5 N_5 \tag{B.3}$$

$$\lambda_5 = \frac{c}{f_1 - f_2} \approx 0.86\,m \tag{B.4}$$

$$N_5 = N_1 - N_2 \tag{B.5}$$

$$P(L5) = \rho - \frac{f_1}{f_2} \cdot d_{ion(L1)} \tag{B.6}$$

The wide-lane pseudo-range is therefore advanced by the ionosphere (range too short), while the wide-lane phase is delayed by the ionosphere (phase-range too long).

**Narrow-Lane combination (L6)**

The narrow-lane combination has a smaller noise and multipath level, and has the following form.

$$\Phi(L6) = \rho - \frac{f_1}{f_2} \cdot d_{ion(L1)} + \lambda_6 \cdot N_6 \tag{B.7}$$

$$\lambda_6 = \frac{c}{f_1 + f_2} \approx 0.10\ m \tag{B.8}$$

$$N_6 = N_1 + N_2 \tag{B.9}$$

$$P(L6) = \rho + \frac{f_1}{f_2} \cdot d_{ion(L1)} \tag{B.10}$$

The narrow-lane pseudorange is therefore delayed by the ionosphere (range too long), while the narrow-lane phase is advanced by the ionosphere (phase-range too short).

L3 can be derived from L5 and L6 as follows,

$$\Phi(L3) = \frac{\Phi(L5) + \Phi(L6)}{2} \tag{B.11}$$

**Combination Comparison on Noise and Ionosphere**

All the combinations can be expressed in the following form.

$$\phi_{i,j} = i\phi(L1) + j\phi(L2) \tag{B.12}$$

which is in units of cycles.

The ionospheric effect of the combinations can be expressed as a scaled ionospheric effect on L1 by a factor. This ionospheric scale factor isf can be calculated with the following equation:

$$isf = \frac{f_1}{f_2} \cdot \left( \frac{if_2 + jf_1}{if_1 + jf_2} \right) \tag{B.13}$$

Similarly, a noise scale factor nsf can be deduced based on the assumption of equal noise on both L1 and L2 when expressed in cycle.

$$nsf = \frac{\lambda_2 \sqrt{i^2 + j^2}}{i\lambda_2 + j\lambda_1} \tag{B.14}$$

**Table B.1 Noise and Ionospheric Effect of Some Common Linear Combinations**

| Some common Linear Combinations of L1 and L2 Phase Observations | | | | |
|---|---|---|---|---|
| Phase Combination | Wavelength (m) | Noise Nsf * L1 | Ion. Delay Isf * dion(L1) | Ambiguity |
| L1 | 0.190 | 1.0 | 1.0 | $N_1$ |
| L2 | 0.244 | 1.28 | 1.65 | $N_2$ |
| L3 (IF) | 0.190<br>0.244 | 3.2 | 0.0<br>0.0 | $\alpha_1 N_1 + \alpha_2 N_2$<br>$\beta_1 N_1 + \beta_2 N_2$ |
| L4 (GF) | | 1.63 | -0.65 | $\lambda_1 N_1 + \lambda_2 N_2$ |
| L5 (WL) | 0.862 | 6.4 | -1.28 | $N_1 - N_2$ |
| L6 (NL) | 0.107 | 0.8 | 1.28 | $N_1 - N_2$ |
| | | | | |
| Double WL | 1.628 | 42.78 | 18.25 | $-3N_1 + 4N_2$ |
| Half WL | 0.431 | 6.41 | -1.28 | $2N_1 - 2N_2$ |
| Semi WL | 0.341 | 4.0 | 2.805 | $-N_1 + 2N_2$ |
| Monster WL | 14.65 | 878 | 350 | $-7N_1 + 9N_2$ |
| Ion-free | 0.006 | 3.22 | 0.0 | $77N_1 - 60N_2$ |